PB82-212499

Measurements in the Wake of an 'Infinite' Swept Airfoil

Iowa Inst. of Hydraulic Research, Iowa City

Prepared for

National Aeronautics and Space Administration
Washington, DC

Apr 82

U.S. Department of Commerce
National Technical Information Service
NTIS

BIBLIOGRAPHIC INFORMATION

PB82-212499

Measurements in the Wake of an 'Infinite' Swept Airfoil,

Apr 82

C. J. Novak, and B. R. Ramaprian.

PERFORMER: Iowa Inst. of Hydraulic Research, Iowa City.
IIHR-240
Grant NSG-1200, Grant NAG-2-110

SPONSOR: National Aeronautics and Space Administration, Washington, DC.

Portions of this document are not fully legible.

This is a report of the measurements in the trailing edge region as well as in the report of the developing wake behind a swept NACA 0012 airfoil at zero incidence and a sweep angle of 30 degrees. The measurements include both the mean and turbulent flow properties. The mean flow velocities, flow inclination and static pressure are measured using a calibrated three-hole yaw probe. The measurements of all the relevant Reynolds stress components in the wake are made using a tri-axial hot-wire probe and a digital data processing technique developed by the authors.

KEYWORDS: *Airfoils, *Trailing edges, *Boundary layer flow.

Available from the National Technical Information Service, Springfield, Va. 22161

PRICE CODE: PC A07/MF A01

PB82-212499

MEASUREMENTS IN THE WAKE OF AN 'INFINITE' SWEPT AIRFOIL

by

C. J. Novak and B. R. Ramaprian

Sponsored by

National Aeronautics and Space Administration
Grants No. NSG-1200 and NAG 2-110

IIHR Report No. 240

Iowa Institute of Hydraulic Research
The University of Iowa
Iowa City, Iowa 52242

April 1982

Approved for public release; distribution unlimited

MEASUREMENTS IN THE WAKE OF AN 'INFINITE' SWEPT AIRFOIL

by

C. J. Novak and B. R. Ramaprian

Sponsored by

National Aeronautics and Space Administration
Grants No. NSG-1200 and NAG 2-110

IIHR Report No. 240

Iowa Institute of Hydraulic Research
The University of Iowa
Iowa City, Iowa 52242

April 1982

ABSTRACT

This is a report of the measurements in the trailing edge region as well as in the report of the developing wake behind a swept NACA 0012 airfoil at zero incidence and a sweep angle of 30 degrees. The measurements include both the mean and turbulent flow properties. The mean flow velocities, flow inclination and static pressure are measured using a calibrated three-hole yaw probe. The measurements of all the relevant Reynolds stress components in the wake are made using a tri-axial hot-wire probe and a digital data processing technique developed by the authors. The development of the three-dmensional near-wake into a nearly two-dimensional far-wake is discussed in the light of the experimental data. A complete set of wake data along with the data on the initial boundary layer in the trailing edge region of the airfoil are tabulated in an appendix to the report.

ACKNOWLEDGEMENTS

The authors wish to thank Professors V.C. Patel and A. Prabhu for many useful discussions. Dr. Prabhu made significant contribution to the development of the triple-sensor instrumentation, which is discussed more elaborately in a separate report.

TABLE OF CONTENTS

LIST OF TABLES

LIST OF FIGURES

LIST OF SYMBOLS

a_i, b_i, c_i	Sensor direction cosines $i = 1,2,3$
A_{2d}	Bradshaw structure parameter as calculated in two-dimensional case
A_{3d}	Bradshaw structure parameter as calculated in three-dimensional case
A', B'	Constants in King's Law
b_x	Half width of longitudinal velocity in the wake
b_z	Half width of spanwise velocity in the wake
C,L	Airfoil chord length = 922 mm
C_p	Pressure coefficient
A_i, B_i, C_i	Variables used in hot wire data analysis, $i = 1,2,3$
a_4, b_4, c_4, d_4, e_4, f_4	Constants used in hot wire data analysis
E	Hot wire mean voltage output
H	Shape factor (δ_1/θ_f)
k	Sensitivity correction factor = .1
n	Exponent in King's Law
$\bar{Q}_1, \bar{Q}_2, \bar{Q}_3$	Effective mean velocities of sensors 1, 2, and 3, respectively
q_1, q_2, q_3	Fluctuating effective velocities of sensors 1, 2, and 3
Q_1, Q_2, Q_3	Instantaneous effective velocities of sensors 1, 2, and 3
$\bar{U}, \bar{V}, \bar{W}$	Mean velocities in the x,y, and z directions
U,V,W	Instantaneous velocities in x,y, and z directions
u', v', w'	Root mean squares of u,v, and w
U_{in}, U_∞	Constant freestream velocity

W_{cl}	W at the centerline
w_x	Defect velocity in the longitudinal or chordwise direction
w_z	Defect velocity in the spanwise or crossflow direction
w_{xo}	w_x at the centerline of the wake
w_{zo}	w_z at the centerline of the wake
e	Fluctuating hot-wire voltage output
u_τ	Friction velocity
δ	Boundary layer thickness
x,y,z	Streamwise (longitudinal or chordwise), normal and spanwise (crossflow) coordinates
ε_x	Eddy viscosity, as calculated from the gradient of U
ε_z	Eddy viscosity, as calculated from the gradient of W
θ	Sensor orientation in the x-z plane
ψ	Sensor orientation in the y-z plane
θ_f	Final station momentum thickness (2-D definition)
θ_t	Trailing edge momentum thickness (2-D definition)
η_x	y/b_x
η_z	y/b_x
δ_1	$\int_{-\infty}^{\infty} (1 - \frac{U}{U_\infty})\, dy$
δ_2	$\int_{-\infty}^{\infty} (1 - \frac{W}{U_\infty})\, dy$
θ_{11}	$\int_{-\infty}^{\infty} \frac{U}{U_\infty} (1 - \frac{U}{U_\infty})\, dy$
θ_{22}	$\int \frac{W}{U_\infty} (1 - \frac{W}{U_\infty})\, dy$

θ_{12} $\int \frac{U}{U_\infty}(1 - \frac{W}{U_\infty})\, dy$

θ_{21} $\int \frac{W}{U_\infty}(1 - \frac{W}{U_\infty})\, dy$

γ Angle between the velocity vector and the x-direction in the case of the swept air foil

ϕ Sweep angle of the airfoil

ATTENTION

AS NOTED IN THE NTIS ANNOUNCEMENT, PORTIONS OF THIS REPORT ARE NOT LEGIBLE. HOWEVER, IT IS THE BEST REPRODUCTION AVAILABLE FROM THE COPY SENT TO NTIS.

CHAPTER I

INTRODUCTION

1. The Problem Introduced

There is a growing interest, in recent years, in the development of calculation methods of three dimensional turbulent shear flows such as boundary layers and wakes. This is largely because of their application in aerodynamics and ship hydrodynamics. Calculation of the drag on the swept wing of an aircraft is a typical example. This problem presents many complexities (especially in the trailing edge and near-wake regions) such as viscid-inviscid interaction, three dimensionality and the modeling of turbulence. Computational techniques capable of handling these complexities are currently under development at various research centers. In order to verify the accuracy of such methods and also to aid the development of new methods, it is essential to have a comprehensive data base on three-dimensional flows in general and three dimensional wake flows with particular reference to the problem cited above. Such data should include information on velocities, pressure and the details of the turbulence properties. Measurement of turbulence properties in three dimensional flows is still a challenging task since the required measurement techniques are only in their early stages of development. Consequently, there is not much data available on the turbulence properties in three dimensional flows. The present research has been aimed at obtaining a set of detailed measurements, in a relatively simple three-dimensional wake, namely the developing wake behind an infinite swept airfoil. Also as a part of this research program, significant effort has been directed towards the development and validation of a suitable technique for turbulence measurements in three-dimensional flows.

Previous work done in the wake of streamlined bodies have been largely restricted to two-dimensional flows. These include the work of Chevray and Kovasznay (1969), Pot (1979), Andreopoulos and Bradshaw (1980) as well as that of Sastry (1981) in the symmetric and asymmetric wakes of flat plates and airfoils. In these studies, the relevant components of the Reynolds stress tensor have been measured. Computational models have also been developed and used to describe these experimental findings. Of the above, Sastry's studies included the two-dimensional wake of a Korn-Garabedian airfoil at incidence. The development of various wake parameters were studied and compared with those in the case of the flat plate wake. It should be noted that most of the data reported by the previous investigators have been restricted to the near or intermediate wake regions.

It is only very recently that experimental studies of wakes exhibiting three-dimensionality have been performed. One study, that of Cousteix and Pailhaus (1980) explored the wake behind a swept 'ONERA D' airfoil at incidence. This study contains hot-wire measurement of all the components of the Reynolds stress tensor in addition to data on mean velocities and flow inclination. Similar hot-wire data in the three-dimensional wakes of turbomachinery blade have been obtained at Penn State University. These data, however, were obtained under very difficult experimental conditions, with many uncertainties introduced by such factors as small physical size, probe orientation, probe dimensions, data reduction, etc. The data of Cousteix and Pailhaus (1980) were obtained under more favorable conditions. Yet, even in these experiments, (the airfoil studied had a chord of 200 mm and a span of 300 mm) tunnel wall interference on the wake development could have been significant.

In the present study some of the limitations of the above experiments have been removed. Present experiments were performed in the wake behind an "infinite" NACA 0012 airfoil swept at 30 degrees, and at zero incidence. Such a flow, being significantly three dimensional, yet relatively simple, is expected to provide useful information on growth rates, viscosity models and other properties of three-dimensional wakes. Also, these flows can be studied with regard to the manner in which they approach two-dimensionality at a large distance from the trailing edge.

A complete set of measurements are obtained both in the boundary-layer in the trailing edge region and in the developing wake behind the airfoil. These measurements include pressure distribution, mean velocity components, in the boundary layer and wake. Additionally, the six components of the Reynolds shear stress were also measured in the wake. The measurements extend up to two chord lengths downstream from the trailing edge. The turbulence measurements have been made using triple-sensor hot-wire anemometry. A significant contribution of this study is the development and validation of a suitable technique for the measurement of turbulence properties using the triple-sensor probe and a comparative study of alternative techniques. In fact, development of the present technique forms a part of a larger program of study on general three-dimensional boundary layer flows, currently in progress at the Institute of Hydraulic Research.

Chapter II will be devoted to the development of the triple-sensor anemometry. A complete description of the method is presented. Particulars concerning the airfoil experiments such as calibration procedures for hot-wire instrumentation, details of the airfoil fabrication, instrumentation, and mounting are discussed in Chapter III. The results and discussion are presented and discussed in Chapter IV. The effects of three-dimensionality are compared with previous two dimensional experiments and theory. Further, Chapter IV also contains the concluding remarks as well as suggestions toward further work.

CHAPTER II

DEVELOPMENT OF THREE-DIMENSIONAL HOT-WIRE INSTRUMENTATION

1. Problem Description and Quantities Requiring Measurement

In studies of three-dimensional turbulent flows, it is necessary to measure the instantaneous values of three mutually orthogonal velocities at a given point in space. The instantaneous values will contain three mean velocities as well as three time-dependent or fluctuating velocities. It is these three instantaneous fluctuating velocity components, in addition to the mean components that require retrieval in this study. This retrieval must be general enough, such that it allows one to study flow fields of arbitrary geometry.

2. Available Techniques and Relative Assessment

Hot-wire anemometry has been the most commonly used instrumentation for velocity measurements especially in three-dimensional flows. Laser velocimetry, which is currently gaining popularity, is complex and not well tested in three-dimensional flows. Two techniques, using hot-wire anemometry have been tried in three-dimensional flows. One of these uses a triple-sensor probe in which there are three independent sensing elements oriented in certain specific relative directions, and the other uses a single sensor or x-wire probe oriented sequentially at different angles to the flow. The first method, used by Gorton and Lakshminarayana (1976) and others, requires that the predominant direction of flow is known and that the probe axis coincides with it. The three instantaneous outputs u,v,w, from the sensors are then processed by an analog computer which solves for the mean values $\overline{U}$,$\overline{V}$, and $\overline{W}$ as well as for the six Reynolds stresses u'^2, v'^2, w'^2, $\overline{uv}$, $\overline{vw}$ and $\overline{uw}$ via the solution of a set of linearized simultaneous equations. One of the drawbacks of this method is that, often, there may not be a predominant direction in the flow. Also, nonlinear effects may affect the accuracy of this method.

The second method, used by Elsenaar and Boelsma (1974), consists of a single inclined wire probe rotating about it's roll axis. The probe outputs at successive orientations of the probe are used to obtain solutions for the mean velocities and turbulent stresses. Here again, the major difficulties are the need for actual physical rotation of the probe itself and the interference of the probe support system with the flow. Elsenaar and Boelsma have noted this and the associated uncertainties.

Apart from the shortcomings mentioned above, information is lost in these methods during the analog processing for time-averaged results. Thus instantaneous velocities, their triple correlations, and higher order moments cannot be determined.

The method selected for the present study use a triple sensor probe oriented in an arbitrary direction to the flow. The instantaneous outputs from the three sensors are used to obtain not only the three mean velocity components and the six Reynolds stresses but also the instantaneous fluctuating velocity components. This is done through digital data acquisition software. Two alternate schemes were developed for comparison purposes. Each of these is described below in detail.

2.1 Method A

Figure 1 shows the probe and flow coordinate system. Consider hot wire sensor 1 with respect to the X,Y,Z (flow) coordinate system. This sensor has an orthogonal coordinate system (ζ_1,ζ_2,ζ_3) associated with its orientation. We, then, have

$$(Q_1) = a_1U + b_1V + c_1W \qquad (1)$$

$$(Q_2) = a_2U + b_2V + c_2W \qquad (2)$$

$$(Q_3) = a_3U + b_3V + c_3W \qquad (3)$$

where Q_1, Q_2 and Q_3 are the instantaneous velocities in the ζ_1,ζ_2,ζ_3 coordinate system, and U,V, and W are the instantaneous velocities in the X,Y, and Z coordinate system. The coefficients a_1, b_1, c_1,..., are the appropriate direction cosines of the X,Y, and Z axis with respect to the (ζ_1,ζ_2,ζ_3) coordinate system as shown in figure 1.

The effective velocity sensed by hot wire sensor 1 is given by [see for example Friehe and Schwarz (1968)]

$$Q_1 = [(Q_2)^2 + (Q_3)^2 + k_1^2 (Q_1)^2]^{1/2} \qquad (4)$$

with k_1 being the cross-sensitivity factor associated with deviation from the cosine law. Q_1 is obtained from the voltage output E_1 of the sensor 1, via its calibration curve. Now, if we substitute Eq. (1,2,3) into Eq. (4), the resulting expression becomes

$$Q_1 = [a_4U^2 + b_4V^2 + c_4W^2 + d_4UV + e_4UW + f_4VW]^{1/2} \tag{5}$$

The coefficients in the above equations are:

$$a_4 = a_2^2 + a_3^2 + k_1^2\ a_1^2 \tag{6}$$

$$b_4 = b_2^2 + b_3^2 + k_1^2\ b_1^2 \tag{7}$$

$$c_4 = c_2^2 + b_3^2 + k_1^2\ c_1^2 \tag{8}$$

$$d_4 = 2(a_2b_2 + a_3b_3 + k_1^2\ a_1b_1) \tag{9}$$

$$e_4 = 2(a_2c_2 + a_2c_3 + k_1^2a_1c_1) \tag{10}$$

$$f_4 = 2(b_2c_2 + b_3c_3 + k_1^2b_1c_1) \tag{11}$$

Similar expressions can be derived for sensors 2 and 3. One, then gets a set of three nonlinear algebraic equations for the three unknowns U,V, and W. These require solution by an iterative scheme. The method used is a Newton-Raphson scheme, which requires an initial guess to start the algorithm.

In practice, the instantaneous outputs E_1,E_2 and E_3 of the three sensors are sampled, digitized and stored. These data are later recalled, calibrated and the velocity components U,V,W are computed on an instant to instant basis using the above procedure. After the entire set of instantaneous velocity components are evaluated, they are time averaged to obtain $\overline{U}$, $\overline{V}$, and $\overline{W}$. The turbulent fluctuations, u, v, and w are then recovered and stored for subsequent processing. Since this method involves the solution of nonlinear equations, for each set of instantaneously sampled data, it is computationally very time-consuming and expensive. However, it does not involve any linearization and can therefore be used even for very large fluctuations.

2.2 Method B

In this method the effective velocities and resultant velocities are both decomposed into their mean and fluctuating components. Eqs. (1-3), then, become:

$$(\overline{Q} + q)_1 = a_1(\overline{U}+u) + b_1(\overline{V}+v) + c_1(\overline{W}+w) \quad (12)$$

$$(\overline{Q} + q)_2 = a_2(\overline{U}+u) + b_2(\overline{V}+v) + c_2(\overline{W}+w) \quad (13)$$

$$(\overline{Q} + q)_3 + a_3(\overline{U}+u) + b_3(\overline{V}+v) + c_3(\overline{W}+w) \quad (14)$$

Now, if they are substituted into Eq. (4), we get

$$[(a_4\overline{U}^2 + b_4\overline{V}^2 + c_4\overline{W}^2 + d_4\overline{UV} + e_4\overline{UW} + f_4\overline{VW}) +$$

$$+ (2a_4\overline{U}u + 2b_4\overline{V}v + 2c_4\overline{W}w + d_4(\overline{U}v+\overline{V}u) + e_4(\overline{U}w+\overline{W}u) + f_4(\overline{V}w+\overline{W}v)$$

$$+ (a_4u^2 + b_4v^2 + c_4w^2 + d_4uv + c_4uw + d_4uv + c_4uw + f_4vw)]^{1/2}$$

$$= (\overline{Q} + q)_1 \tag{15}$$

which can be written (collecting terms from Eq. 15 such that A_1 contains $\overline{VW}$ terms, B_1 contains terms as $\overline{V}u$, and C_1 contains uv terms):

$$\overline{Q}_1 + q_1 = [A_1 + B_1 + C_1]^{1/2} \tag{16}$$

If we assume that $B_1 + C_1 \underline{<<} A_1$, we can linearize Eq. (16) as

$$\overline{Q}_1 + q_1 = A_1^{1/2} [1 + \frac{B_1 + C_1}{2A_1} - \frac{1}{8} \frac{(B_1 + C_1)^2}{A_1} + \ldots] \tag{17}$$

Squaring Eq. (16), time-averaging and neglecting terms of higher order, the resulting expressions for hot-wire sensor 1 in terms of the mean and fluctuating velocity components are

$$\overline{Q}_1^{\,2} = a_4\overline{U}^2 + b_4\overline{V}^2 + c_4\overline{W}^2 + d_4\overline{UV} + e_4\overline{UW} + f_4\overline{VW} \tag{18}$$

$$q_1 = \frac{1}{2A_1^{1/2}} [u(2a_4\overline{U} + d_4\overline{V} + e_4\overline{W}) + v(2b_4\overline{V} + d_4\overline{U} + f_4\overline{W}) +$$

$$+ w(2c_4\overline{W} + e_4\overline{U} + f_4\overline{V})]. \tag{19}$$

$$= \frac{1}{2A_1^{1/2}} (uP_1 + vS_1 + wR_1) \quad (20)$$

where P_1, R_1 and S_1 denote the terms in parentheses in Eq. (19). Simultaneous solution of the three nonlinear algebraic equation like Eq. (18) will directly yield the mean velocity components $\overline{U}, \overline{V}$, and $\overline{W}$. Now, looking at (20) we find that it contains, as constants, the predetermined mean velocities and those of geometry. The variables remaining are the instantaneous fluctuations about the mean. Eq. (20) and the corresponding equations for the other two sensors will again yield three linear equations for the instantaneous turbulence velocities. Thus, the instantaneous details can be recovered in this method also, as was done in Method A. Since the equations for u,v,w are linear in nature, this procedure requires much less computer time (less by an order of 10) than method A, and also ensures absolute convergence. However, it should be reminded that this method involves the process of linearization and is therefore acceptable only for flow situations where the linearization assumption is valid.

2.3 Method C

If we consider Eq. (20) again, square it and time-average, we get

$$\overline{q_1^2} = \frac{1}{4A_1} [\overline{u^2}P_1^2 + \overline{v^2}S_1^2 + \overline{w^2}R_1^2 + 2\overline{uv}\,P_1S_1 + 2\overline{uw}\,P_1R_1 +$$

$$+ 2\overline{vw}\,S_1R_1] \quad (21)$$

Also for the effective shear stresses, the resulting expression is

$$\overline{q_1 q_2} = \frac{1}{4A_1^{1/2} A_2^{1/2}} [\overline{u^2} P_1 P_2 + \overline{v^2} S_1 S_2 + \overline{w^2} R_1 R_2 + \overline{uv}(P_1 S_2 +$$

$$P_2 S_1) + \overline{uw}(P_1 R_2 + P_2 R_1) + \overline{vw}(S_1 R_2 + S_2 R_1)] \qquad (22)$$

Similarly, one can obtain two such equations for each of the other two sensors. There would be a set of six linear algebraic equations with known coefficients, which can be solved once for all, for the six Reynold's stress components $\overline{u^2}$, $\overline{v^2}$, $\overline{w^2}$, $\overline{uv}$, $\overline{vw}$, and $\overline{uw}$ in terms of the corresponding effective components as sensed by the three sensors. This method does not allow the instantaneous u ,v, and w values to be recovered. It is, however, very economical computationally. This procedure is very similar to that used by Gorton and Lakshminarayana (1976), and has been used in the present studies chiefly to provide a comparison with methods A and B. In fact, the linearization assumption implied in this is less restrictive than in the method of Gorton and Lakshminayama.

2.4 Description of the Probe

Two probes were used for the test of the methodology and software. One of these (Probe 1) was developed in house and the other (Probe 2) was a commercial probe, Disa triaxial hot-wire probe. Probe 1 has dimensions and sensor orientation, as shown in Fig. 2a. It can be seen that the ratio of probe diameter to sensor support length is such that significant probe interference may be present. This probe was a first attempt at constructing a 3-wire probe at the Institute. The Disa probe, Fig. 2b, has a much longer sensor support as well as a small head diameter. Sensing elements in the Disa probe sense over the central 1.25 mm, whereas the in-house probe senses over its entire length (approximately 2.1 mm). This is due to the fact that the Disa sensor is a gold plated tungsten wire of 5 micron diameter, with the central portion etched to give a 1.25 mm sensing length. The in-house sensor is a bare platinum-rhodium wire of the same diameter. It is obvious that the spatial resolution of the Disa probe is much better. However, for flow measurement where spatial resolution was not crucial, the in-house probe proved to be quite adequate.

2.5 Signal Processing: Hardware and Software

Each hot-wire sensor of the triaxial probe was operated by a Disa model 55M10 constant temperature anemometer. These instantaneous output voltages from the three anemometers were filtered using a high pass filter of 36 db/octave roll-off, set at 0.1 Hz. The voltage signals were then amplified by 3 Preston SW 8300 amplifiers and sampled at a rate of 50 samples per second for 50 seconds by a Preston GMAD-3 analog to digital converter (with a 3-channel 'sample and hold' front end). The data were stored on disk file on an HP-1000 minicomputer. At the end of the experiment the data were recalled from the disk file and processed to obtain the velocities. A block diagram of the instrumentation is shown in Fig. 3.

The computer program used for data acquisition records the time and date when the samples were taken. This information is used to apply corrections for small drifts in probe calibration caused by temperature changes in the tunnel and probe contamination. This is done by calibrating the probe at the beginning and end of the experiment and applying a simple linear correction to the calibration coefficients with respect to time. The corrected calibration constants are then used to convert the voltages to effective velocities in each case. Time-associated changes in the calibration for the hot-wire anemometry are therefore eliminated.

Double precision arithmetic was used in calculating accumulated sums while computing average values where the numerics were suspected to exceed the single precision register size. This way, round-off and truncation errors were held to a minimum. Any errors still remaining have to be associated with the uncertainties in the overall process (i.e., probe orientation, tunnel speed, ... etc).

2.6 Accuracy of the Software

The stability of the Newton-Raphson algorithm used in Method A depends on the "closeness" of the initial velocity guesses as well as the convergence criteria specified. Tests on the program itself were performed to provide values of accuracy and reliability. In these tests, dummy values for the effective velocities, computed (independently) for a set of known velocities, were input to the program. The resultant velocities output by the program were compared with the correct values. It was found, that, in each case, the algorithm converged to the correct value in approximately 5 iterations with a convergence criterion of one part in one thousand. The initial guess needed to be only of the same order of magnitude as the final converged correct value. In order to make the scheme converge quicker, the equations were analyzed and certain characteristics were noted. The predominant term in the three equations (Eqs. 5), were those that involved the U^2 terms and if the effective velocities were averaged and divided by the sum of the coefficients the resultant velocity was found to be within 2% of the final value. For the other two velocities the relative magnitudes of the effective velocities were noted and the appropriate sign for one of the two could be recovered. The remaining velocity was guessed as the mean of all the velocities in that direction by averaging first the effective velocities and then using that solution as the starting point for the discrete solution in question. Furthermore, a relaxation factor was applied to U such that instabilities were damped. These techniques helped in arriving at the final result for the particular sample set. However, if convergence was not achieved, the set would be discarded and calculation would proceed to the next sample set. This dropout rate would be recorded and later examined to decide whether or not the results should be accepted. Typical dropout rates were .05 per cent.

2.7 Triaxial Hot Wire Probe Calibration

Each sensor of the probe was calibrated at the beginning and end of an experiment. The probe was traversed to the freestream in the wind tunnel with the probe axis aligned with the flow direction. This condition represents a limiting case for the three simultaneous equations, namely the equivalent velocities sensed by each sensor must be equal.

This is true, of course, if the sensors are all symmetrically oriented with respect to the probe axis. A computer program was developed exclusively for probe calibration.

For the hot-wire anemometer, the output voltage across the sensor varies as a function of velocity, this variation being given by the well-known King's law. This law most commonly takes the form

$$E^2 = A + BV^n \tag{23}$$

where n is generally between .45 and .55.

The computer program developed would sample the sensor output at 50 samples per second for 50 seconds. These values were time averaged to obtain E. The calibration was carried out at several wind tunnel velocities. The computer program would fit Eq. (23) to these data by a least square procedure. This method of calibration required a minimum amount of time due to the fact that the three sensors were calibrated simultaneously.

2.8 Validation Tests of Hot Wire Anemometry

Two of the well known two-dimensional flow fields, namely, a flat plate boundary layer and a wake were used to validate the performance of the triple-sensor probe and the related software and hardware. The results obtained by the methods A, B, and C, in each case were compared with those obtained earlier in the same flow with a conventional x-wire probe by Sastry (1981). In the case of the flat plate boundary layer measurements, the triaxial probe results were also compared with the data of Klebannof (1955). In this situation, however, only the in-house probe was tested.

The flat plate used by Sastry (1981) was mounted as in the earlier experiments. Velocity traverses were made in the boundary layer (at -76.3 mm from the leading edge), and in the wake (at 177.8 mm from the trailing edge). Various tests were then performed on the probe and the software to determine uncertainties, accuracies, as well as the sensitivity to errors in orientation of the probes with respect to the flow field. Effect of sample sizes and rates on drop out rates (in Method A) and accuracy was also studied.

Sensor orientation angles were measured to be within $\pm$ 1° in the θ plane and $\pm$ 3° in the ψ plane (see Fig. 1). Effects of uncertainties in probe orientation were estimated by simulating these uncertainties in probe yaw, pitch and roll in the processing algorithm. Values determined from the adjusted geometric inputs deviated from the best known inputs substantially enough (approximately 5 to 10%) to verify the uncertainty ranges and their centers. Sample size and rates were varied also to find an efficient rate and size. The values used by Sastry (1981) were rechecked to see if such rates and sizes were adequate for the three dimensional probe, and were, in fact, found to be so. The convergence criterion specified for the Newton-Raphson scheme was 0.1% of the free-stream velocity, and further constraining (reducing the value) resulted in negligible changes (less than 2%) in the shear stresses (the most sensitive of the results).

2.9 Test Results

It is seen from Fig. 4 that at $y/\delta = .2$ in the boundary layer, the predominant turbulent shear stress $\overline{uv}$ (obtained by Method A) is 25% below the data of Klebanoff (1955), whereas the results obtained by Method C, developed by the authors and very similar to that of Gorton and Lakshimaryana (1976) appear to agree very well with the data of Klebanoff. Intensities u' and v' determined by Method A or C show smaller departures from the data of Klebanoff than in the case of the shear stress $\overline{uv}$ (see Fig. 5). However, the most disturbing observation was that the nonprincipal shear stresses $\overline{uw}$ and $\overline{vw}$ (which should be zero) were found to be as large as the principal component $\overline{uv}$ at some y locations. Results in the wake (shown in Table A1) for the in-house probe were found to be even worse in this regard, even though values for the principal stress $\overline{uv}$, were found to be of proper magnitude and to deviate by less than 20% from those of Sastry (1981).

The Disa triaxial probe 55P91 was traversed only in the wake because of probe support and mounting problems encountered in the boundary layer traverse. Principal shear stress component $\overline{uv}$, shown in Fig. 6 is in good agreement with the previous measurements. However, it was found that even though the nonprincipal stresses had decreased substantially in comparison with the inhouse probe, they are still as high as 30% of $\overline{uv}_{max}$ in the worst case. Also shown for this case is a comparison of the three methods of data reduction presented earlier It is seen that methods A and B agree well with each other and also with the data of Sastry (1981), especially in the evaluation of $\overline{uv}$. On the other hand, the time-averaged method C, while still giving good results for u', v', and w', estimates the shear stresses very poorly (see Figs. 6, 7, 8, 9). Since method B takes about 1/10 the computer time of method A and shows comparable accuracy, it is concluded that this is the most useful procedure for data reduction.

Looking at the spatial resolution of the two probes, Disa 55P91 and the in-house probe, and the corresponding values of the $\overline{vw}$ and $\overline{uw}$ obtained using them provides some insight into the requirements for three-dimensional flow measurement. The in-house probe with a spatial resolution of approximately 5 mm has failed to determine turbulent quantities in the moderately high shear regions. On the other hand, the DISA 55P91 probe with a resolution of 3.2 mm has given better results. It is therefore recommended that a probe of even smaller size (such as the custom made Disa subminiature triaxial probe with a resolution of 1.2 mm) be used in future measurements. It is felt that such a probe is needed to measure $\overline{uw}$ and $\overline{vw}$ to a better level of accuracy.

2.10 Accuracies

An uncertainty of ± .007 meters per second, due to micromanometer error, is inherent in the calibration procedure. Other uncertainties are associated with the software as well as with probe size and orientation. The convergence criteria for velocities in the software is less than .001U. This is the maximum uncertainty associated with software, hence, remaining inaccuracies are best described as being well within the uncertainty associated with geometry. However, in high shear regions, the errors extend beyond this and are due to size and displacement effects. Those errors due to misalignment and sensor angle error are approximately .5%

in the mean velocity components and 5% and 15% for the intensitites and shear stresses respectively. However, because of the finite size, the accuracies are reduced even further. While the probe size effect is not significant on the intensities u', v', w', the estimated values of $\overline{vw}$ and $\overline{uw}$ may be in error by as much as ± 35% of $\overline{uv}_{max}$.

CHAPTER III

DESCRIPTION OF AIRFOIL EXPERIMENTS

In selecting a suitable airfoil for the study, several design requirements had to be satisfied before construction could begin. The test section of the wind tunnel used is octogonal throughout, with a distance of 1.67 m between the flats. This dimension provided the constraint for the span of the airfoil. The requirement of 'infinite' span conditions restricted the maximum chord. By combining these two constraints with the range of velocities possible in the wind tunnel used, the sweep angle, span and chord could be specified.

The profile selected is the NACA 0012 symmetric airfoil - a well studied profile. For the purpose of fabrication the coordinates describing the profile geometry were taken from Abott and Van Doenhoff (1959).

A sweep angle of 30° was chosen, so that a sizeable crossflow component would be present at the trailing edge. The construction of the airfoil is shown in Fig. 10. Blocks of aluminum, milled to size, were secured to a central frame 12.5 mm thick aluminum plate, to form spanwise ribs. A wooden nose cone was attached to the central frame with pressure taps on both sides. Two aluminum sheets (0.75 mm) used as skins, were wrapped around the aluminum blocks on each side of the frame and were feathered to give a nominal trailing edge thickness of 1 mm. Pressure taps of 1.2 mm diameter (totaling 92) were provided on both sides of the airfoil along midspan, and along two off-mid span planes 15 cm away on either side of the midspan plane.

The airfoil was mounted in the wind tunnel with its spanwise direction located 30° from vertical. A false floor and boundary layer fence were used to remove end-wall boundary effects. This provided conditions close to the desired infinite airfoil configuration (see Fig. 11). Tubing and other mounting fixtures were concealed so as not to affect the flow under measurement. Flow visualization studies made, using wool tufts did not indicate any areas of separation or tunnel-wall effects. These tests also showed that the fence had no appreciable effect on the flow and hence was not used during the main experiments.

1. Coordinate System

The coordinate system used is a right handed orthogonal system, the freestream velocity direction corresponding to the x-direction. The y-direction is normal to the airfoil surface and towards the near wall of the tunnel. The z-direction is perpendicular to the tunnel ceiling. This system is shown in Fig. 10 and it should be noted that the sensor's direction cosines are referenced to this system.

Traversing the boundary layer and wake in the y-direction was accomplished by a servo-controlled stepping motor with a range of 20 cm and an accuracy of .025 mm. The traverse is movable in the x-direction for the longitudinal repositioning. A list of traverse stations and their locations are shown in Table 1.

2. Pressure Measurements on the Airfoil

Measurements of static pressure were used to insure that the airfoil was mounted at zero incidence, and more importantly to provide the actual pressure distribution on the airfoil. A total of 92 pressure taps were used for this purpose. In the midplane of measurement, 22 taps were located on each side of the airfoil with additional 11 taps $\pm$ 15 cm from the midplane. These were also located on both sides of the airfoil.

To perform the measurements a 48-port-selecting scani-valve was used in conjunction with an alcohol micromanometer. The micromanometer had an accuracy of .025 mm and was used for monitoring tunnel speed as well as measuring the static pressure.

Static pressure taps on the two sides of the airfoil and directly opposite to each other were used for initial alignment of the airfoil. For a further and more accurate check on alignment complete scans of all the pressure taps were made at a tunnel speed of 21.84 meters per second. The coefficients of pressure, C_p, defined as

$$C_p = \frac{P-P_\infty}{\frac{1}{2}\rho U_\infty^2} \tag{24}$$

are shown in Figs. 12 and 13. It is seen that the static pressure distributions at the three spanwise locations coincide reasonably well. This is an indication that the airfoil can be considered to be nearly 'infinite' in span. However, it should be noted that this test will be pressure, which, according to Bussman and Ulrich (see Schlichting (1974)) is the region where natural transition occurs on an NACA 0012 airfoil. Past experience at the Institute has shown that sand paper strips perform better than trip wires often used for this purpose. With this tripping, the boundary layer on the airfoil was found to be fully turbulent and the Reynolds number based on the momentum thickness at 2.5 cm upstream of the trailing edge was 7280.

5. Experimental Procedure

The wind tunnel was started and allowed to warm up before starting the experiment. Typically, the temperature rise over the duration of an experiment was of the order of 1°C. First, yaw probe traverses were made in the boundary layer and wake. These included profiles on either side of the airfoil to check for symmetry and profiles at spanwise locations 15 cm above and below the midspan plane to check for infinite conditions. These locations are indicated in Table 1, referred to earlier. The yaw probe traverses were followed by traverses of the Disa 55P91 triaxial hot-wire probe in the wake. Location of the wake centerline was inferred from the minimum in the velocity distribution across the wake.

Uncertainty in the velocity measurements is estimated to be 2%. Static pressure is considered to be accurate within 15 - 20% and the flow angle within 0.5°. Hot wire uncertainties are primarily due to errors in probe alignment and resolution. Preset yaw is expected to be less than $\pm 0.5°$ and a preset error in pitch is likely to be less than $\pm 2°$. Inaccuracies in probe manufacturing were of the order of 2° as determined by direct measurement through a steroscope with a graduated reticle. Roll inaccuracies were eliminated through the Disa type mounting that fixed the roll axis to the traversing mechanism. The overall uncertainties in the turbulence measurement were u', v', w': 5%, $\overline{uv}$: 15%, $\overline{vw}$: 30%. The uncertainties in the $\overline{uw}$ were too large to be acceptable. Hence, these data are not discussed in this report. Further miniaturization of the probe is necessary in order to improve these results. Also not used in the discussion are the data on the various triple correlations such as $\overline{u^3}$, $\overline{u^2v}$, etc., since their accuracy has not been established so far. All the data are, however, reported in the Appendix, for the purpose of documentation.

followed by boundary layer traverses in "the midplane" and "off-planes" for this aspect to be further verified.

3. Flow Angle Measurement and Calibration

Magnitude and direction of the velocity vector were determined by a directionally sensitive three-hole yaw probe. This probe of similar type and size to that used by Ramaprian, Patel, and Choi (1978) and was calibrated in a similar manner. However, several changes were made to make the calibration more accurate. The probe was also calibrated to yield the local static pressure, in addition to the magnitude and direction of the velocity. Details of this calibration, including probe dimensions are shown in Fig. 14. The yaw probe outputs were read via a set of three STATHAM pressure transducers, amplified, scanned, digitized and recorded by the HP/1000 computer. The results were averaged over 20 seconds to obtain the mean pressure for each tube. The transducer calibration was repeated several times each day to see if the instrumentation and methodology used ensured repeatability.

4. Experimental Conditions

The experiments were performed at a tunnel velocity of about 22 meters per second corresponding to a trailing edge Reynolds number of approximately 1.36×10^6. To fix transition to turbulence, a boundary layer 'trip' consisting of a strip of 20-grid sandpaper, 15 cm wide and extending over the entire span, was glued to the surface on both sides of the airfoil at a distance of 20 cm from the leading edge. The location of the sand paper corresponds roughly to the region of lowest

CHAPTER IV

RESULTS AND DISCUSSION

1. General

The results of the experiments are presented and discussed in this chapter. A complete set of tabulated experimental data is provided in Appendix A.

2. Mean Flow Measurements

The variation of static pressure across the trailing edge boundary layer and wake is shown in Fig. 15. It is interesting to see that the static pressure varies across the wake and reaches a maximum value at the wake centerline. This trend persists mildly even at the last measuring station in the wake. This observation confirms similar observations made by Sastry (1981) in the developing two-dimensional wake of an airfoil. The static pressure variation across the wake can be viewed as the result of the interaction among the boundary layer, wake and the external inviscid flow. These data should, therefore, provide a good test case for interactive calculation methods.

Figure 16 shows the distributions of the longitudinal velocity component U across the boundary layer in the trailing edge region. Specifically, the velocity profiles at $x/L = -0.220$ and $x/L = -0.014$ are shown. It is seen that these profiles, especially the latter, resemble a typical distribution in a moderate adverse pressure gradient. The profile does not show any evidence of flow separation. The variation of the crossflow angle γ in the boundary layer at the same locations are also shown in Fig. 16. It is seen that the crossflow increases towards the trailing edge. Also, at the trailing edge, the crossflow is strong ($\gamma = 15°$) enough to introduce significant three-dimensional effects into the wake flow. Furthermore, at x/L = - .124, spanwise variations in the boundary layer are seen to be small (see Fig. 17).

Figures 18 and 19 show the distributions across the wake of the chordwise velocity component. A close study of these profiles shows that there is slight asymmetry in the flow. The reason for this is not known. Also, the profile at the last station has been shown only for half of the wake since the traverse could not be extended to cover the other half of the wake at this station. The crossflow angle, (γ) profiles across the wake shown in Fig. 20 exhibit similar properties as the chordwise velocity profiles, namely decay of the crossflow angle and the increase in spread with distance downstream. It is also seen that at the last measuring station, the crossflow is very small, indicating that the mean flow is virtually two-dimensional beyond this point.

3. Integral Parameters

We now define the following integral parameters for the wake:

displacement thickness $$\delta_1 = \int_{-\infty}^{\infty} \left(1 - \frac{U}{U_\infty}\right) dy \qquad (25)$$

momentum thickness $$\theta_{11} = \int_{-\infty}^{\infty} \frac{U}{U_\infty} \left(1 - \frac{U}{U_\infty}\right) dy \qquad (26)$$

momentum thickness $\theta_{21} = \int_{-\infty}^{\infty} \frac{W}{U_\infty} (1 - \frac{U}{U_\infty}) \, dy$ (27)

shape factor $H = \frac{\delta_1}{\theta_{11}}$ (28)

The distributions of these parameters with downstream distance are shown in Figs 19-22. First, Fig. 21 shows the variation of θ_{11}. In this figure the reference length scale used is the momentum thickness θ_f at the far wake, defined as

$\theta_f = \theta_{11}\big|$ at the last measurement location

From Fig. 21 certain aspects concerning the flow may be noted. Clearly, the momentum thickness increases in the boundary layer due to the adverse pressure gradient. There is a small increase in θ_{11} again in the very near wake due to the finite thickness of the trailing edge of the airfoil. Continuing into the wake we see a gradual decrease of θ_{11} brought about by the combined contributions from the favorable longitudinal pressure gradient and the rotation of the velocity vector towards the streamwise direction. The effect of the gradual weakening of three-dimensionality in the flow is also seen from Fig. 22 which shows that the momentum deficit thickness θ_{21} decreases nearly to zero at the last station. Unfortunately, measurements could not continue beyond x/L = 1.928. It is assumed that the flow will be two-dimensional beyond this distance and hence θ_{11} will remain constant at its value θ_f at the last station. This value is, therefore, used as the reference length scale in the rest of the figures.

Figure 23 shows the variation of the displacement thickness along the streamwise direction. The initial increase in the boundary layer is caused again by the adverse pressure gradient in the trailing edge region. Subsequent reduction in δ_1 is primarily due to the evolution of the wake-like profile from the original boundary-layer-like profile. This trend is, of course, also influenced by factors such as the prevailing favorable pressure gradient and gradual decay of three-dimensionality. The changes in profile shape are more clearly seen from Fig. 24, which shows the variation of the shape factor H with θ_f. It is seen that the shape factor, at the trailing edge, has a value of about 1.5, indicating that the boundary layer is only under a moderate adverse pressure gradient. The shape factor is seen to drop quickly and at x/θ_f = 326, is only slightly greater than 1, its asymptotic value at very large distances.

4. Growth and Decay of the Velocity Defect and Wake Width

The decay of the maximum longitudinal velocity defect w_{xo} is shown in Fig. 25 in the usual coordinates used for two-dimensional wakes. The distance downstream is normalized with θ_f. Also shown in the figure is the asymptotic decay law [See Sastry (1981)].

$$\left(\frac{U_\infty}{w_{xo}}\right)^2 = .4\left(\frac{x}{\theta_f}\right) \qquad (29)$$

for two-dimensional far-wake. The data seem to indicate that the decay rate approaches this law near the farthest downstream station (x/θ_f = 326). Likewise, Fig. 26 shows the half-width of the wake again plotted in the usual two-dimensional coordinates. The theoretical two-dimensional far-wake behavior given by [Sastry (1981)].

$$\left(\frac{b_x}{\theta_f}\right)^2 = .355\ (x/\theta_f) \tag{30}$$

is also shown in the figure. The wake width does not show any clear signs of approach to two-dimensional far-wake state, though changes in slope qualitatively resemble two-dimensional flow results. In Figure 25, if the dotted line can be assumed to represent the decay process at large distances, it intersects the x-axis, at a virtual origin corresponding to $x/\theta_f = 70$. If, this point is joined to the last data point in Fig. 26 the line is approximately parallel to the asymptotic growth line. This is a very rough indication that the wake has perhaps reached very nearly the two-dimensional far-wake state at $x/\theta_f = 326$. This observation is in conformity with the findings of Sastry (1981), who inferred that the two-dimensional wake behind a flat plate reaches an asymptotic state around $x/\theta_f = 350$. The present data, are inadequate to confirm this definitively. More closely spaced data as well as data extending further downstream are needed to substantiate the present observations.

Figures 27 and 28 show the corresponding decay and growth rates of parameters w_{zo} and b_z, the maximum defect velocity in the z-direction and half-width of this profile. The velocity defect in this case is normalized by $U_\infty \sin\phi$ (where ϕ is the sweep angle), since this is the maximum value that w_z can attain. It is seen that the crossflow defect velocity decays very rapidly compared to the longitudinal velocity. The wake half-width behaves qualitatively like b_x but is seen to be much larger.

5. Self Similar Velocity Profiles

The velocity data plotted in the conventional self-similar coordinates are shown in Figs. 29 and 30. In Fig. 29 showing the streamwise velocities, it is seen that beyond $x/L = 0.138$ ($x/\theta_f = 23.4$) the profiles become very nearly self-similar and that the profiles follow closely the profile for asymptotic two-dimensional far-wakes. The spanwise velocity profiles shown in Fig. 30 also appear to approach self-similarity. Compared to the w_{xo} profile, however, the half-width of this self-similar profile is approximately 25% larger.

6. Turbulent Stress Measurement

The turbulence quantities measured using the three-dimensional hot wire probe can be analyzed in different ways. First of all, the three intensities u', v', w' and the three shear stresses $\overline{uv}$, $\overline{uw}$ and $\overline{vw}$ are normalized with respect to the freestream velocity so tha. general trends may be observed. These results are shown in Figs. 31 thru 36. In general, the intensities are of similar magnitude and behave in a similar way. This indicates that the turbulence is not too far from isotropy. Furthermore, in Figs. 31, 32, and 33 it is seen that the profiles exhibit a minimum in the center and are fairly symmetric about the wake centerline. The shear stresses $\overline{uv}$, $\overline{vw}$ and $\overline{uw}$ are shown in Figs. 34, 35 and 36. It is seen that $\overline{uv}$ and $\overline{vw}$ are nearly anti-symmetric about the wake centerline changing sign as expected. In contrast, however $\overline{uw}$ measurements are considerably in error. This stress has almost the same magnitude as $\overline{vw}$. This trend is similar to that observed during the validation tests in the flat plate wake mentioned earlier. The ratio of $\overline{vw}$ to $\overline{uv}$ is shown in

Fig. 37. This ratio is a good measure of the three-dimensionality of the shear flow field. It is seen that at the last station (x/θ_f = 326), $\overline{vw}$ is of the order of 15% of $\overline{uw}$, indicating the near two-dimensionality of the flow field. Next, the decay rates for u'_{max} $\overline{uv}_{max}$ and $\overline{vw}_{max}$ are shown in Fig. 38. The centerline turbulent intensity is seen to increase continuously with distance downstream. The normalized Reynolds shear stress $\frac{\overline{uv}_{max}}{w_{xo}^2}$ is also increasing, but at the last measuring station its value is only slightly higher than the value of 0.48 for the asymptotic two-dimensional far-wake (Sastry 1981). The shear stress $\frac{\overline{vw}_{max}}{w_{zo}^2}$ on the other hand is found to be slowly decreasing at large values of x/θ_f. It is difficult to predict from the present measurements whether it would continue to decrease or reach an asymptotic value farther downstream. The development of $\overline{uv}_{max}$ is faster than in the case of the flat plate wake of Sastry or Pot (1979), but otherwise qualitatively similar in that it approaches the asymptotic value from "below". This is in contrast with the behavior of either the wake behind a cylinder or that behind a two-dimensional airfoil at incidence [Sastry (1981)]. In both these cases, $\overline{uv}_{max}$ decreases to the asymptotic value from 'above". The trends in all these cases are consistent with the relative influence of the wall on the velocity profile just before the flow detaches from the wake generator.

7. Self Preservation of the Turbulence Profiles

Figures 39-41 show the profiles of u', $\overline{uv}$ and $\overline{vw}$ in self preserving coordinates. It is seen that the profiles are evolving continuously.

It appears that the turbulence properties have not attained self-similarity even at the last location. However, since $\overline{uv}_{max}$ at x/θ_f = 326 is nearly equal to the asymptotic value, further data in the far wake are needed to determine whether the turbulence profiles indeed have attained the asymptotic self-preserving form.

8. Eddy Viscosity Results

The present data can be used to calculate the eddy viscosity in both x and z directions defined by

$$\varepsilon_x = \frac{\overline{uv}}{\partial U/\partial y} \tag{31}$$

and

$$\varepsilon_z = \frac{\overline{vw}}{\partial W/\partial y} \tag{32}$$

Plots in self-preserving coordinates of both ε_x and ε_z are shown in Figs. 42 and 43. From this it is seen that both viscosities are evolving continuously. The eddy viscosity in the z direction exhibits considerable scatter, but is still of similar magnitude as ε_x. As to whether or not the flow has reached asymptotic behavior it is difficult to confirm because of the lack of adequate data points between x/θ_f = 180 and 326. However, the value of ε_x obtained from the present experiments can be compared with the asymptotic values given by Schlichting (1979) and Sastry (1981). At x/θ_f = 326 the present value for $\varepsilon_x/U_\infty\theta_f$ is .039. This compares with .032 quoted by Sastry and a value of .044 by

Schlichting. Therefore, it seems reasonable to say that at $x/\theta_f = 326$ the streamwise flow is sufficiently close to the two-dimensional far-wake.

If we now assume an average eddy viscosity from Figs. 42 and 43 for each x/L location, we should in turn be able to recalculate the stresses. Typical results for $\overline{uv}$ and $\overline{vw}$ are shown in Figs. 44-47. These figures allow us to compare the extent to which it is realistic to use a constant eddy viscosity model to describe the shear stress in the wake. For the shear stress $\overline{uv}$ it is seen that the agreement with experiment is good. The plots for $\overline{vw}$ show the difference in result obtained by using ε_z or ε_x (scalar eddy viscosity assumption). Average values of the viscosity for the given x-location were used in each case. The comparison (considering experimental scatter) shows little difference and hence we conclude, that for calculation purposes, ε_x can be used as a scalar eddy viscosity at least for mild crossflows.

9. The Structure Parameter

Nash proposed for three-dimensional turbulent shear flow, the following relations (see Nash and Patel 1972):

$$|\overline{uv}| = a\, \overline{q}^2 \frac{\partial U/\partial y}{\left[\left(\frac{\partial U}{\partial y}\right)^2 + \left(\frac{\partial W}{\partial y}\right)^2\right]^{1/2}} \tag{33}$$

$$|\overline{vw}| = a\, \overline{q}^2 \left(\frac{\partial \overline{W}}{\partial y}\right) / \left[\left(\frac{\partial \overline{U}}{\partial y}\right)^2 + \left(\frac{\partial \overline{W}}{\partial y}\right)^2\right]^{1/2} \tag{34}$$

where $q^2 = (u'^2 + v'^2 + w'^2)/2$ and "a" is often called the structure parameter. For two-dimensional flows, the proposal takes the form

$$|\overline{uv}| = a\ \overline{q^2} \tag{35}$$

Results of calculating 'a' from Eq. (34) are shown in Fig. 48. It is seen that except near the centerline and in the outer intermittent region, 'a' has a nearly constant value. Typical comparisons of the value of 'a' obtained using the alternate definitions Eq. (34) and Eq. (35) (three-dimensional and two-dimensional definitions) are shown in Fig. 49. It is seen that two-dimensional definition is adequate to evaluate 'a' in this mildly three-dimensional flow. Again, to assess the validity of the model for practical use in three-dimensional flows an average value for a (= .15) was used in Eq. (34) to calculate $\overline{vw}$ for a few near-wake locations. These results are compared with measurements in Fig. 50. The agreement is seen to be moderate considering the uncertainties in measurement. Therefore, it can be concluded that the structure parameter model in the form of Eqs. (33) and (34) is reasonably satisfactory for describing dimensional wakes.

10. Conclusions

The following conclusions can be arrived at from the study reported in this thesis.

1. A triaxial hot-wire probe can be used, with one of the techniques developed in the present study, for turbulence measurements in three-dimensional shear flows. The accuracy of such measurements,

critically depends on probe orientation, probe size and correct knowledge of sensor angles.

2. The present techniques A and B are superior to that used by Gorton and Lakshminarayana (1976) both in accuracy and versatility.

3. At present, the measurement of $\overline{uw}$ is unsatisfactory. Further miniaturization of probe is necessary to get better results.

4. The study of the developing three-dimensional wake behind an infinite swept airfoil shows that the static pressure varies across the near-wake with the maximum occurring at the wake centerline.

5. The longitudinal and crossflow wake defect components reach near self-similar distributions within about 10 momentum thicknesses downstream of the trailing edge.

6. Three-dimensionality of the flow becomes negligible within about 325 momentum thicknesses. Also, at this distance, the wake begins to exhibit many of the mean and turbulent flow properties of two-dimensional far-wakes.

7. A scalar eddy viscosity, constant across the wake, can be used to describe both the shear stress components $\overline{uv}$ and $\overline{vw}$ reasonably well.

8. The turbulence in the wake exhibits structural similarity in the manner proposed by Nash.

REFERENCES

Abbott, I.H. and Von Doenhoff, A.E., 1959 "Theory of Wing Sections," Dover Publications, Inc., New York, N.Y., USA.

Andreopoulos, J. and Bradshaw, P., 1980 "Measurement of Interacting Turbulent Shear Layers in the Near Wake of a Flat Plate," J. Fluid Mech., 100, 639-668.

Chevray, R. and Kovasznay, L.S.G., 1969 "Turbulence Measurements in the Wake of a Thin Flat Plate," AIAA J. 7, 1641-1643.

Cousteix, J. and Pailhaus, G., 1980 "Measurements of Mean Velocity and Reynolds Stress Tensor within a Wake of a Swept Wing," CERT, Rapport Technique OA 41/2259 AYD.

Elsenaar, A. and Boelsma, S.H., 1974 "Measurements of the Reynolds Stress Tensor in a Three-Dimensional Turbulent Boundary Layer," NLR, TR 74095 U.

Friehe, C.A., and Schwarz, W.H., 1968 "Deviations from the Cosine Law for Yawed Cylindrical Anemometer Sensors," Trans. ASME, Series E, Vol. 35, p. 655.

Gorton, C.A. and Lakshminarayana, B., 1976 "A Method of Measuring the Three-Dimensional Mean Flow and Turbulence Quantities Inside a Rotating Turbo-Machinery Passage," Engineering for Power, 98, 2, 137-146.

Klebanoff, P.S., 1955 "Characteristics of Turbulence in a Boundary Layer with Zero Pressure Gradient," NACA Rep. 1247.

Nash, J.F. and Patel, V.C., 1972 "Three-Dimensional Turbulent Boundary Layers," SBC Technical Books, Sybucon Inc., Atlanta, Ga., USA.

Pot, P.J. 1979 "Measurements in a 2-D Wake and in a 2-D Wake Merging into a Boundary Layer. Data Report. NLR TR-79063 L (Provisional Issue).

Ramaprian, B.R., Patel, V.C. and Choi, D.H., 1981 "Mean-Flow Measurements in the Three-Dimensional Boundary Layer over a Body of Revolution at Incidence," J. Fluid Mech., 103, 479-504.

Sastry, M.S. 1981 "Turbulent Wake Development Behind Streamlined Bodies," Ph.D. Thesis, Dept. of Mechanics and Hydraulics, University of Iowa, Iowa City, Iowa, USA.

Schlichting, H., 1979 "Boundary Layer Theory," McGraw-Hill Book Co., New York, N.Y., USA.

Table 1

Boundary Layer and Wake Traverse Stations

Station #	x/L	x/θ_f
1	-.220	-36.7
2	-.124	-21.0
3	-.014	- 2.37
4	+.014	2.37
5	.027	4.57
6	.041	6.94
7	.055	9.32
8	.138	23.4
9	.275	46.6
10	.399	67.6
11	.661	112.0
12	.992	168.1
13	1.928	326.7

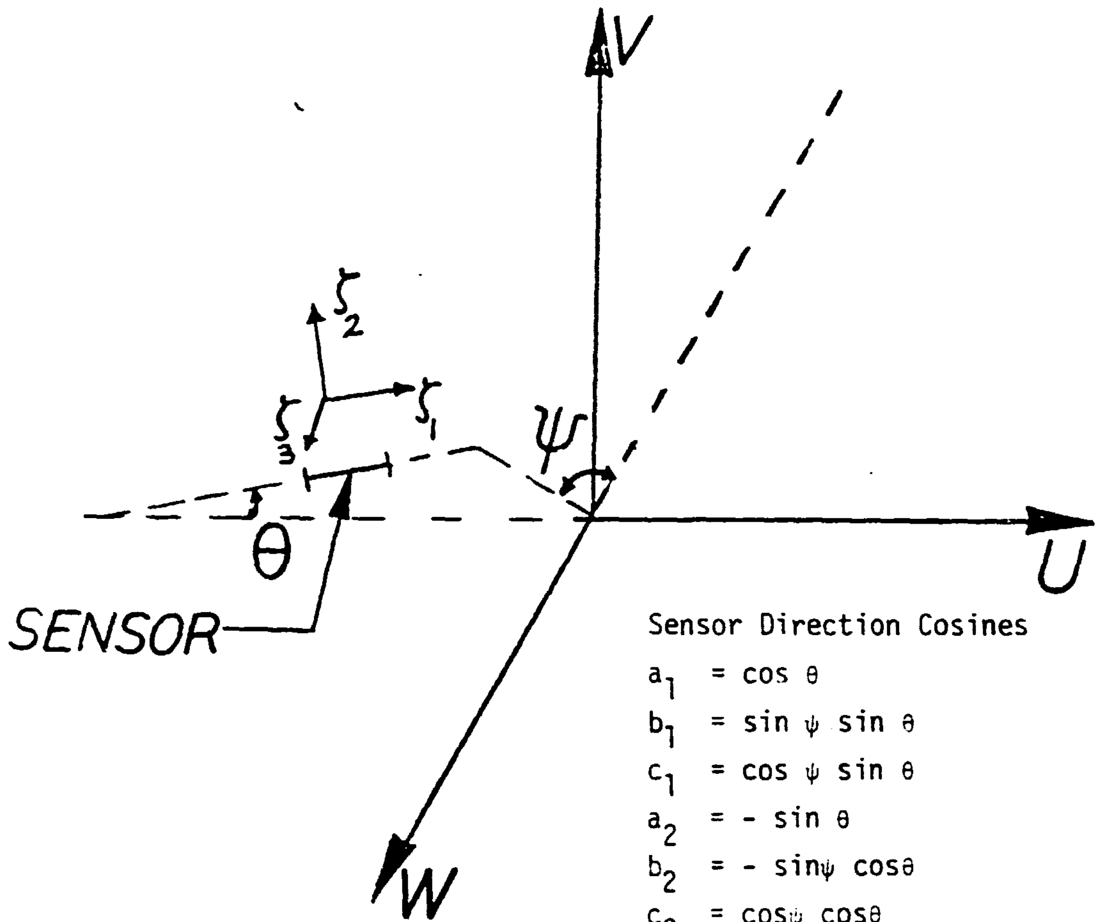

Sensor Direction Cosines

$a_1 = \cos\theta$

$b_1 = \sin\psi \sin\theta$

$c_1 = \cos\psi \sin\theta$

$a_2 = -\sin\theta$

$b_2 = -\sin\psi \cos\theta$

$c_2 = \cos\psi \cos\theta$

$a_3 = 0$

$b_3 = \cos\psi$

$c_3 = \sin\psi$

Figure 1. Sensor coordinate system and sensor direction cosines

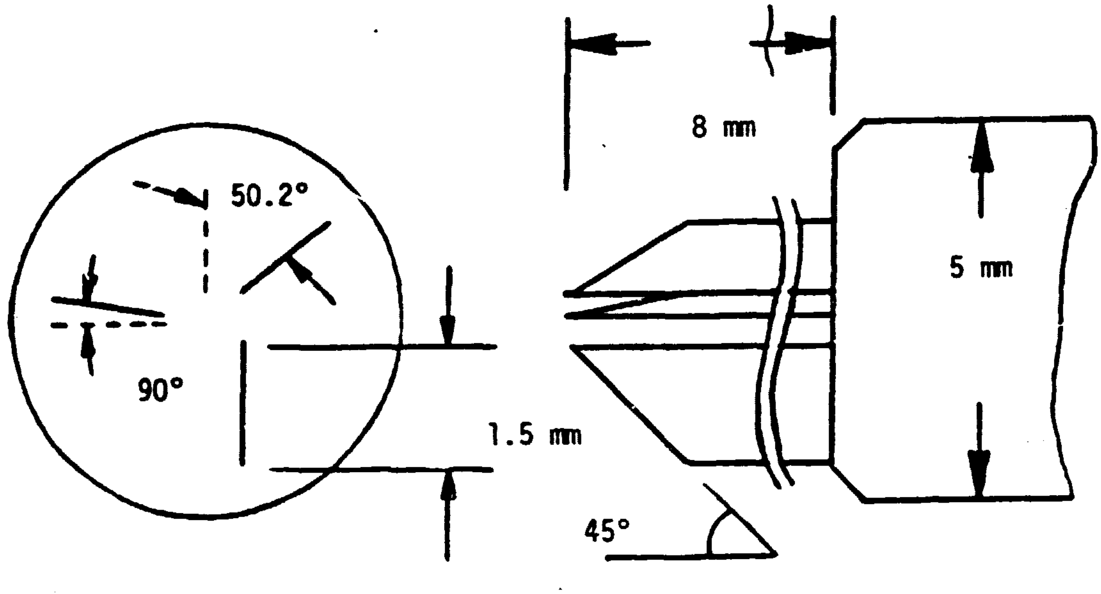

a. IIHR constructed three-dimensional hot-wire probe

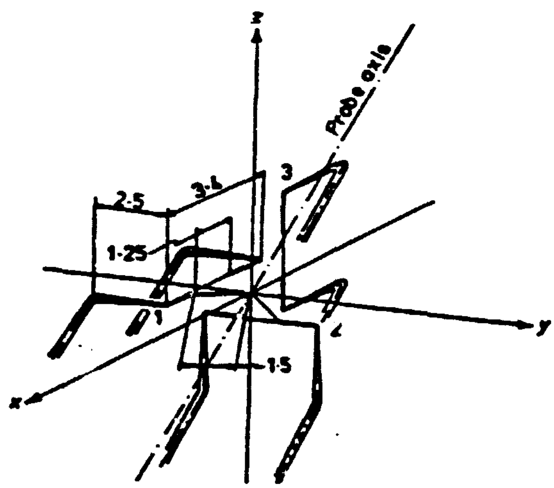

b. Disa 55P91 three-dimensional hot-wire probe

Figure 2. Hot-Wire Probes

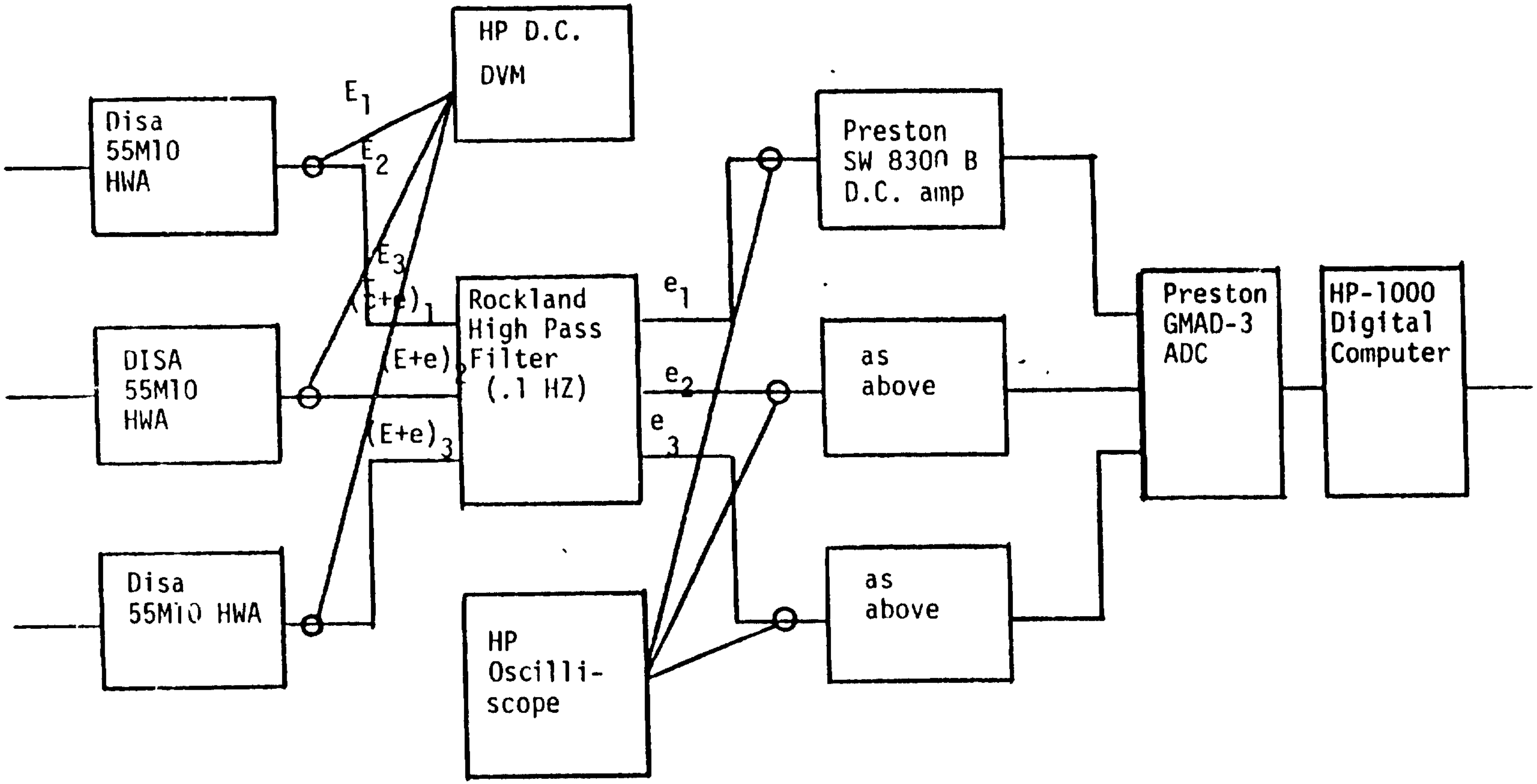

Figure 3. Instrumentation block diagram

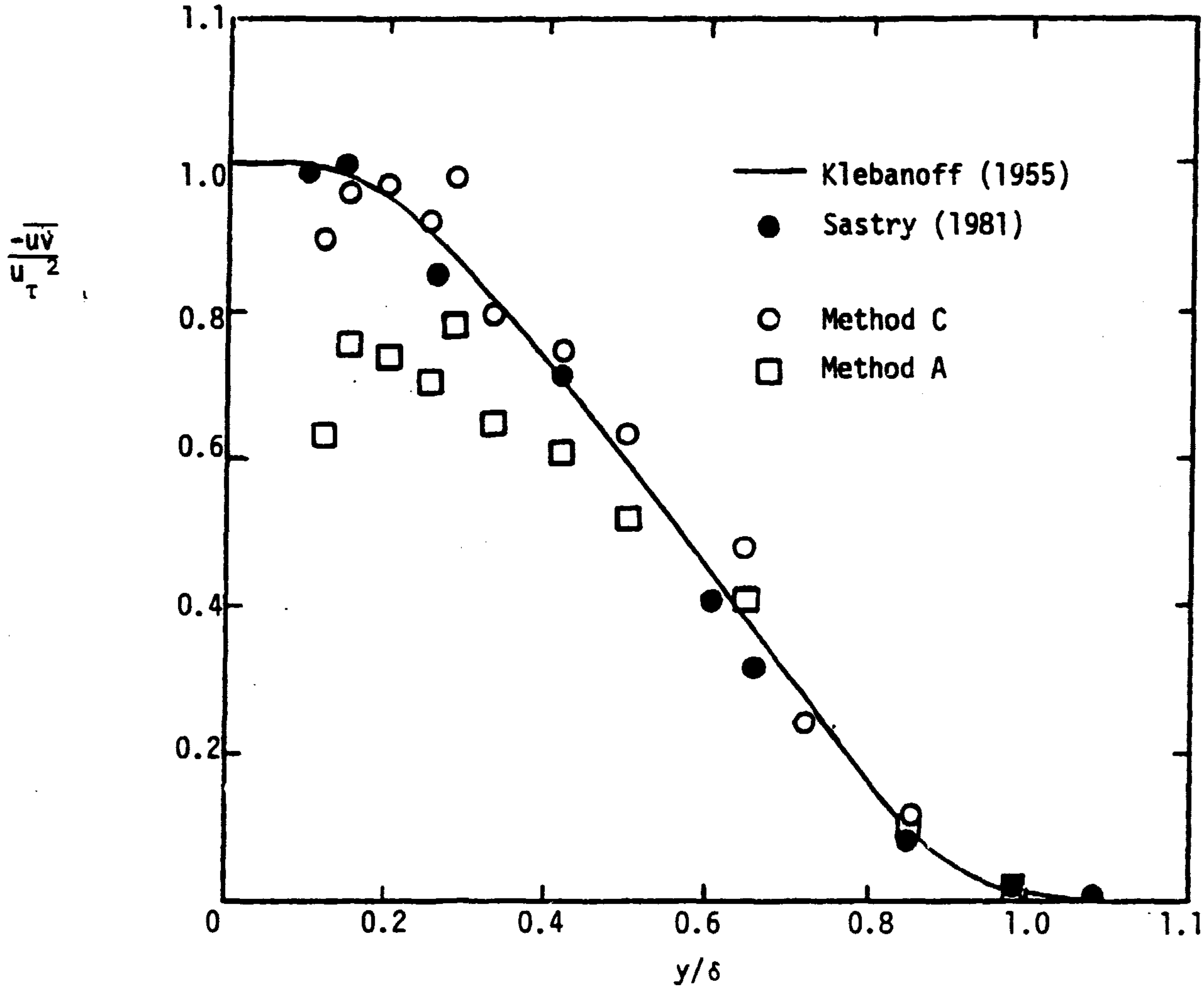

Figure 4. Distribution of $\overline{uv}$ in the flat plate boundary layer at -76.3 mm

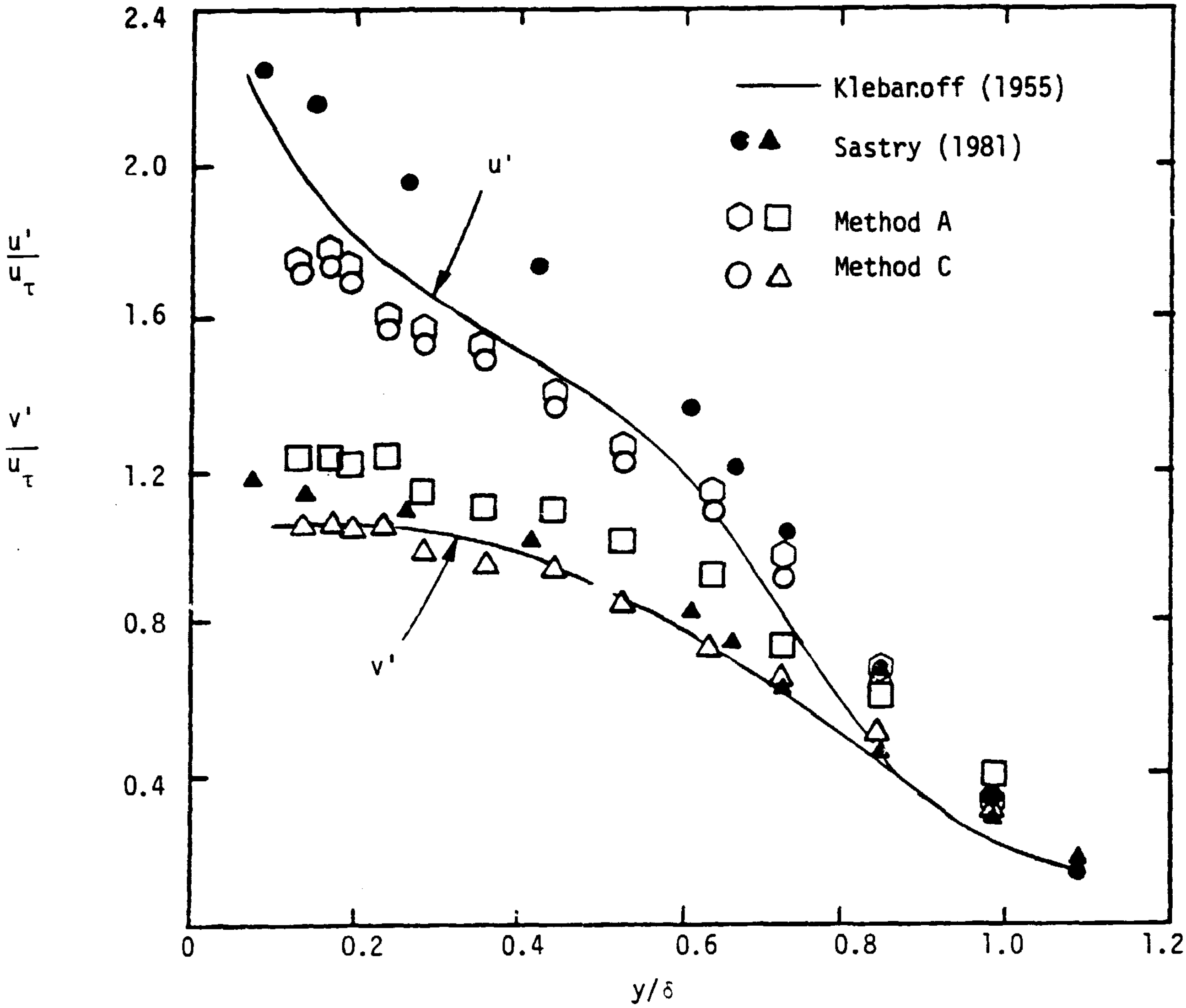

Figure 5. Dist⁻ibution of u' and v' in flat plate boundary layer at -76.3 mm

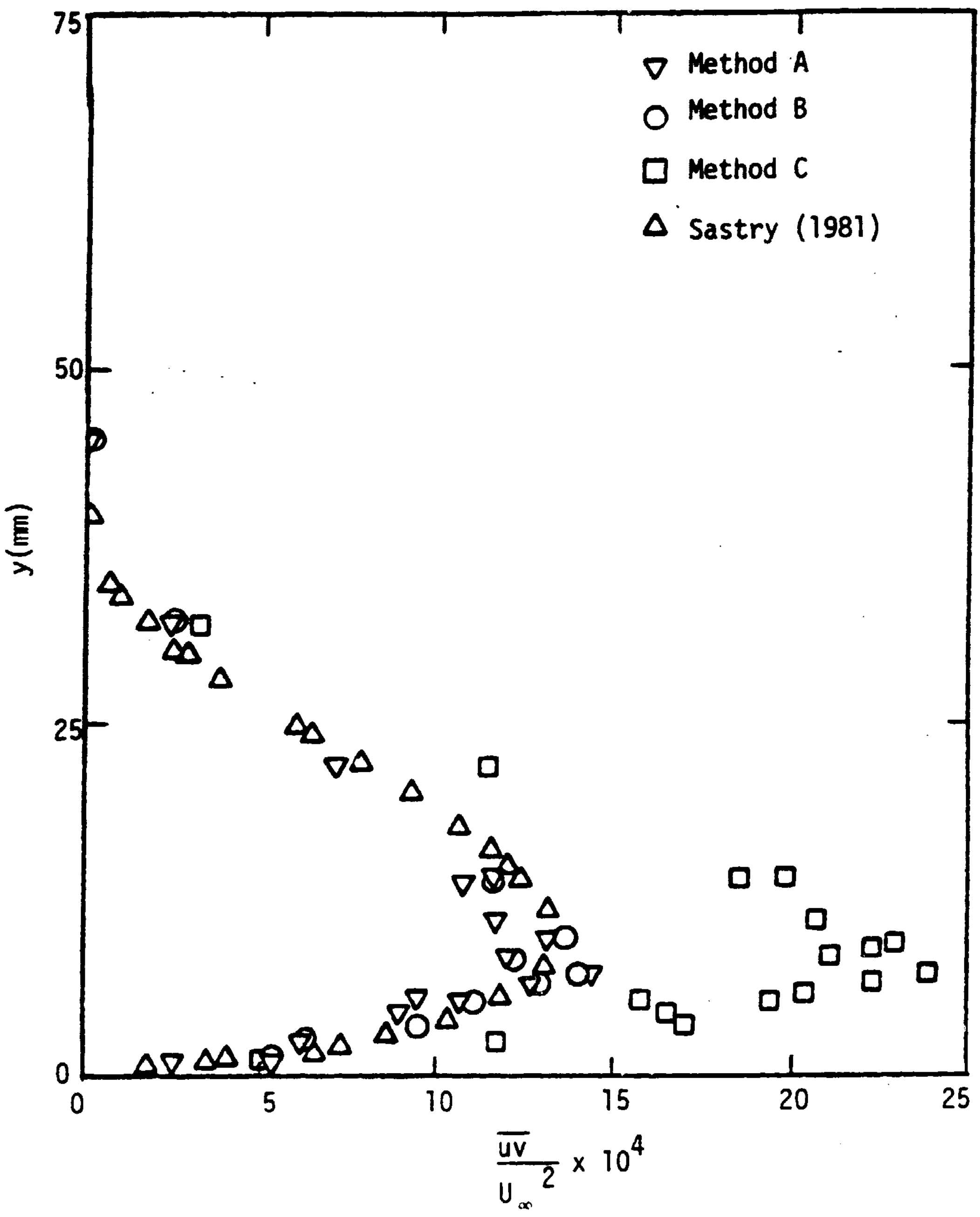

Figure 6. Distribution of $\overline{uv}$ in the flat plate wake at 177.8 mm

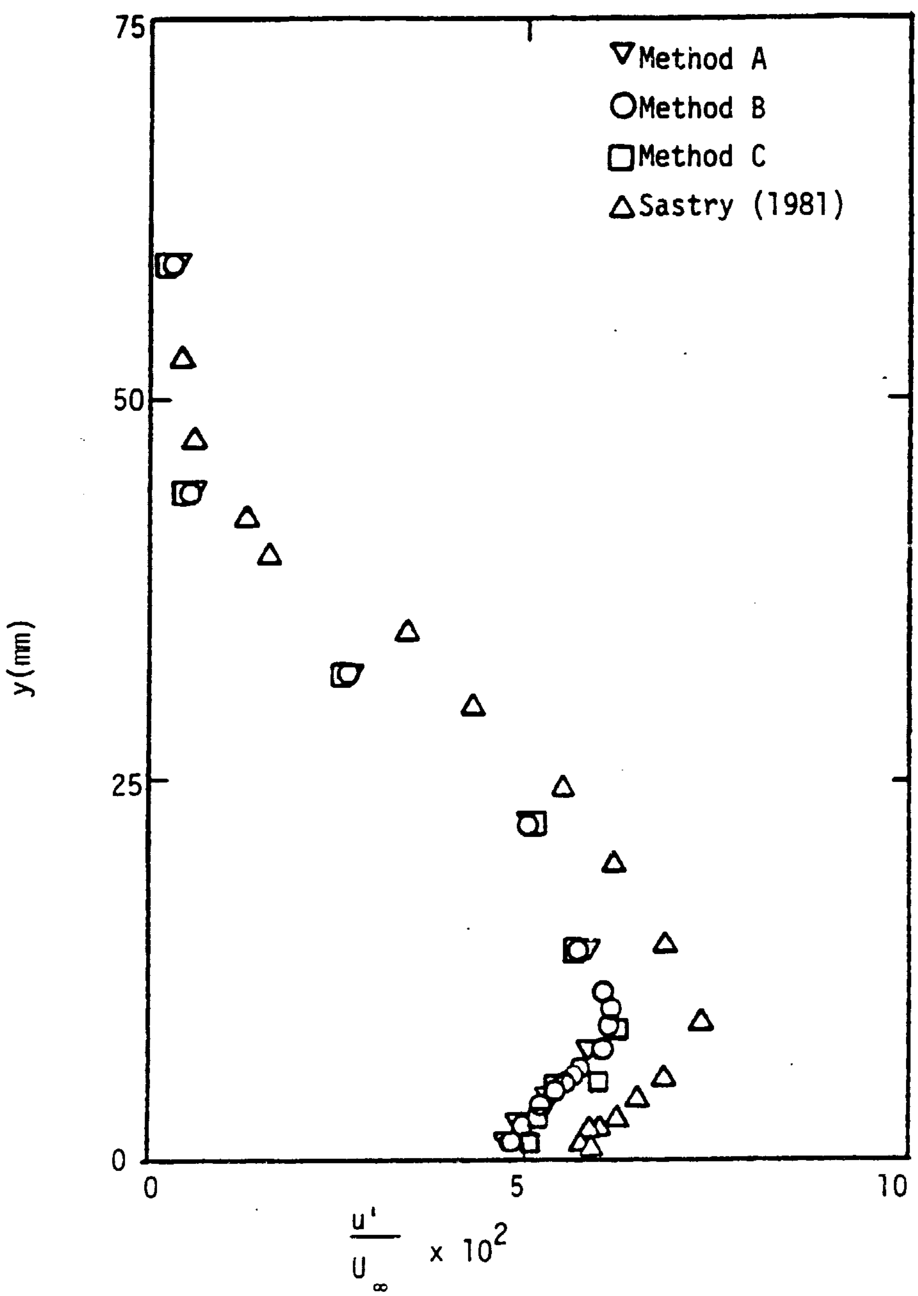

Figure 7. Distribution of u' in the flat plate wake at 177.8 mm

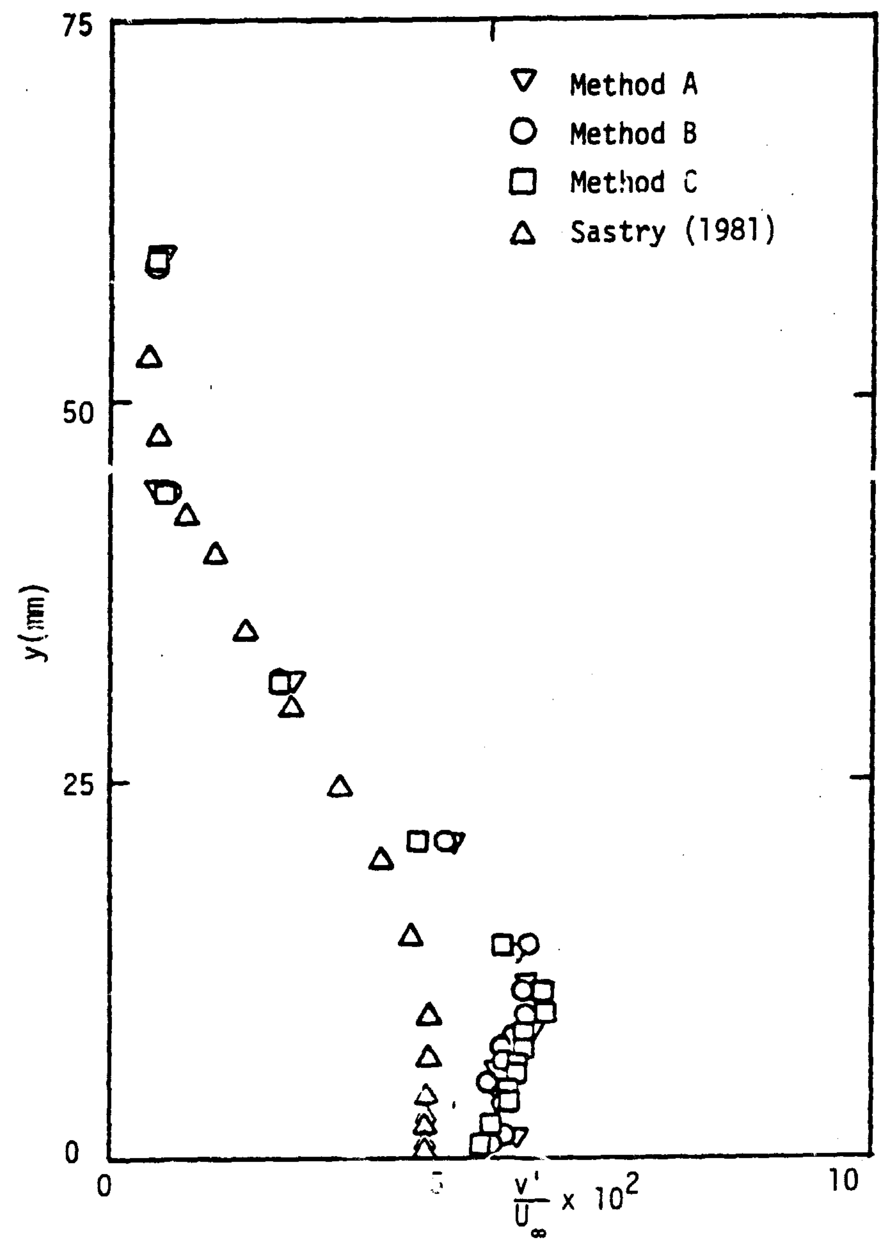

Figure 8. Distribution of v' in the flat plate wake at 177.8 mm

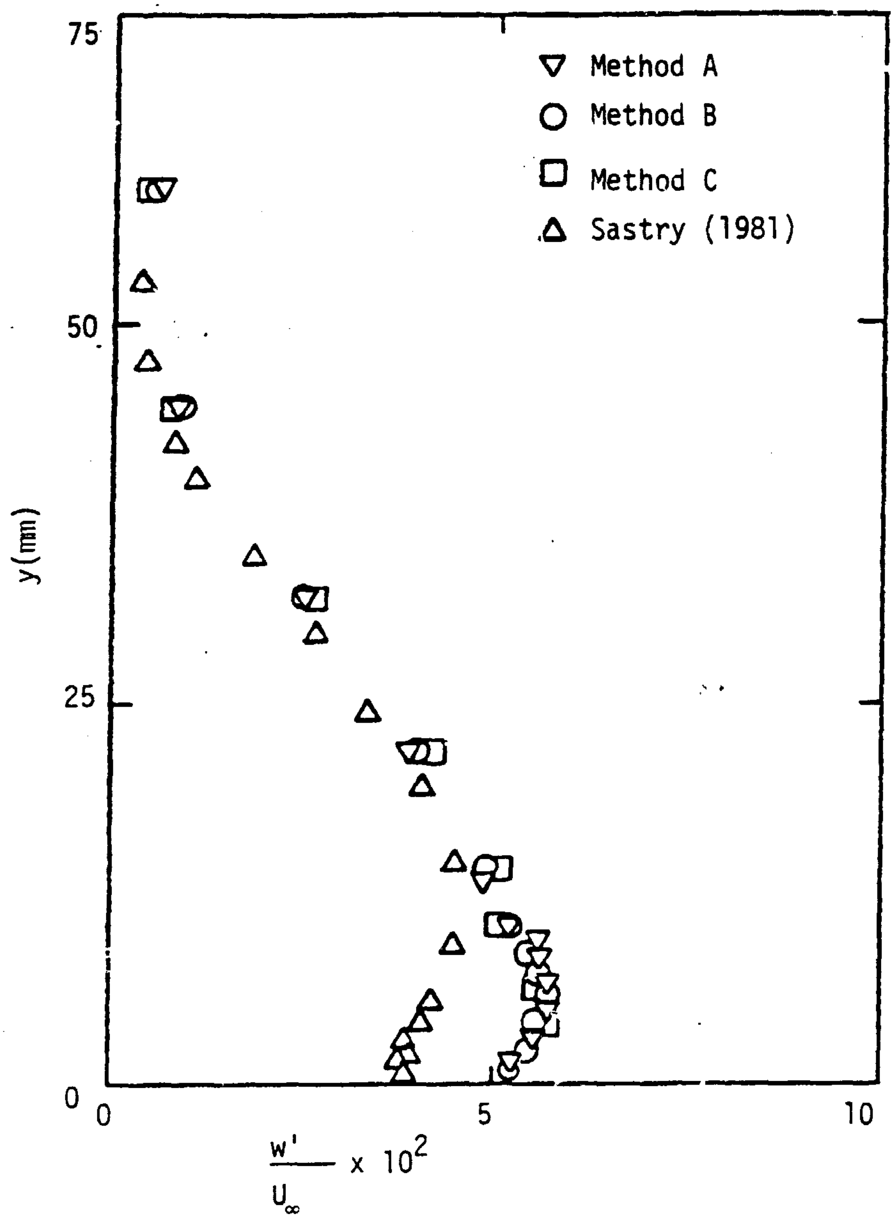

Figure 9. Distribution of w' in the flat plate wake at 177.8 mm

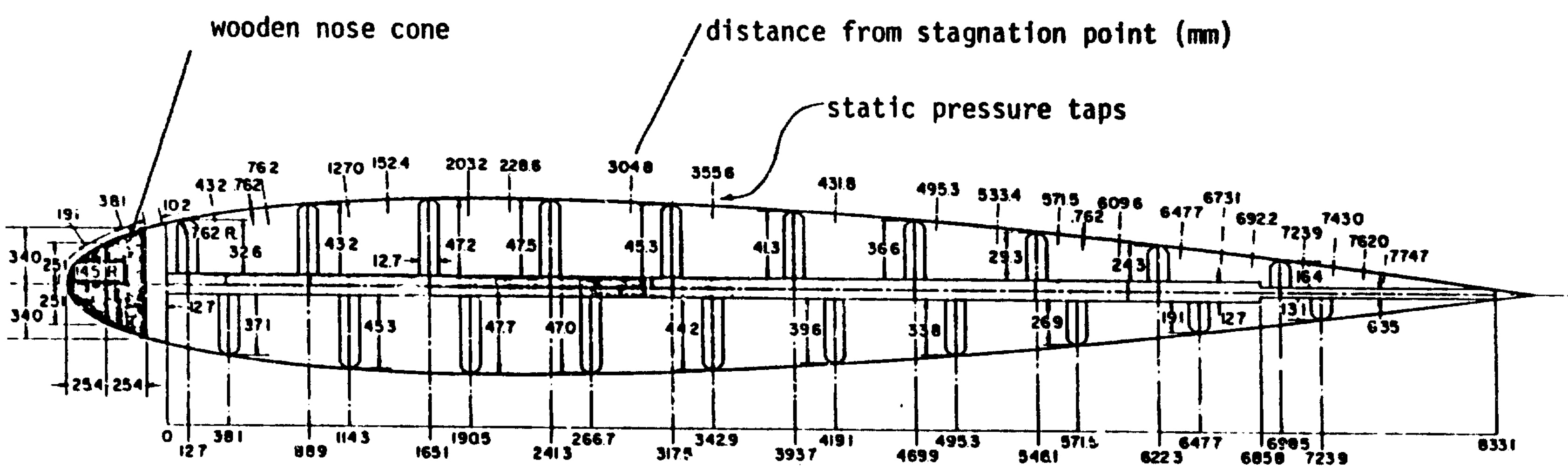

Figure 10. Airfoil cross-section (dimensions in mm)

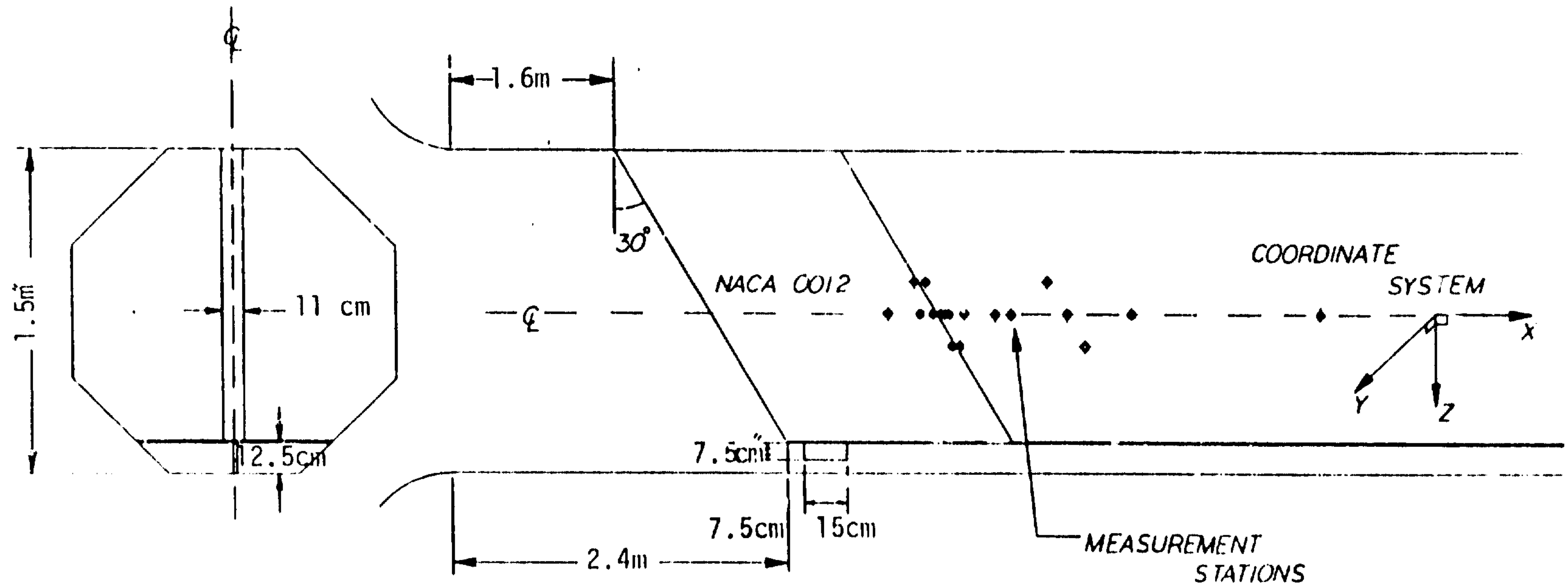

Figure 11. Airfoil in tunnel with measurement station locations

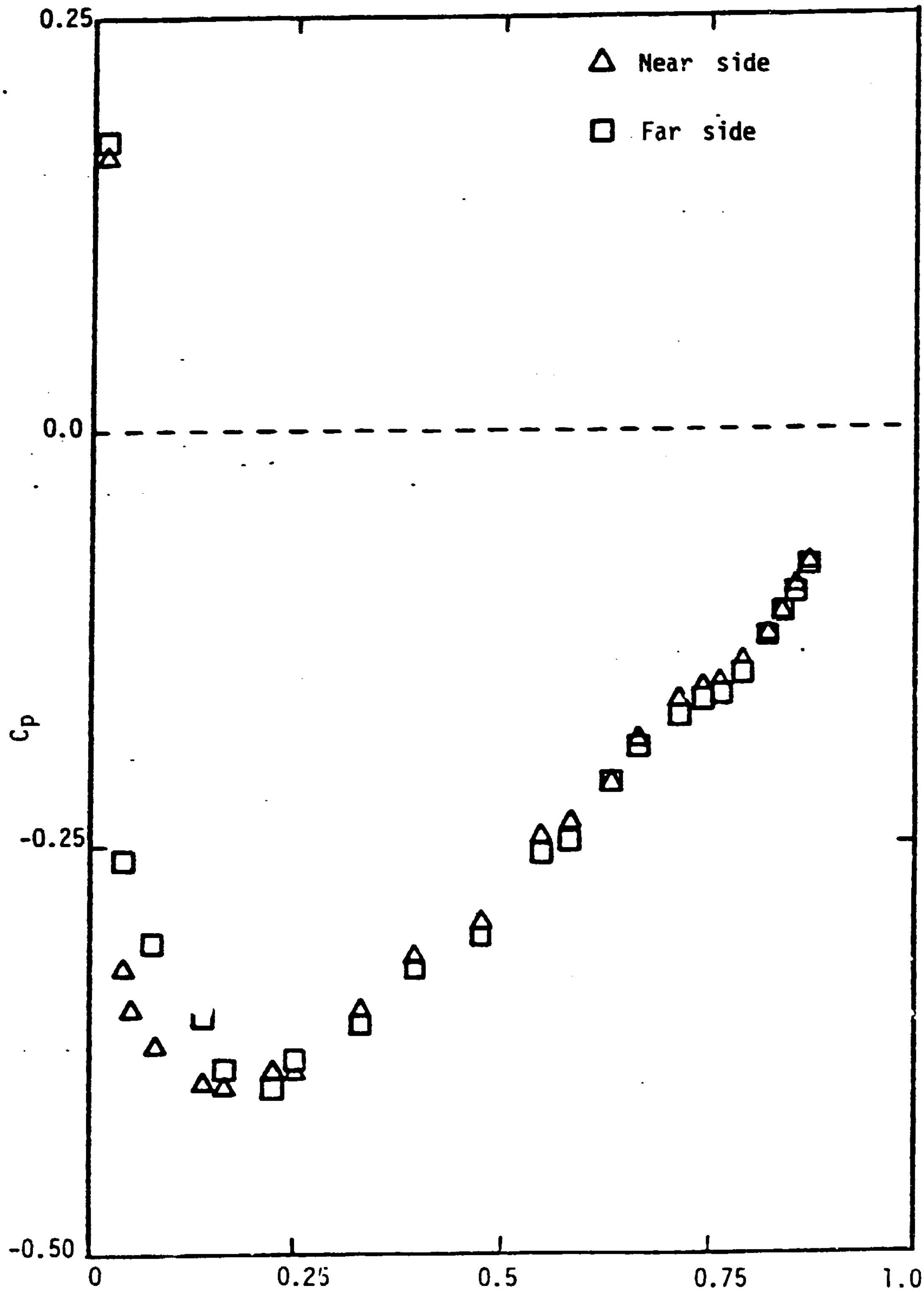

Figure 12. Coefficient of pressure variation on both sides of wing

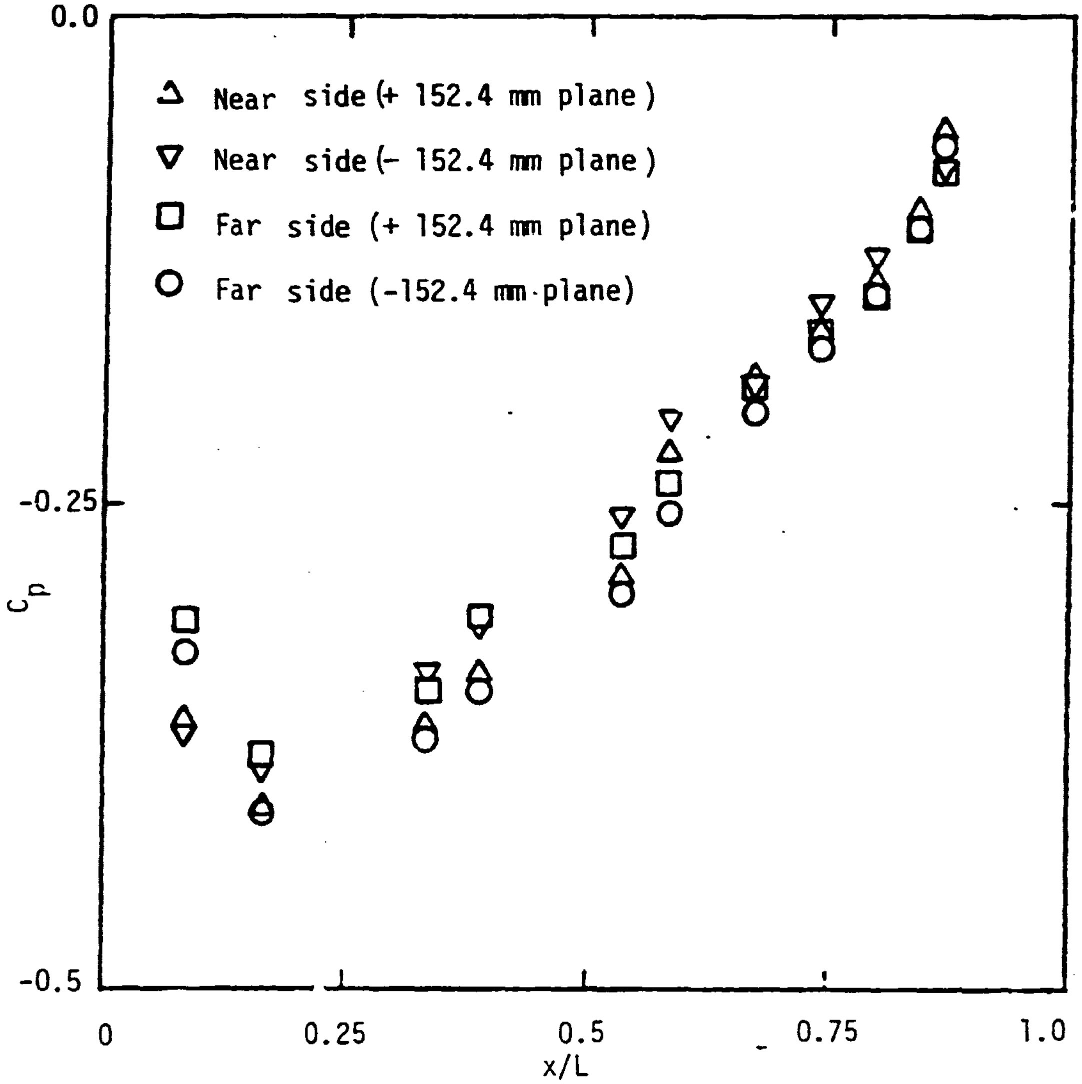

Figure 13. Coefficient of ⌐ressure variation on both sides of wing on a s .nwise basis

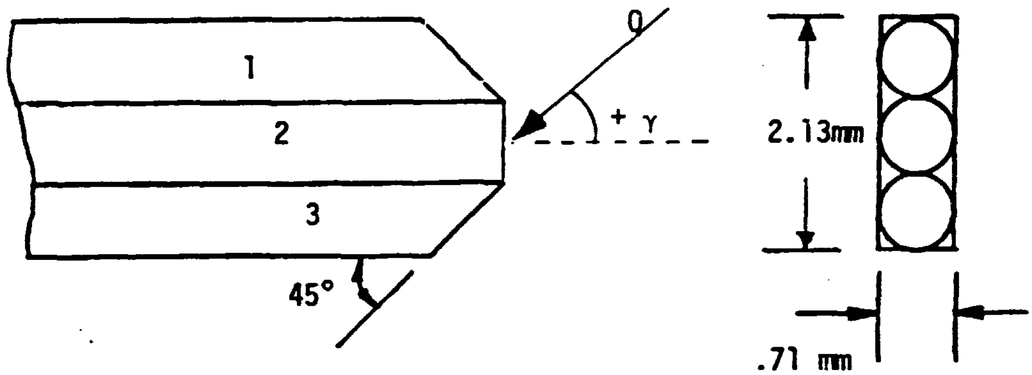

$$AKP = \frac{P_1 - P_3}{P_2 - [\frac{P_1+P_3}{2}]}$$

$$AK23 = P_2 - P_3$$

$$1/2\ \rho Q^2 = AK23/[.51885 + .023779 * \gamma - .0000142 * \gamma^2 - .0000035 * \gamma^3 - .0000001 * \gamma^4]$$

$$\gamma = -1.4345 + 10.28219 * AKP + .04959500 * AKP^2 - .0246590 * AKP^3 - .0148545 * AKP^4$$

$$P_{static} = P_2 - [1.0088296 - .0011767 * \gamma - .0002621\ \gamma^2] * 1/2\ \rho Q^2$$

Figure 14. Yaw probe description and calibration

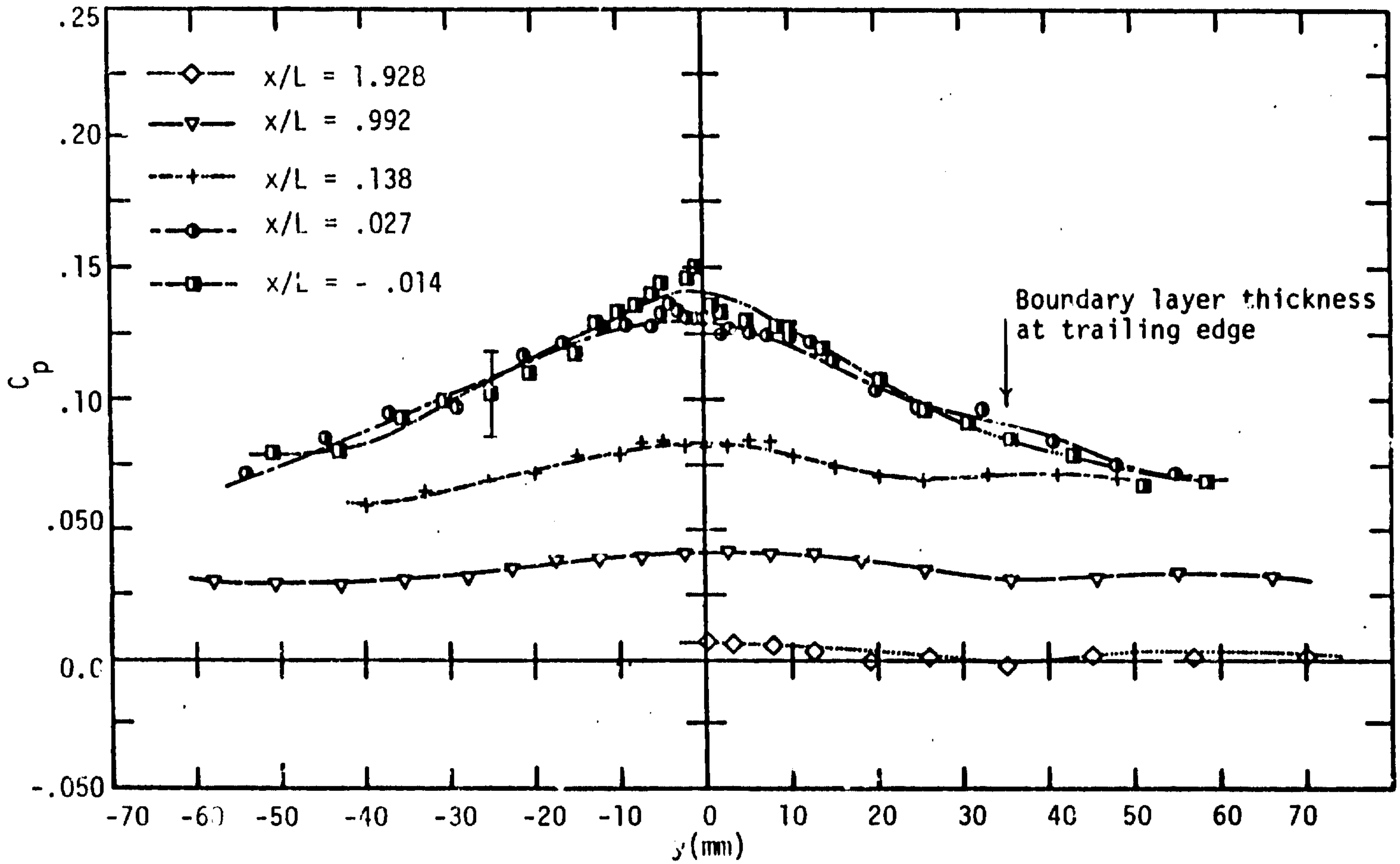

Figure 15. Static pressure variation across trailing edge and wake

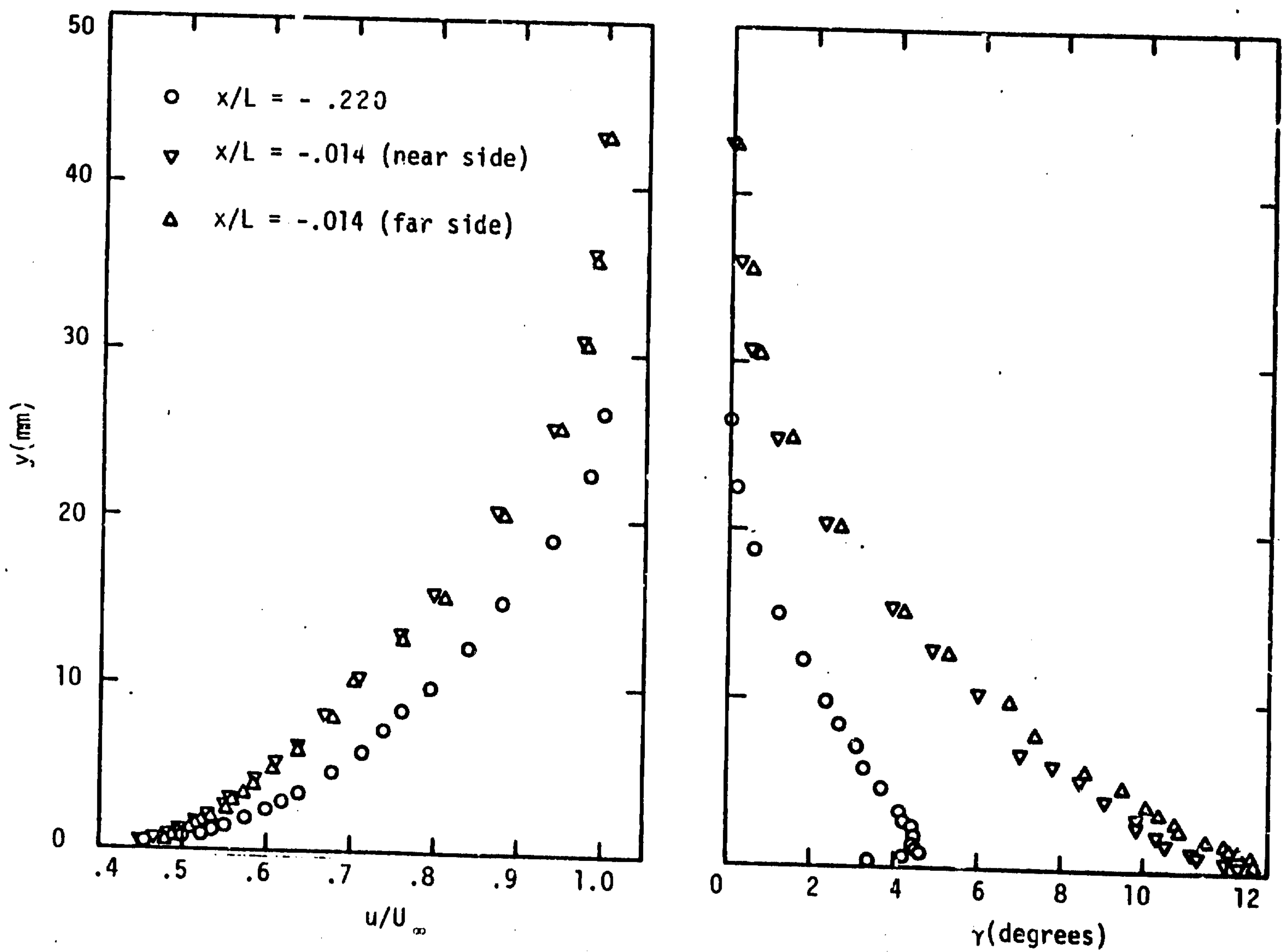

Figure 16. Boundary layer profiles at x/L =-.014 and -.220

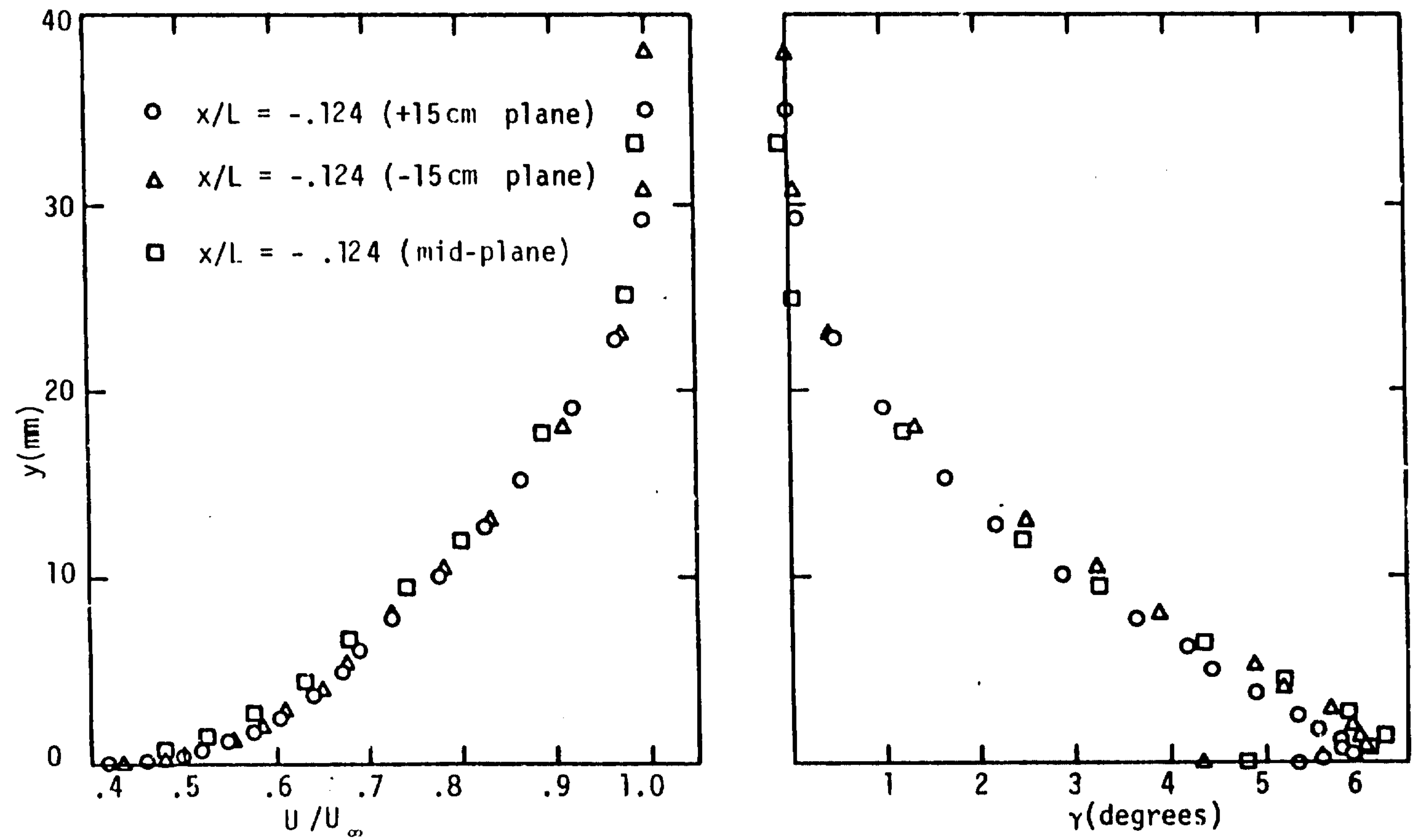

Figure 17. Boundary layer profiles at various spanwise location

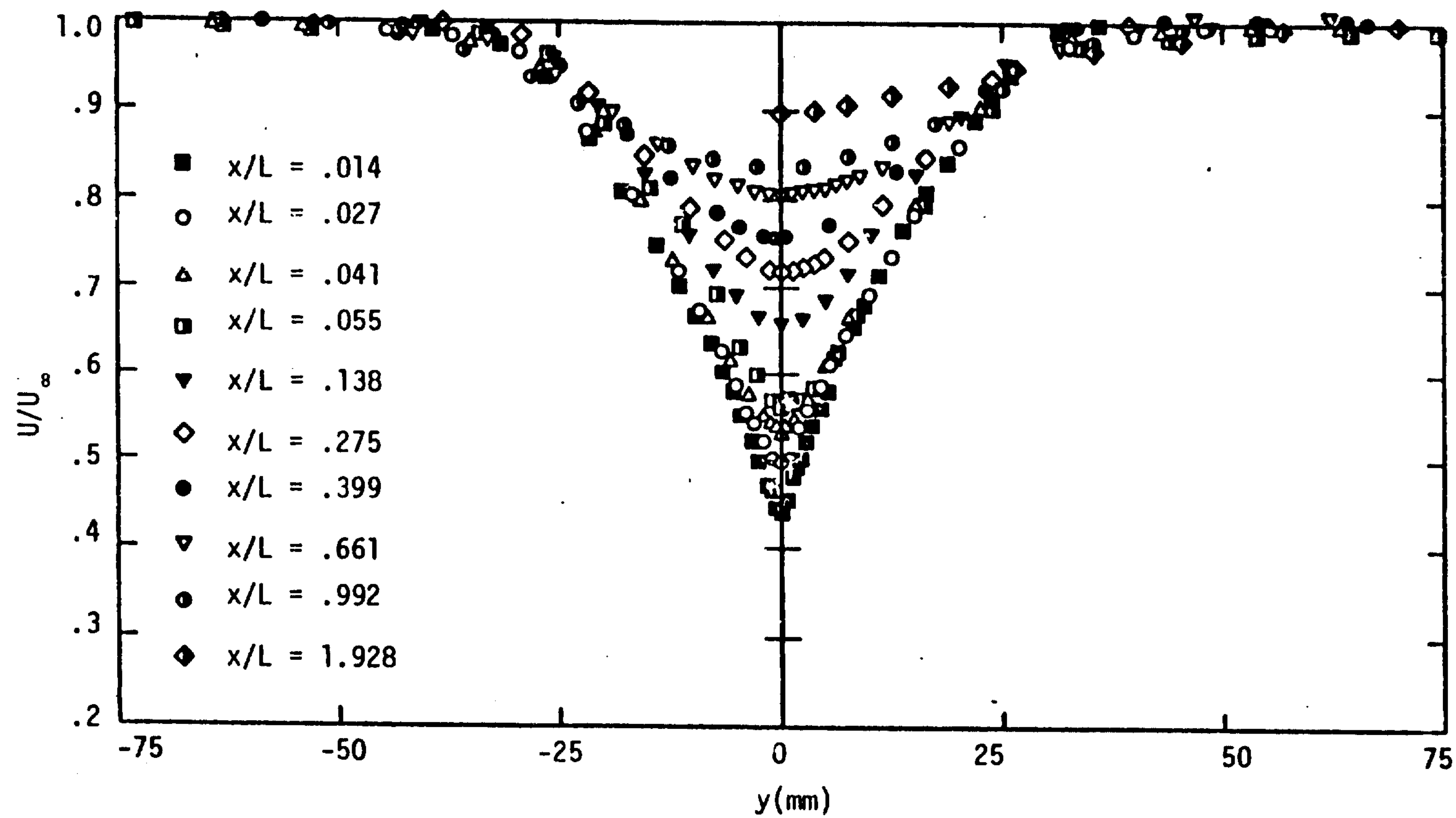

Figure 18. Variation of mean longitudinal velocity in the wake

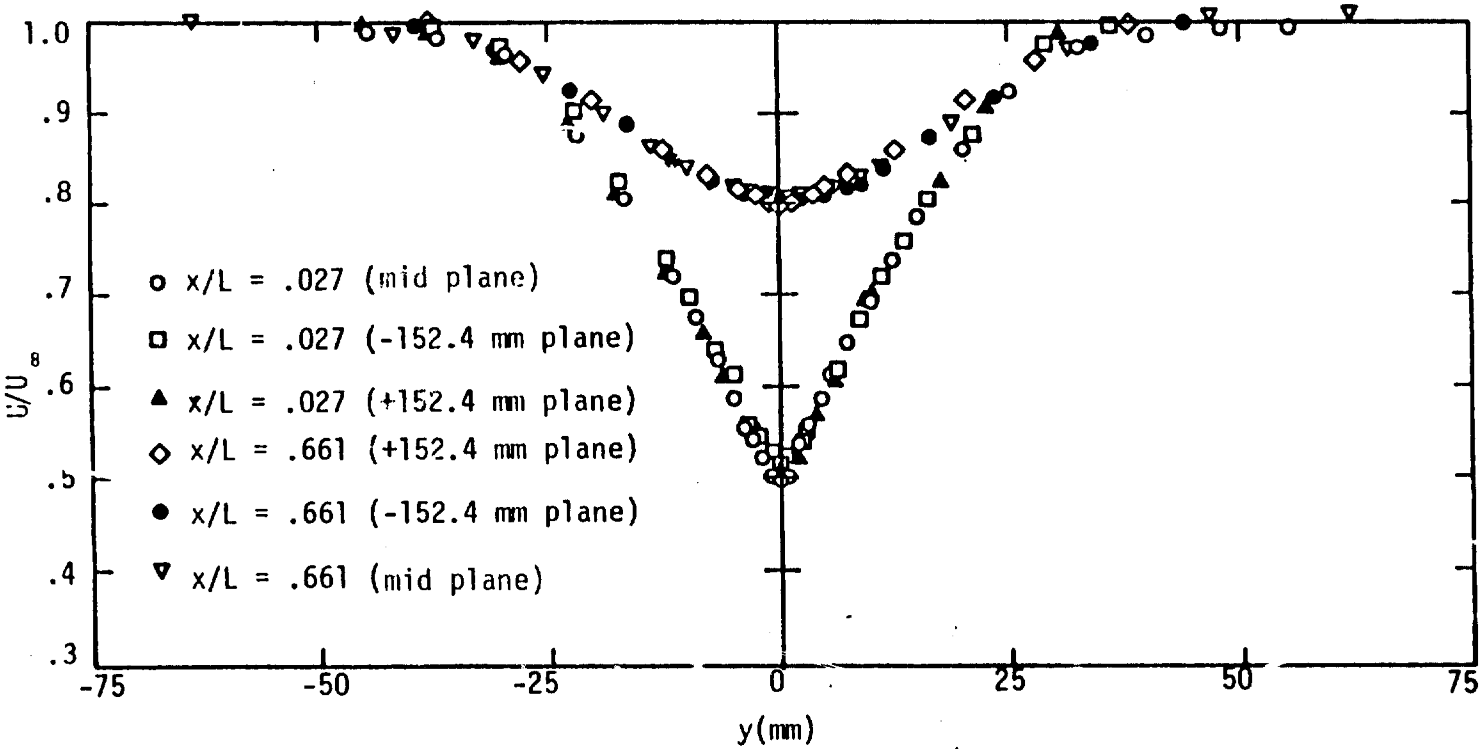

Figure 19. Variation of mean longitudinal velocity in the wake at different spanwise locations

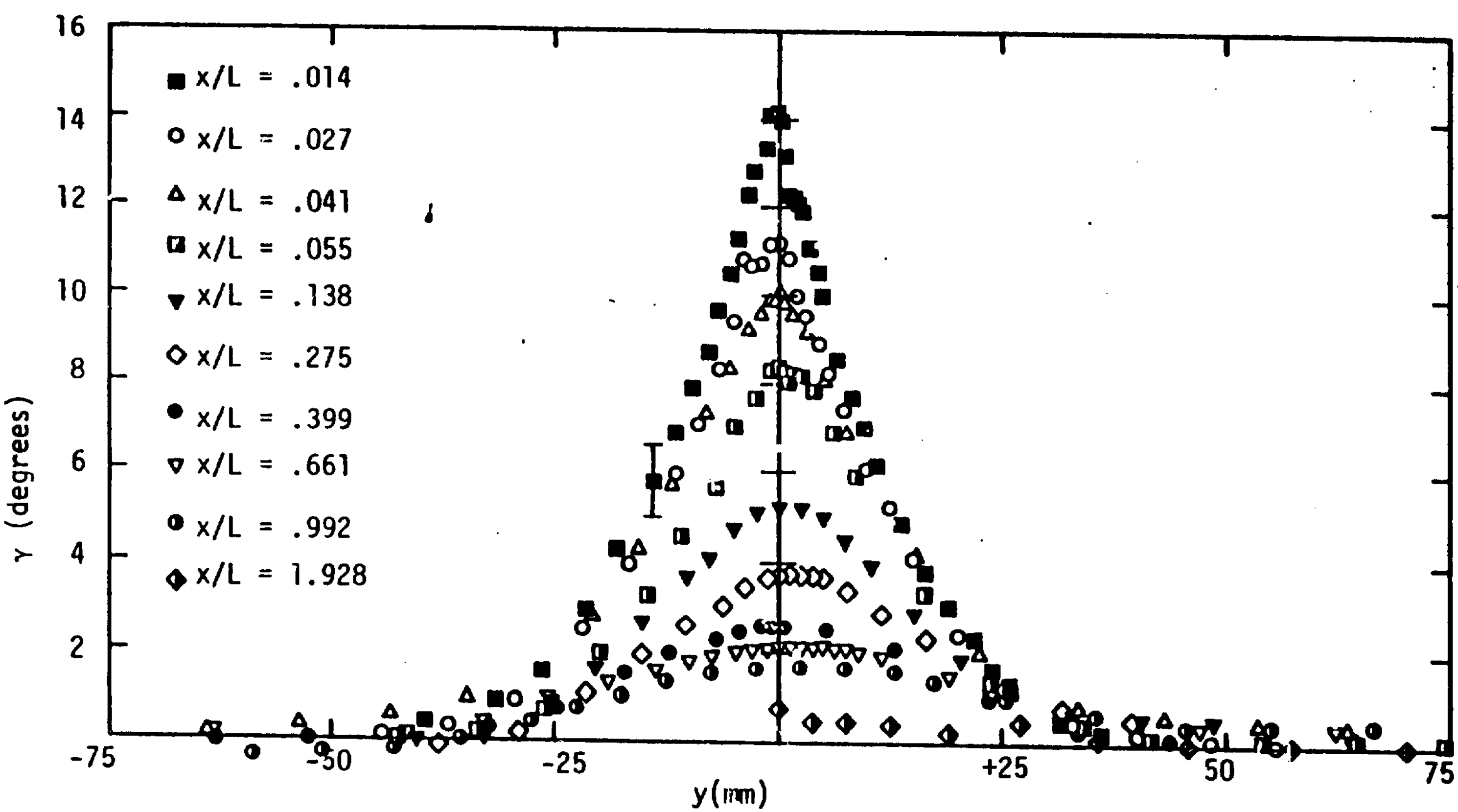

Figure 20. Variation of crossflow angle in the wake

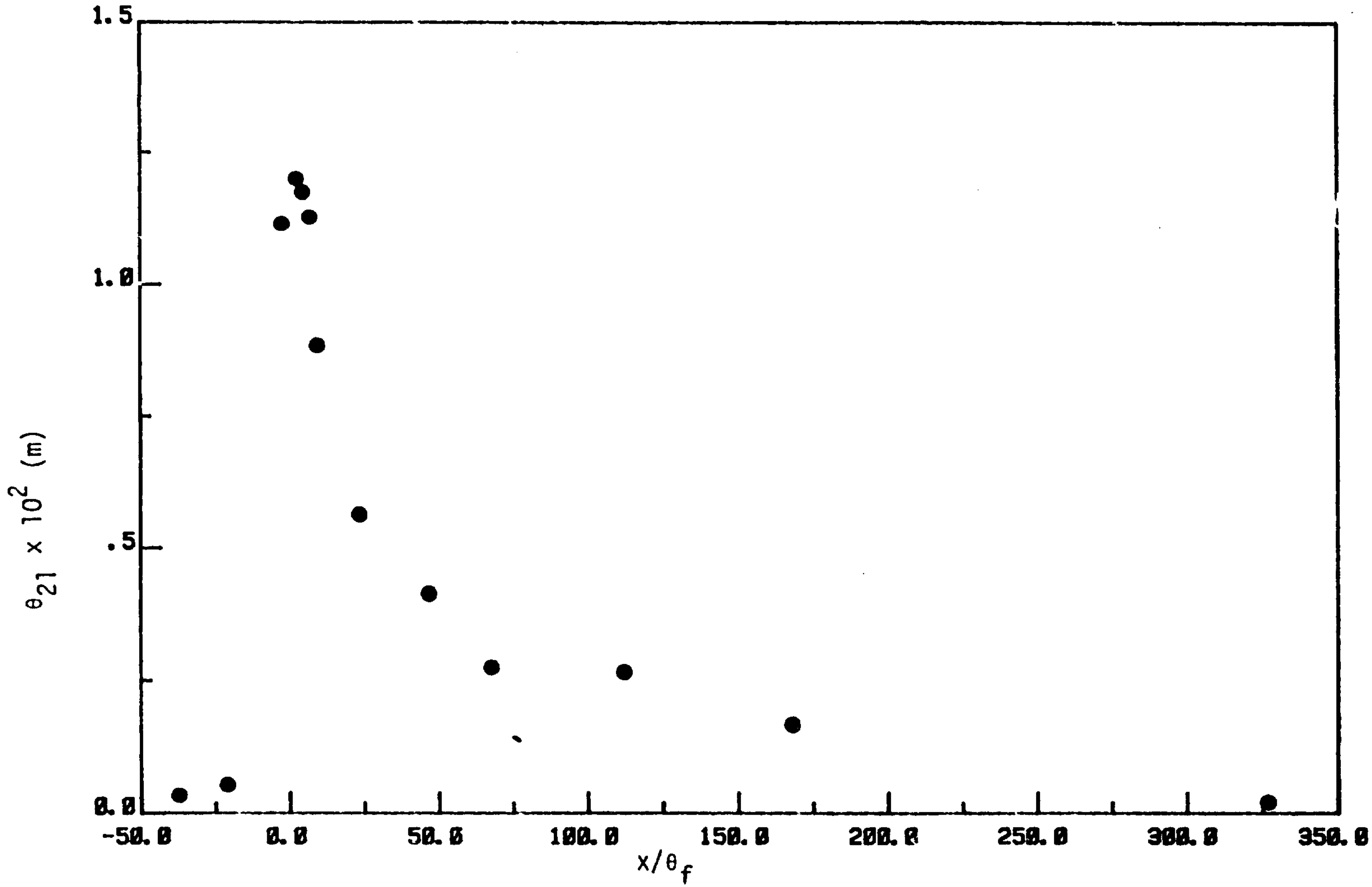

Figure 22. Variation of θ_{21} in the boundary layer and wake

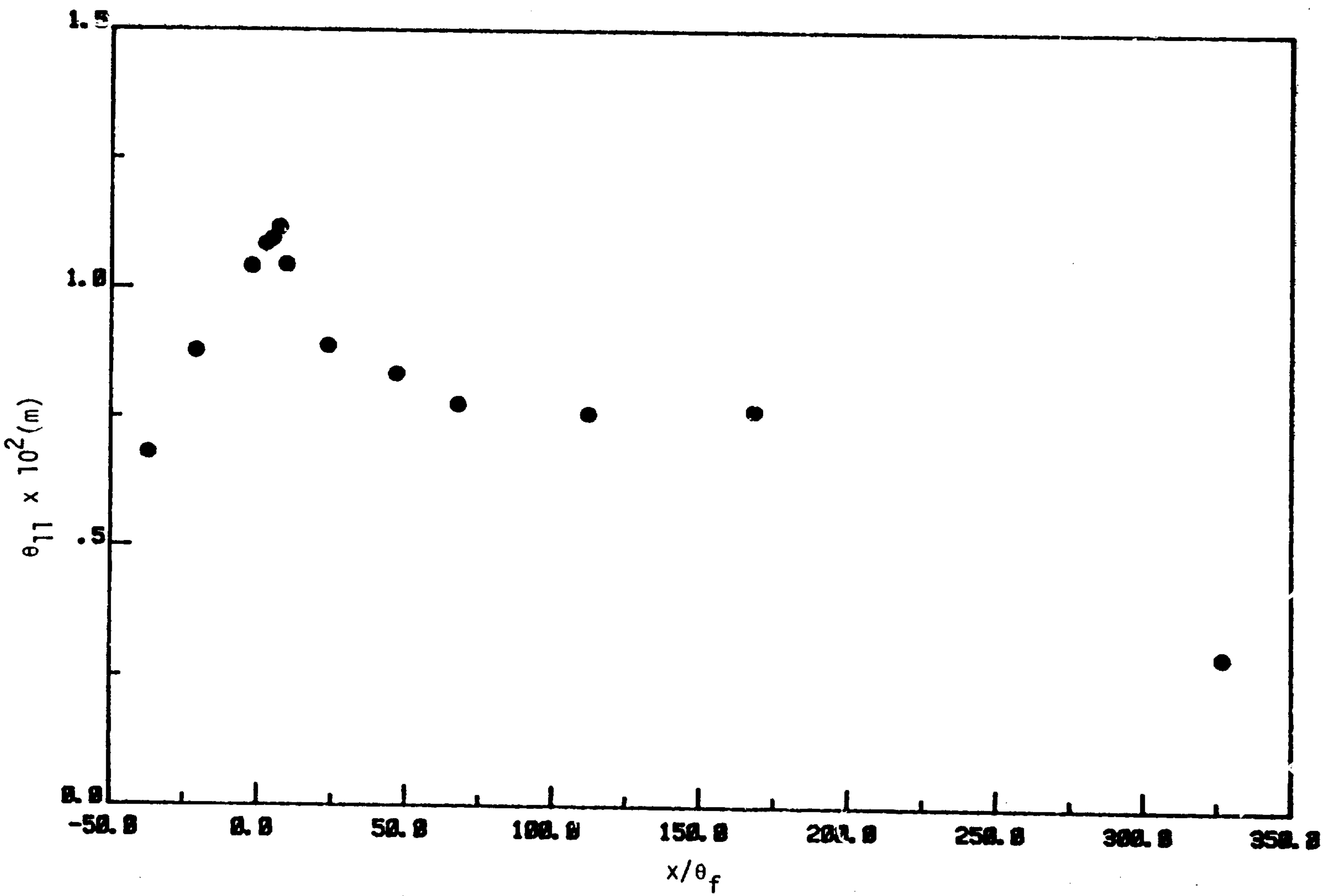

Figure 21. Variation of θ_{11} in the boundary layer and wake

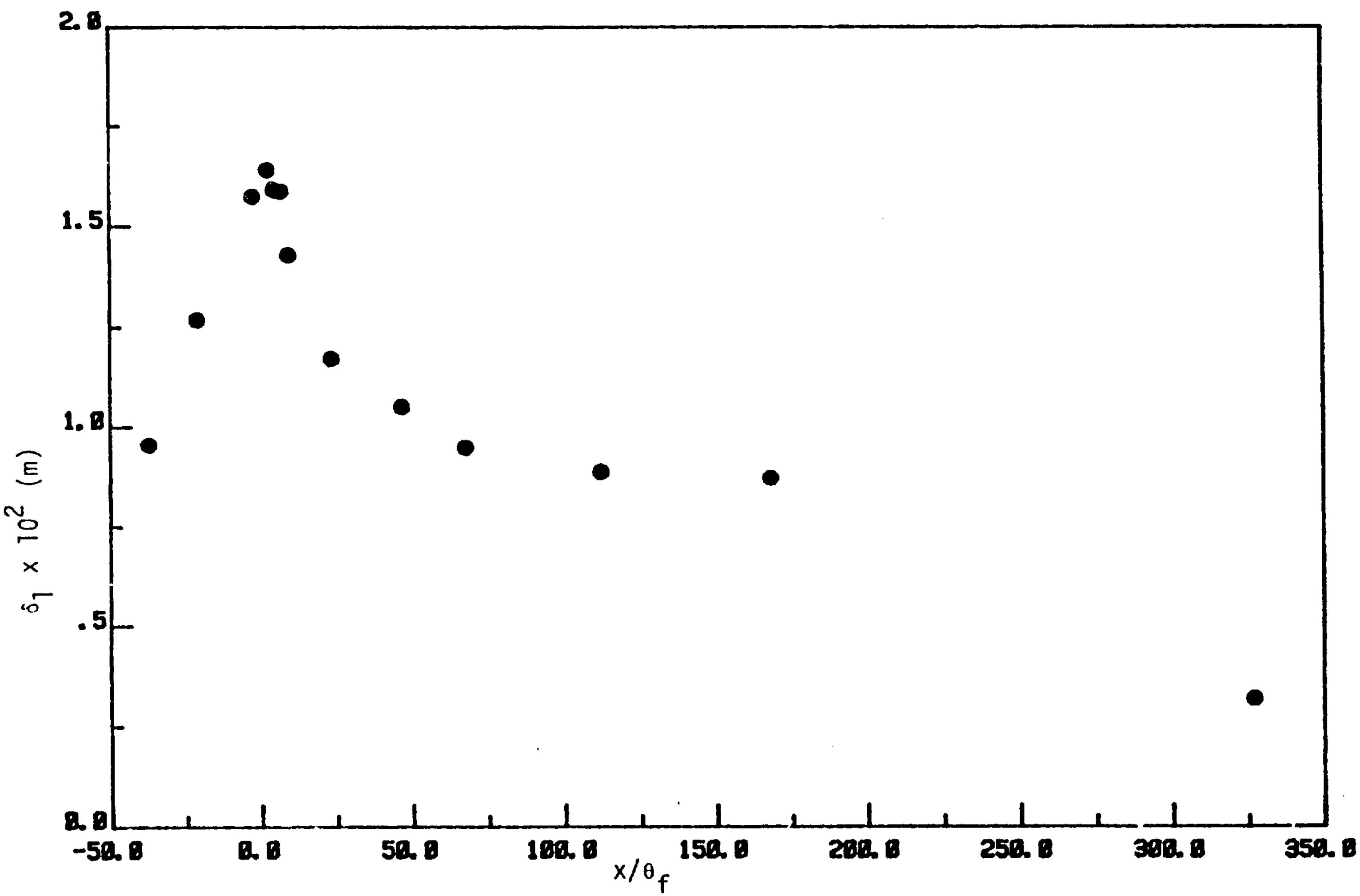

Figure 23. Variation of δ_1 in the boundary layer and wake

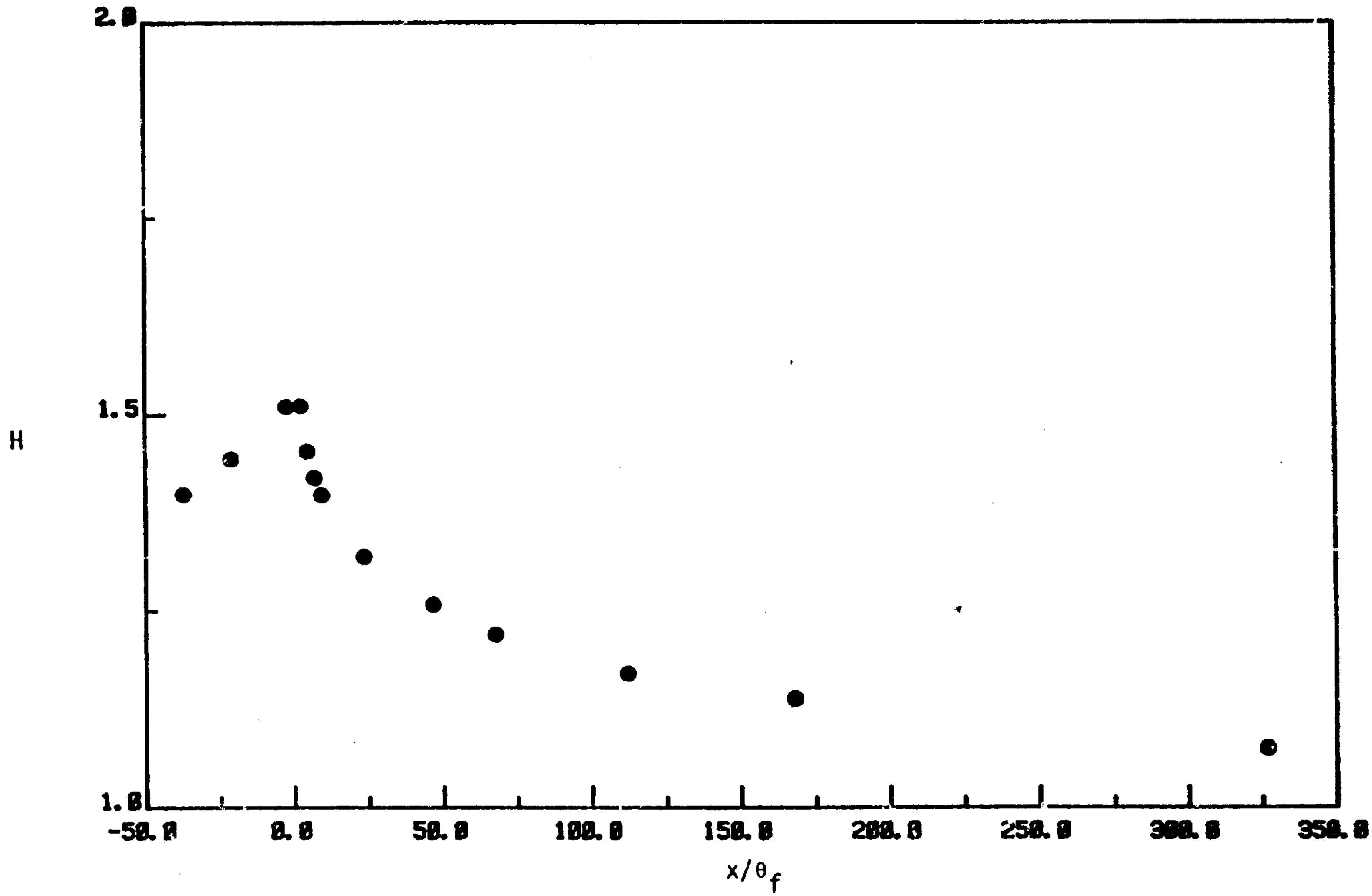

Figure 24. Variation of shape factor in the boundary layer and wake

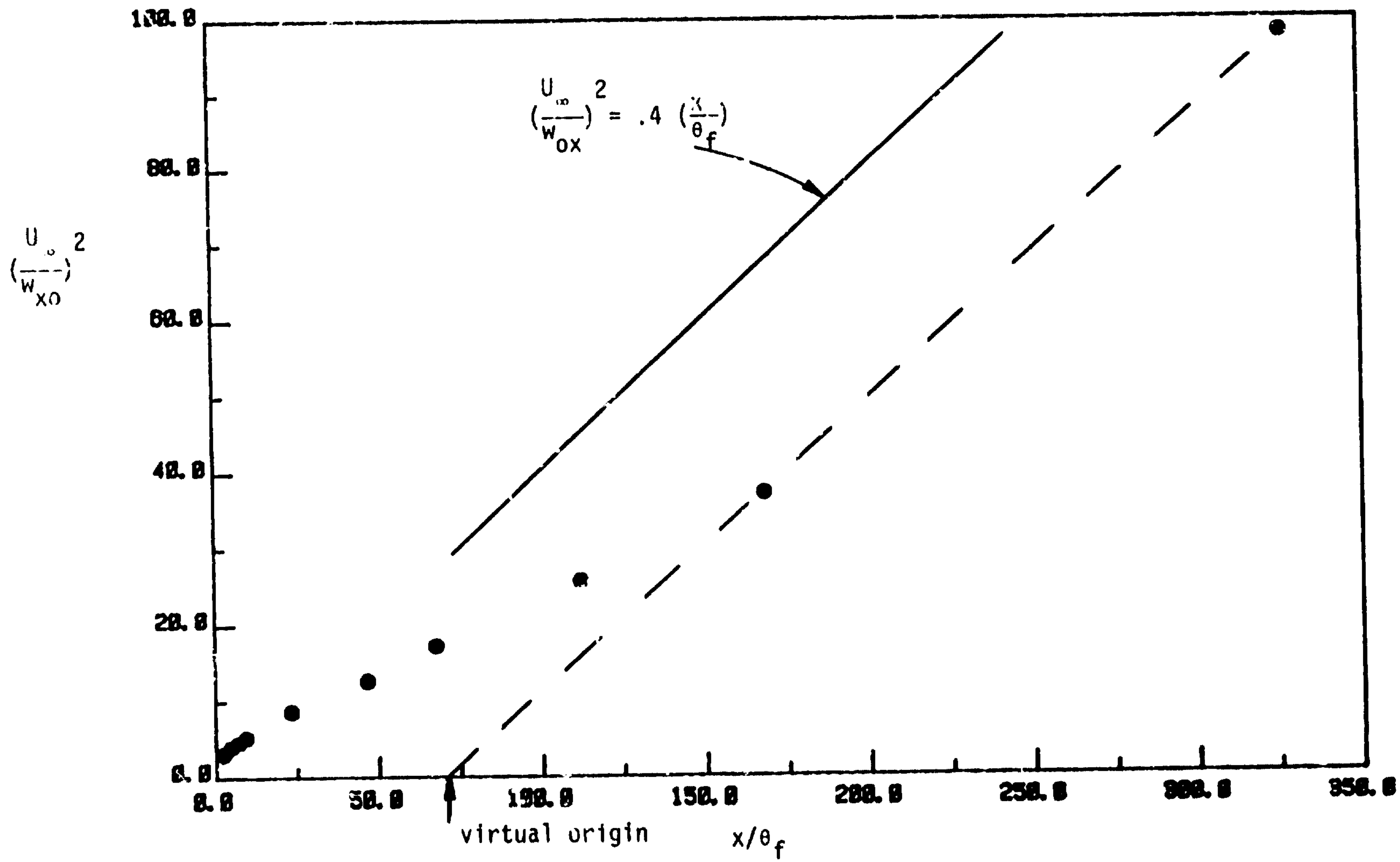

Figure 25. Defect velocity w_{xo} vs. x/θ_f

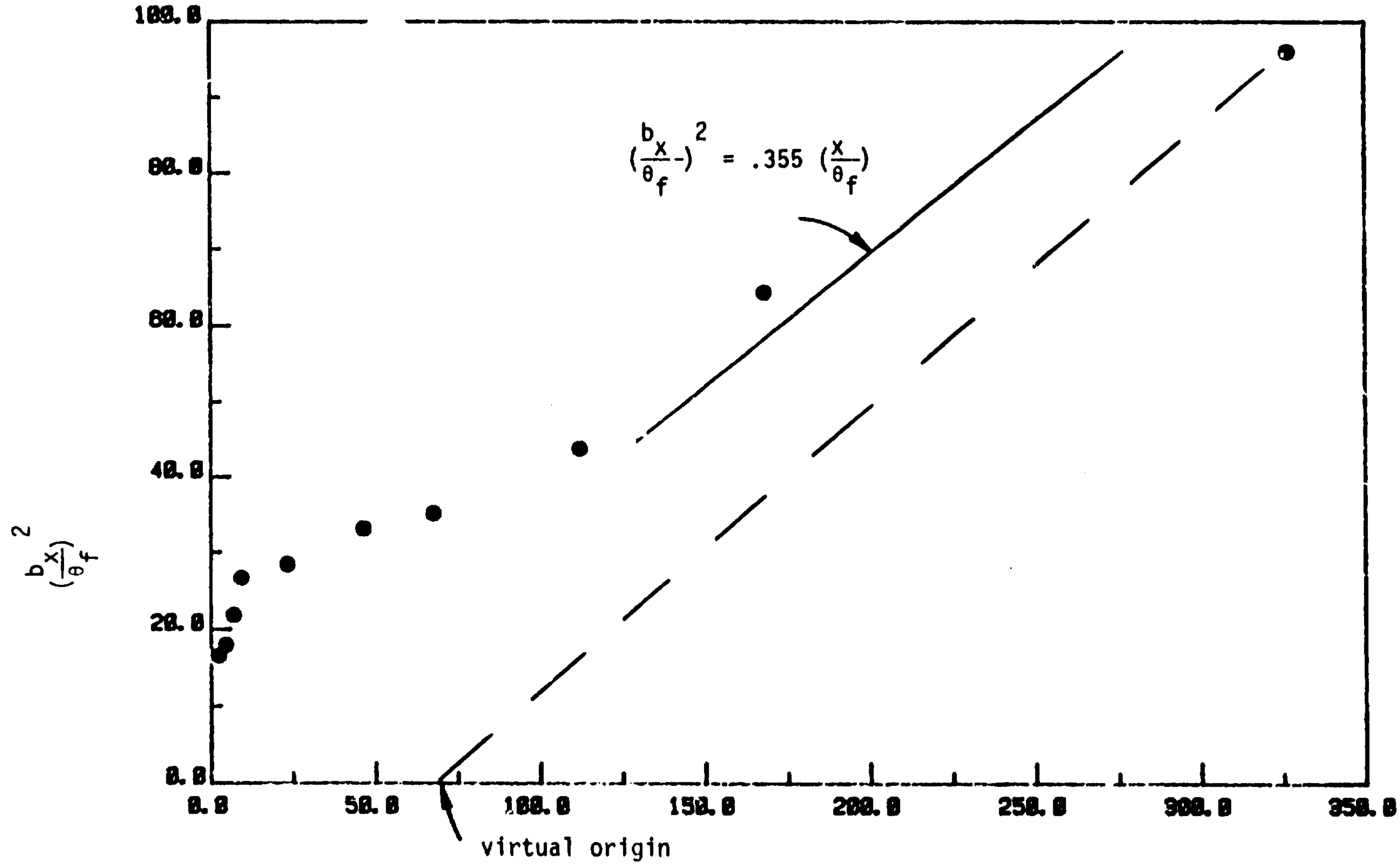

Figure 26. Half-width b_x vs. x/θ_f

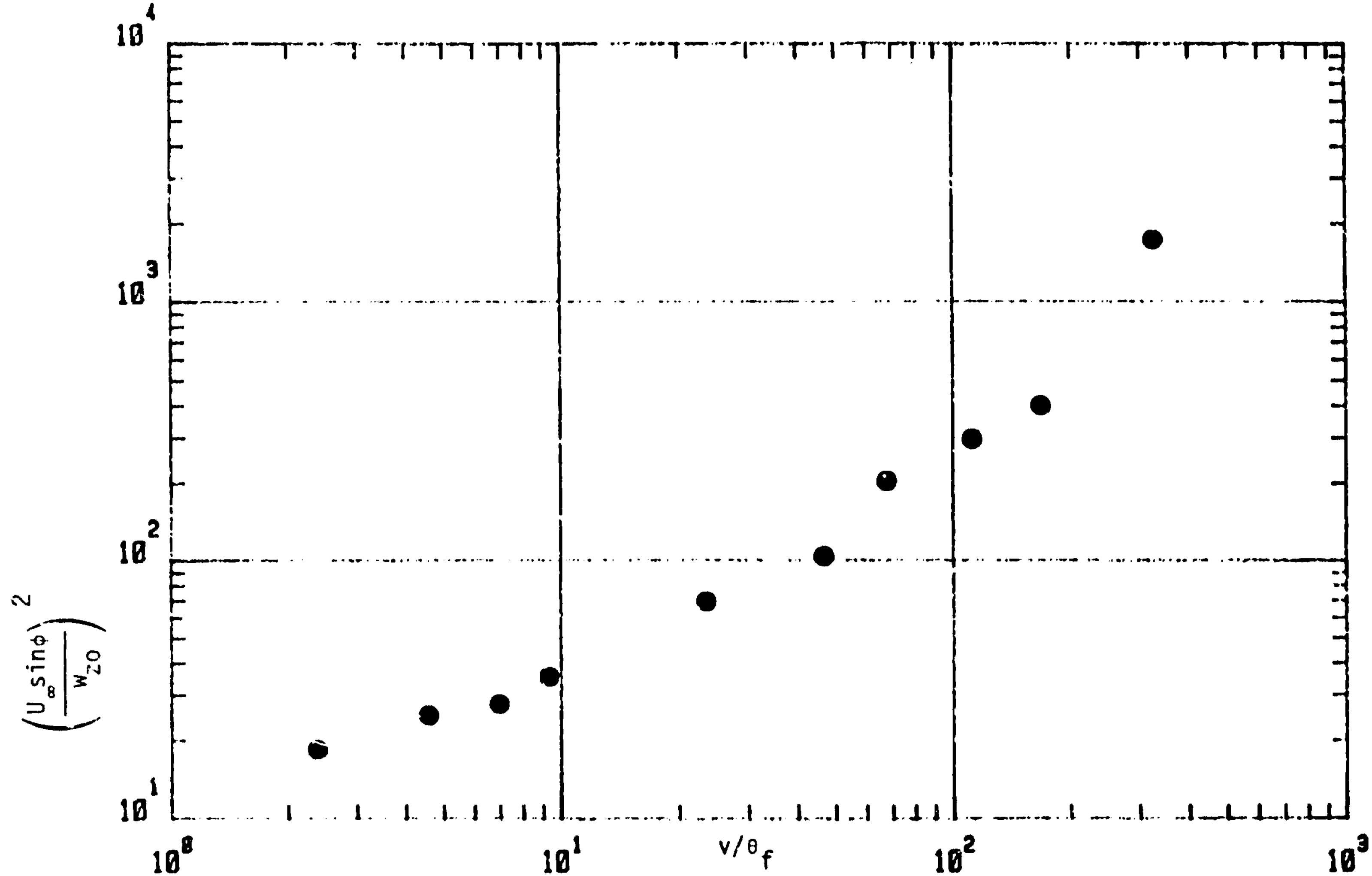

Figure 27. Defect velocity w_{zo} vs x/θ_f in log-log coordinates

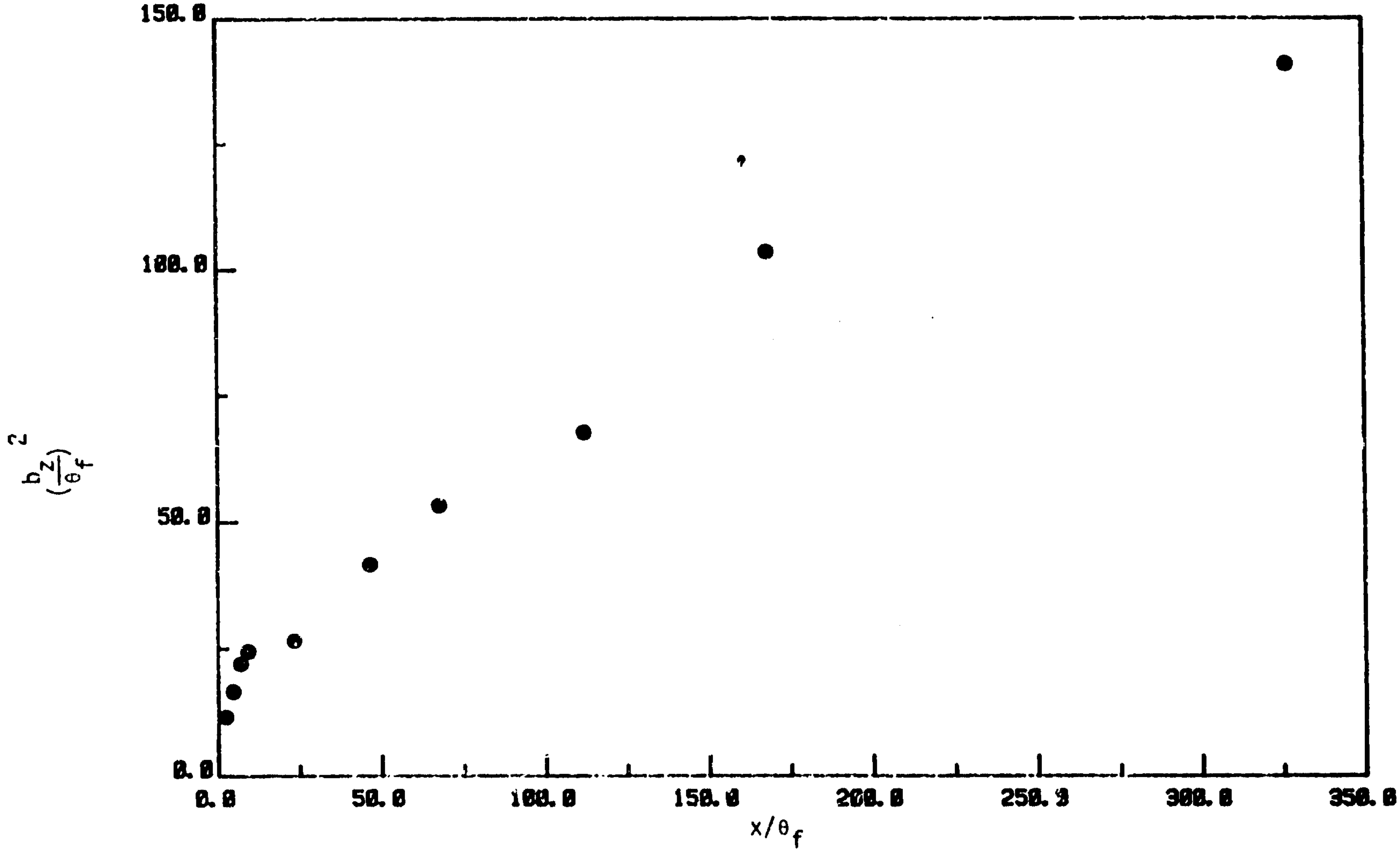

Figure 28. Half-width b_z vs. x/θ_f

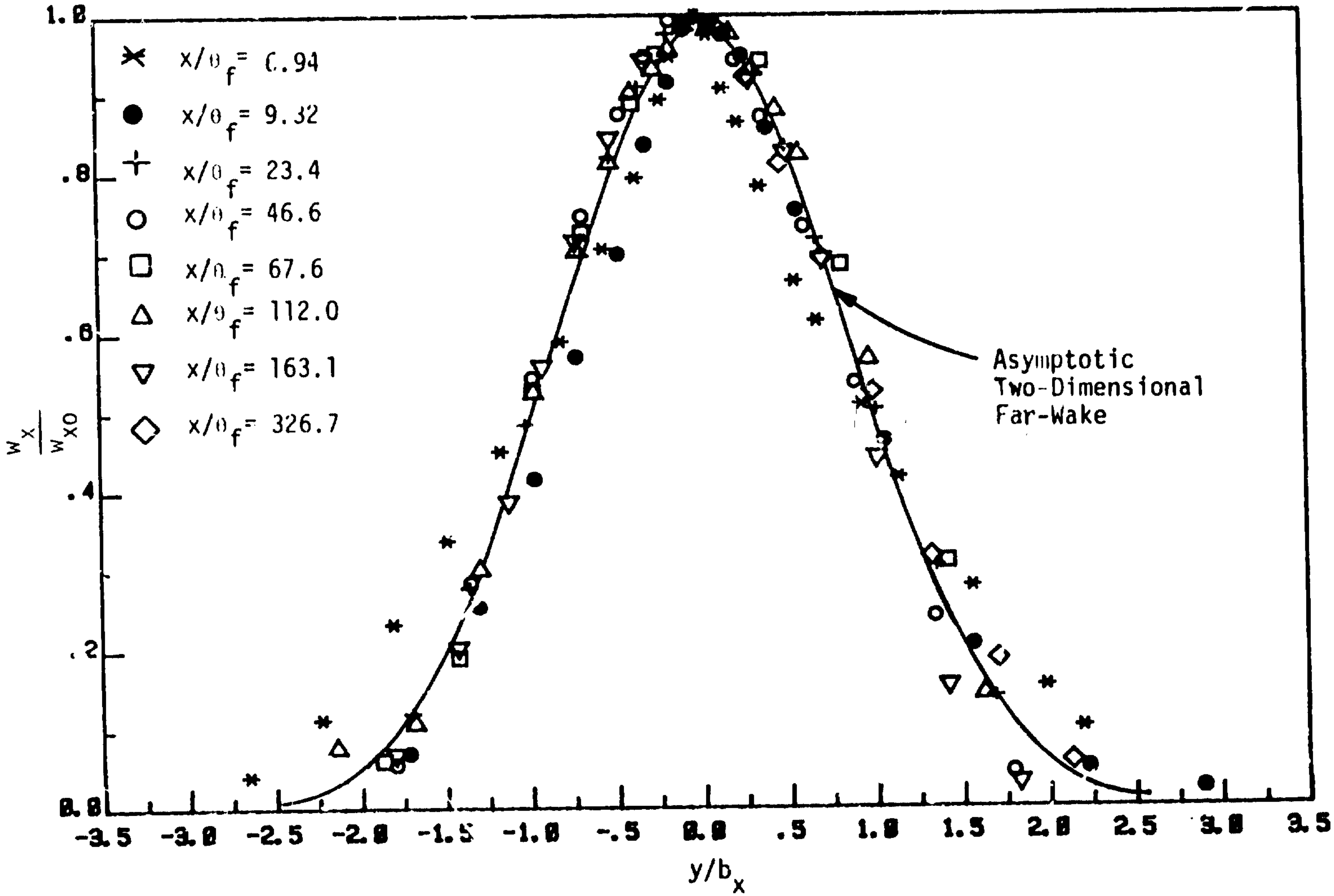

Figure 29. Self-similar streamwise velocities

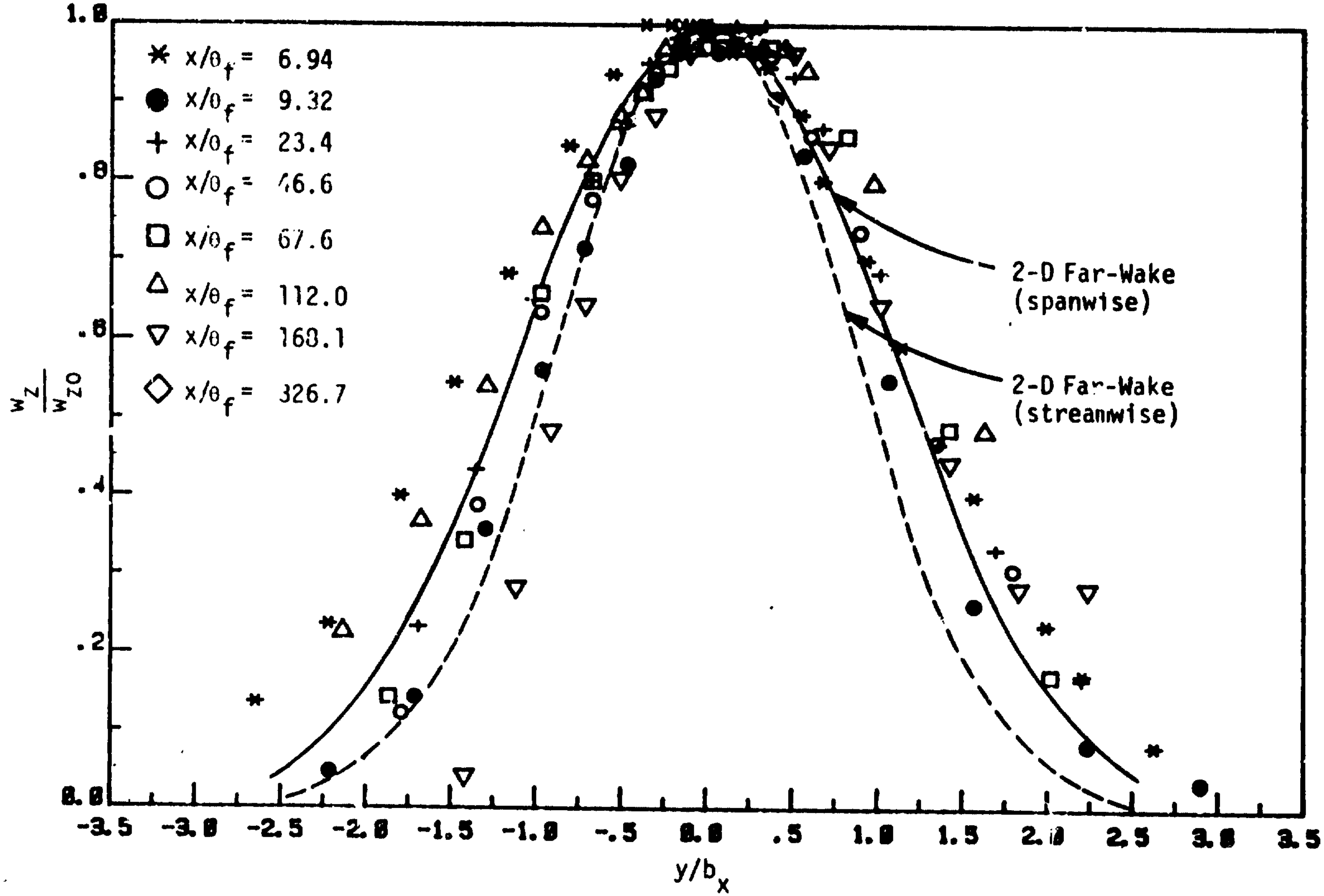

Figure 30. Self-similar spanwise velocities

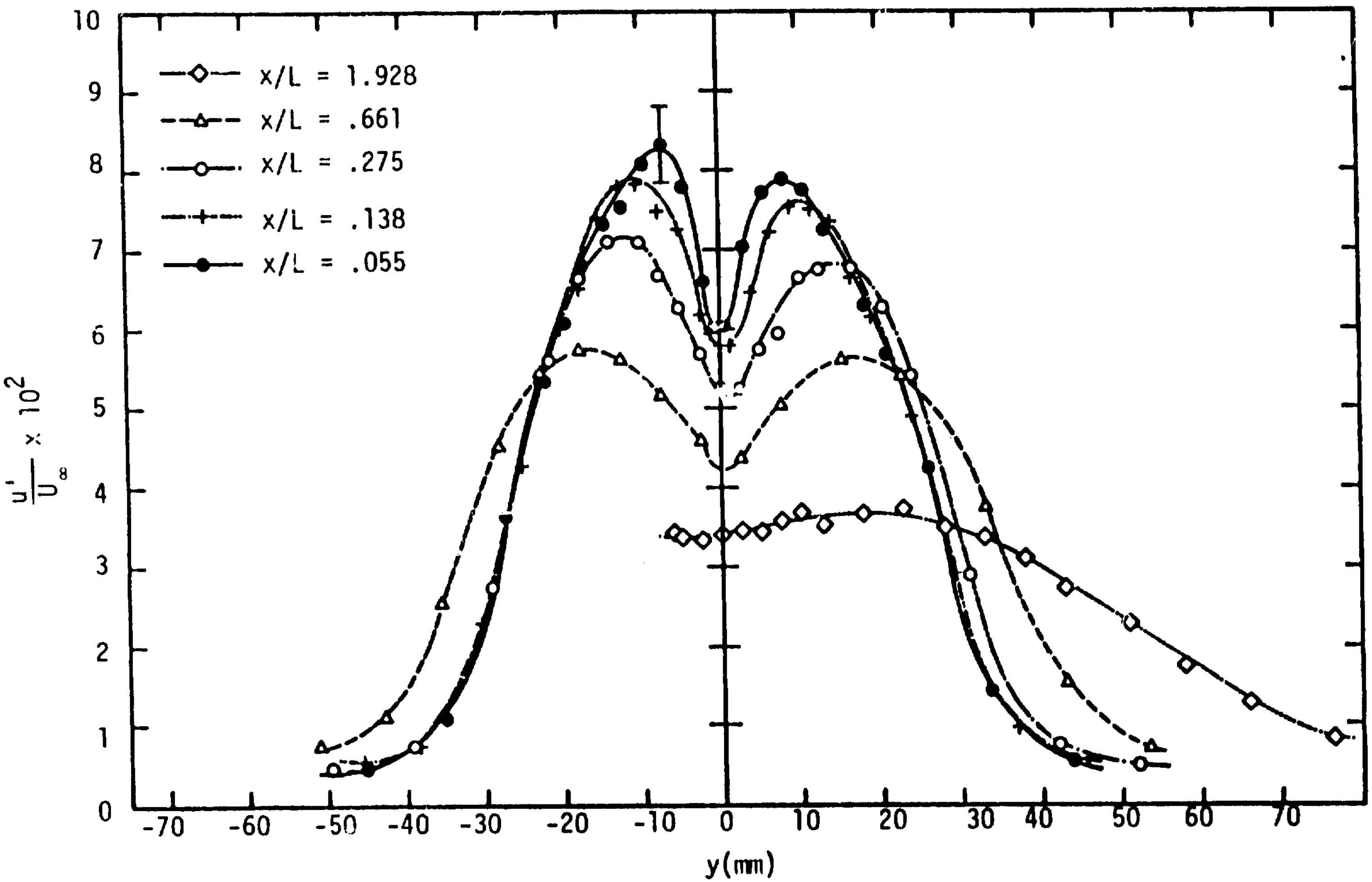

Figure 31. Variation of u' across the wake

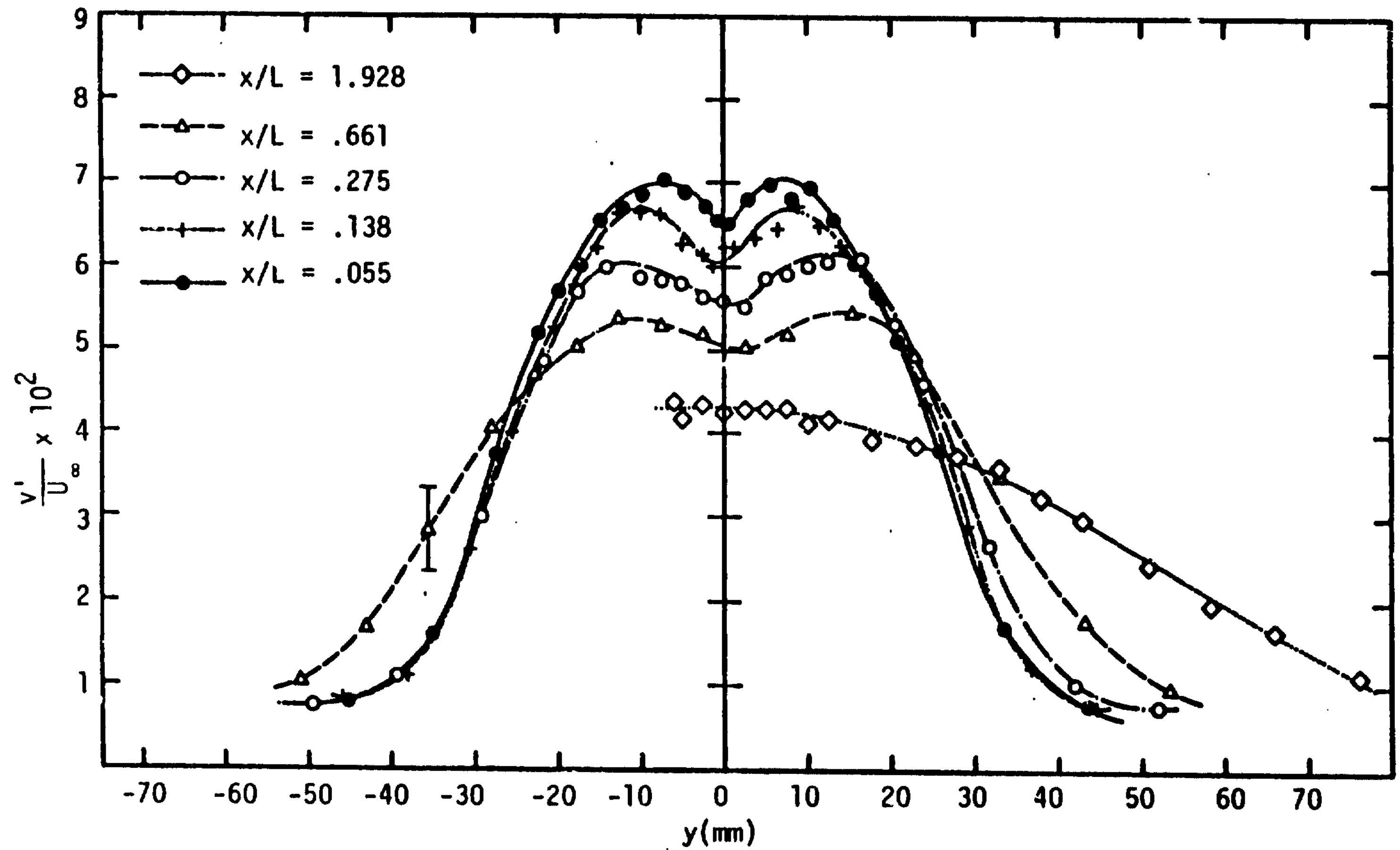

Figure 32. Variation of v' across the wake

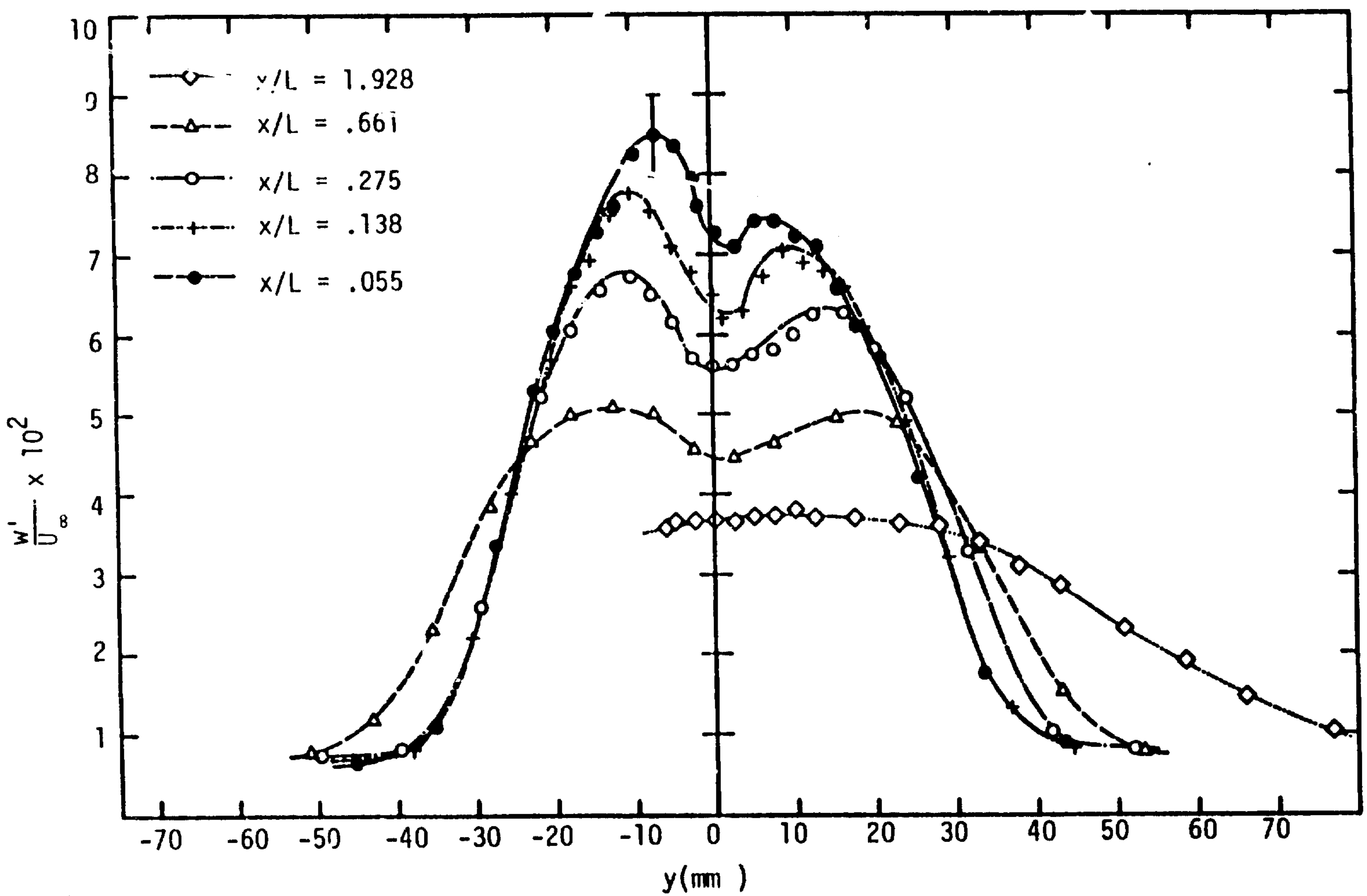

Figure 33. Variation of w' across the wake

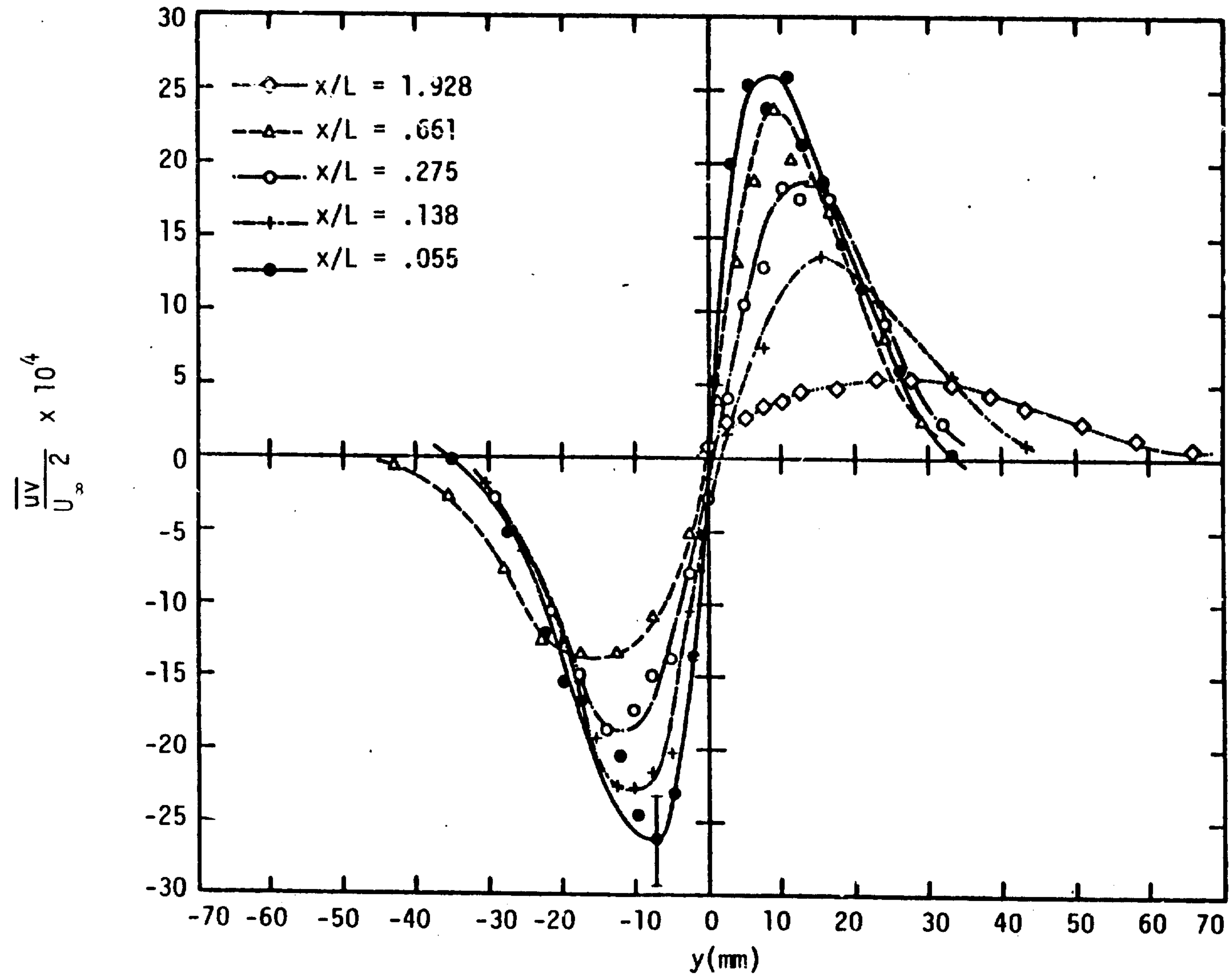

Figure 34. Variation of $\overline{uv}$ across the wake

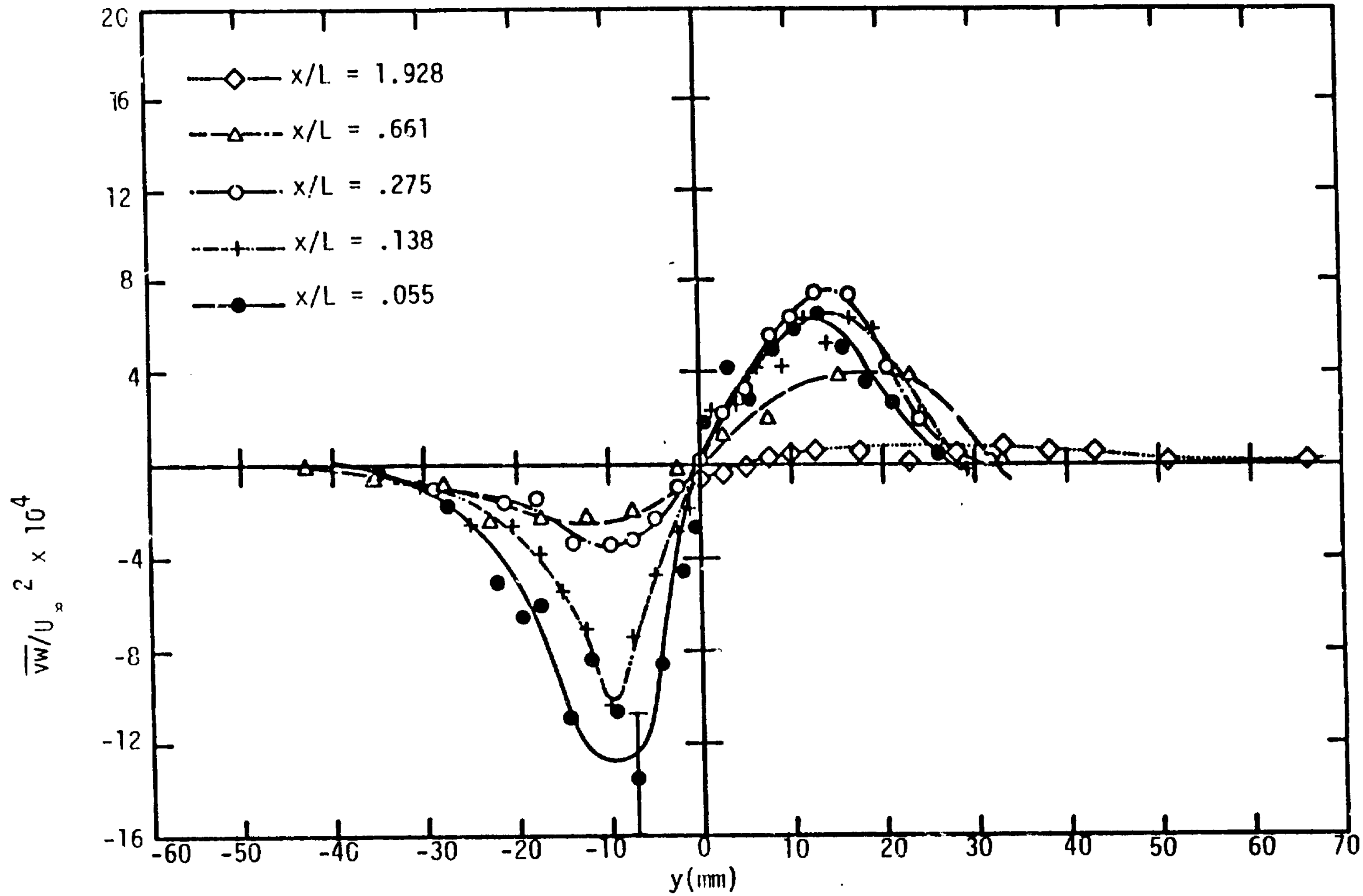

Figure 35. Variation of $\overline{vw}$ across the wake

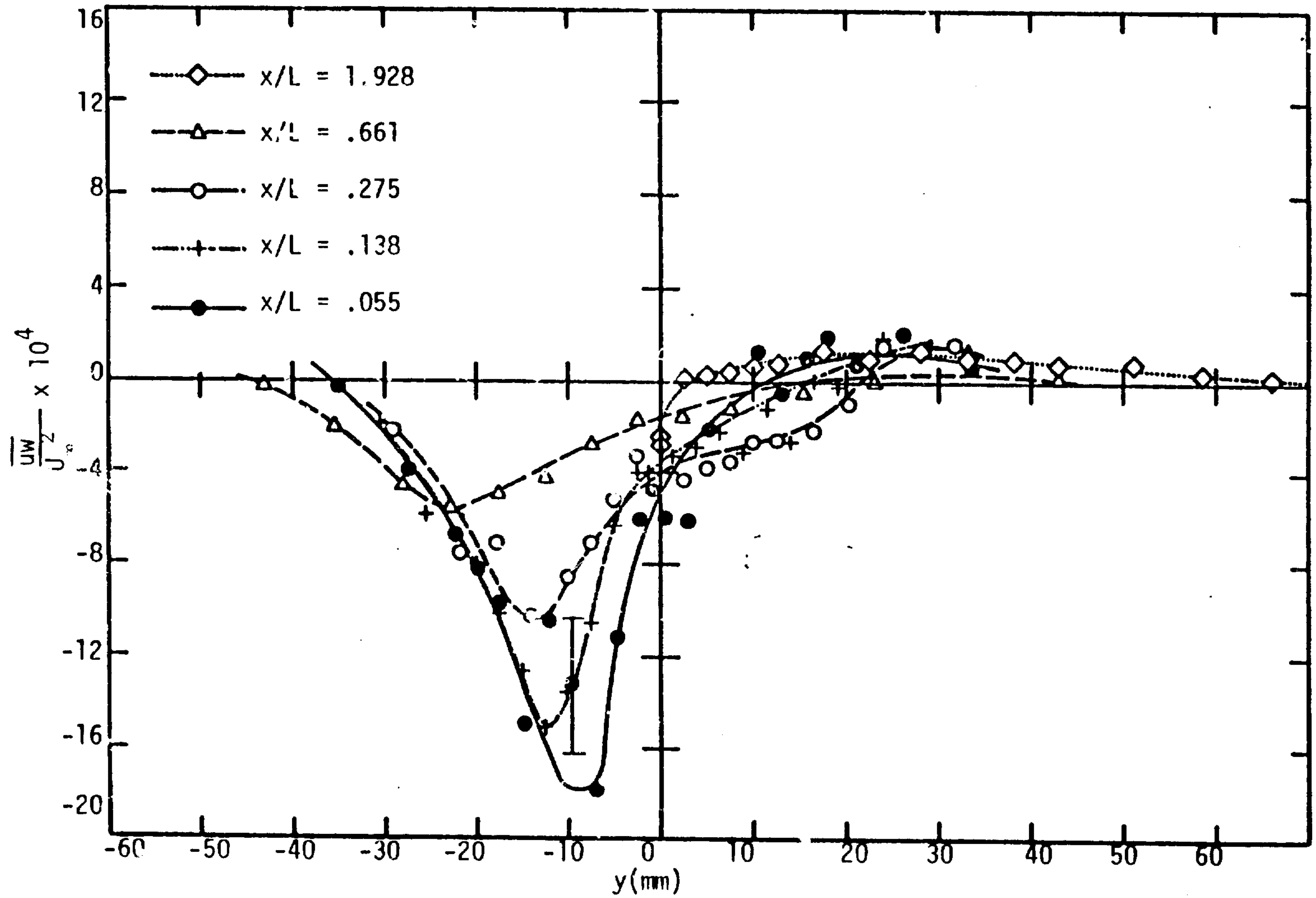

Figure 36. Variation of $\overline{uw}$ across the wake

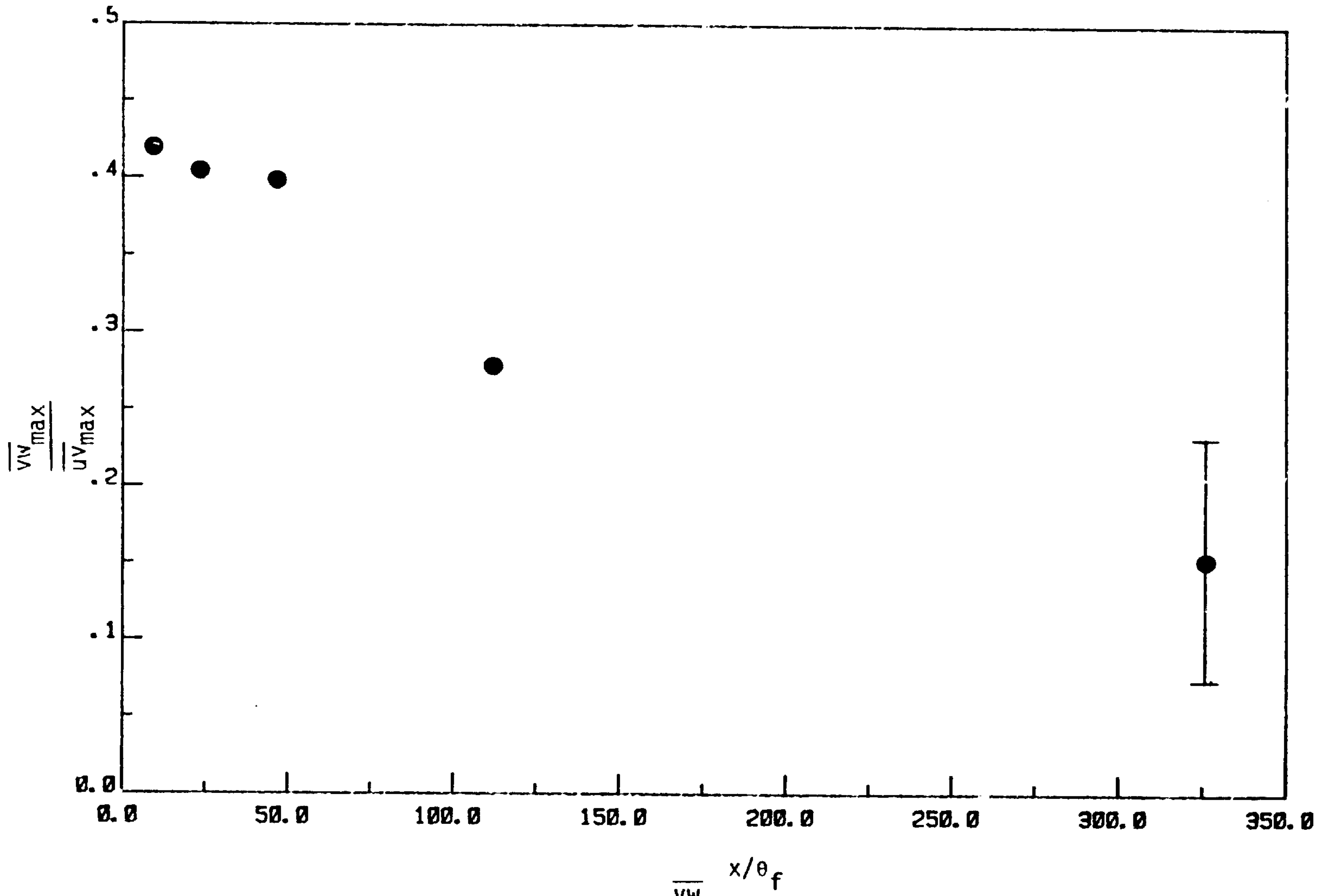

Figure 37. Variation of $\frac{\overline{vw}_{max}}{\overline{uv}_{max}}$ with x/θ_f

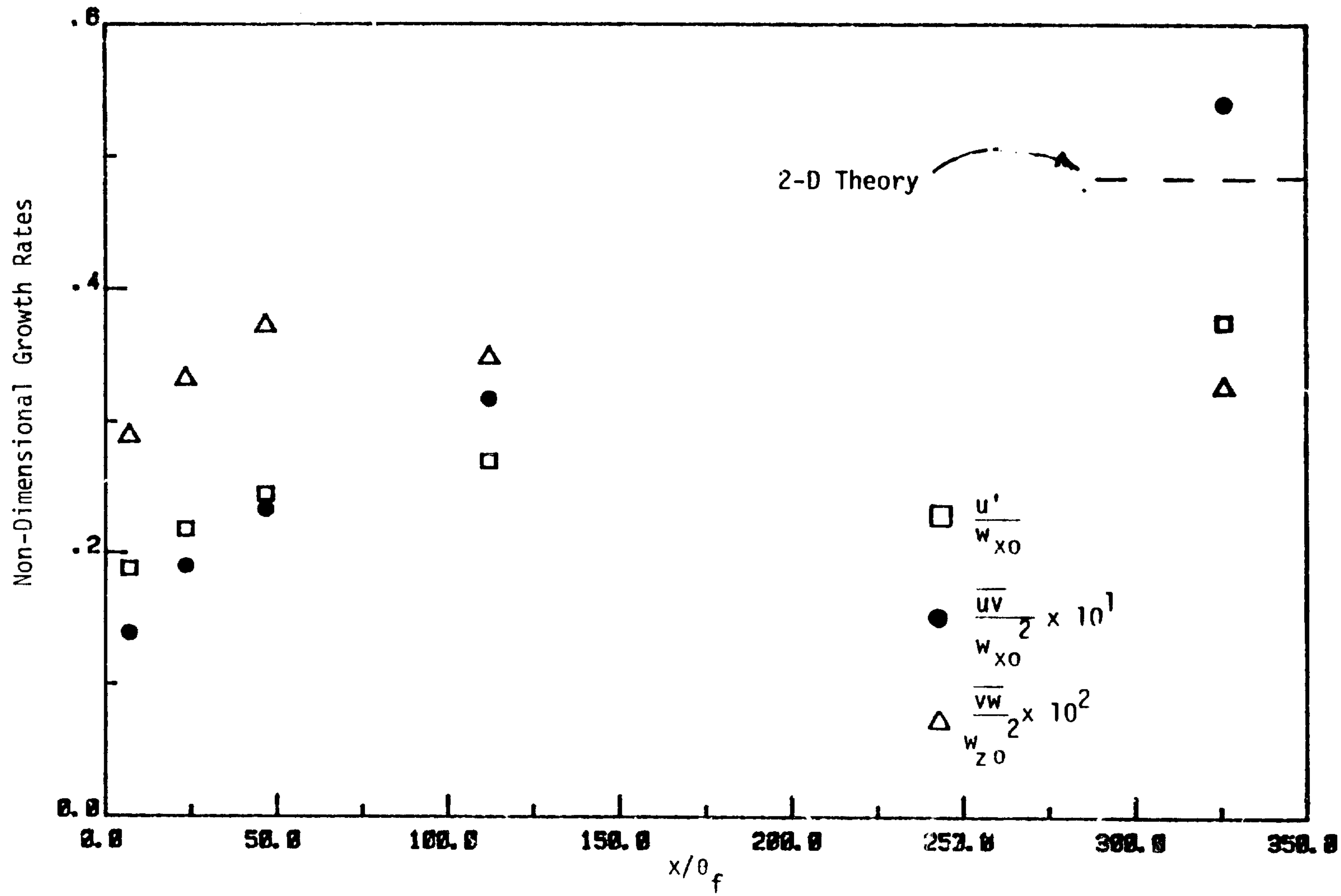

Figure 38. Decay rates of u', $\overline{uv}$ and $\overline{vw}$ with respect to x/θ_f

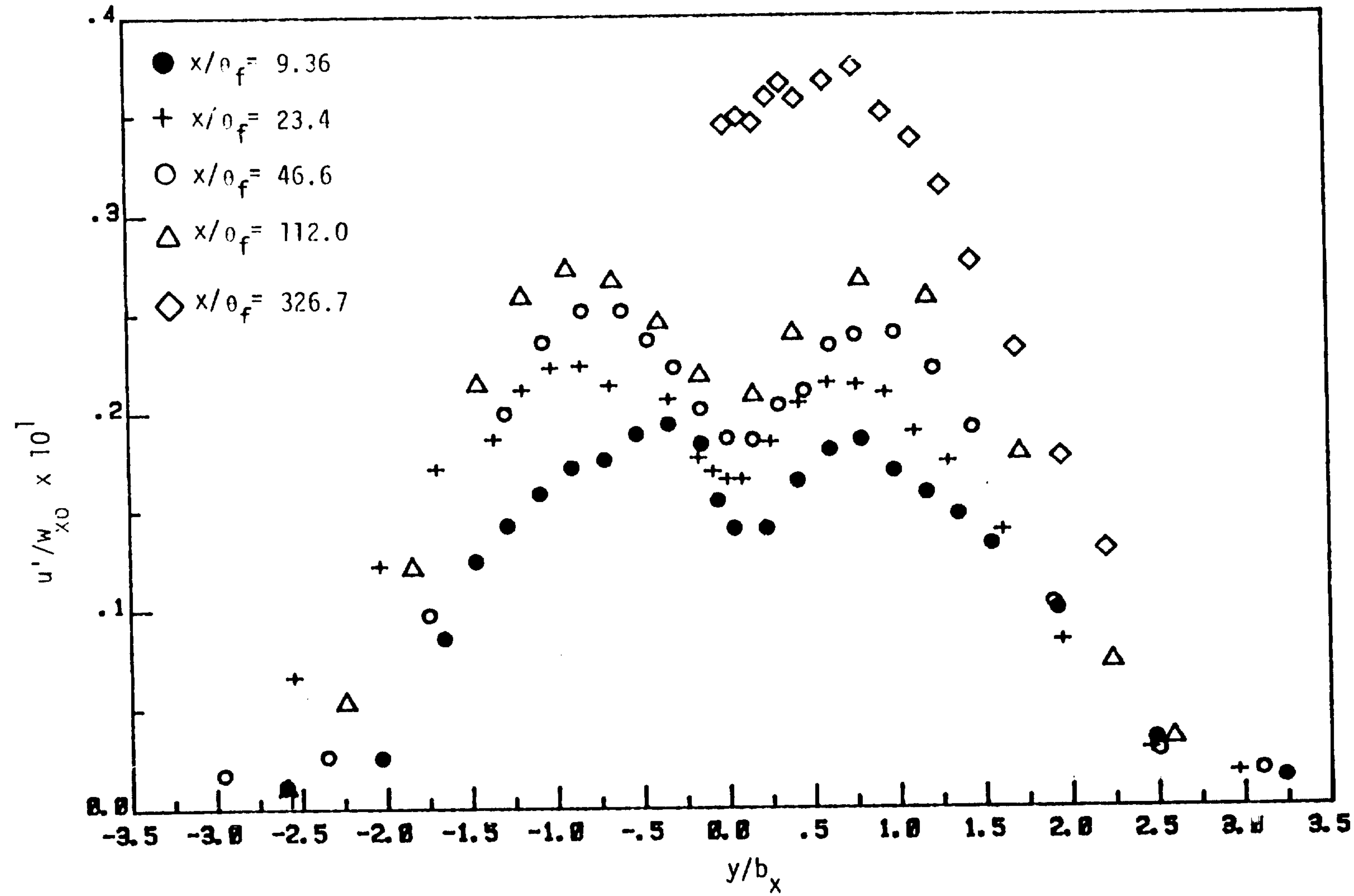

Figure 39. u' in self-preserving coordinates

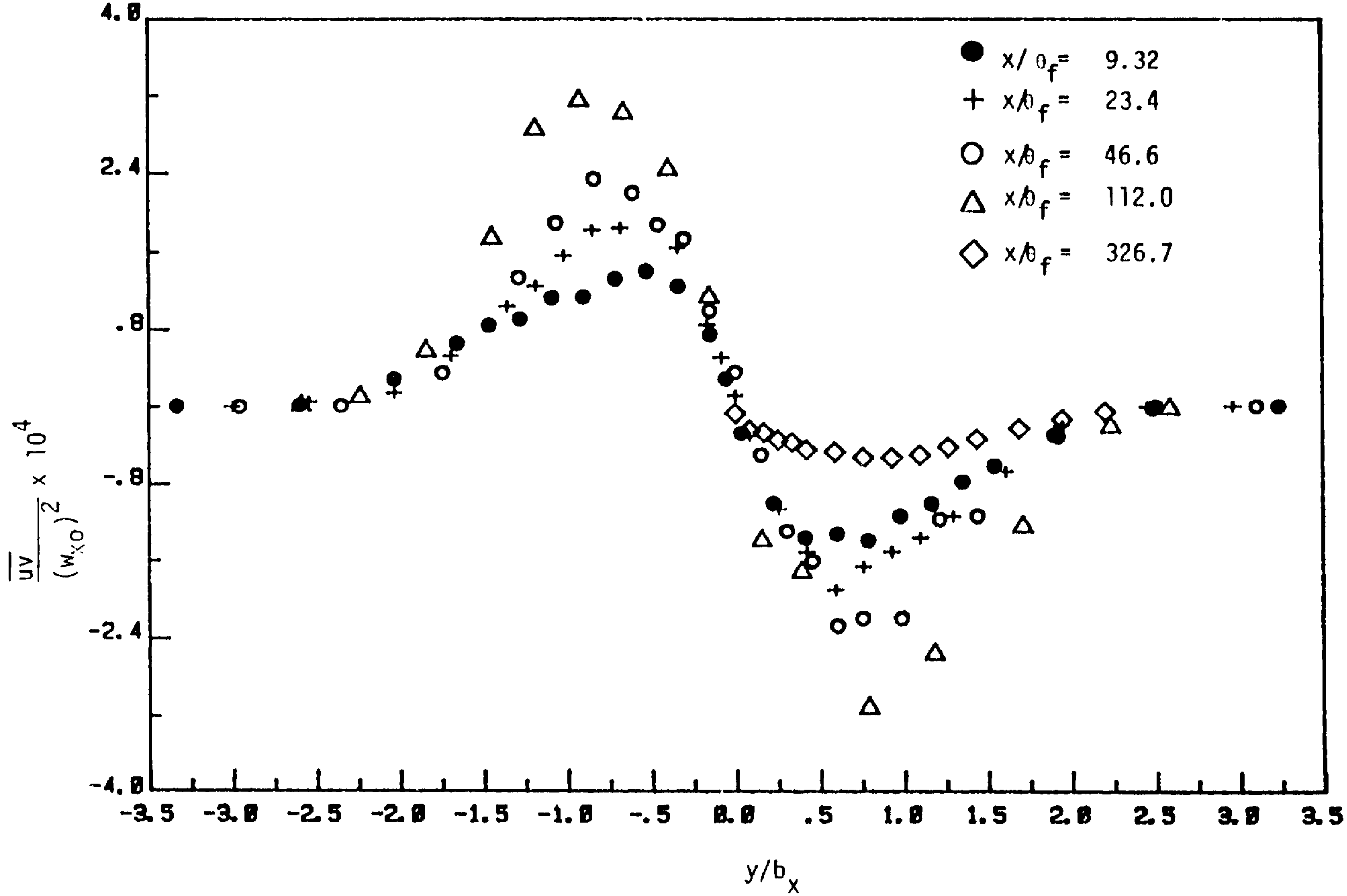

Figure 40. $\overline{uv}$ in self-preserving coordinates

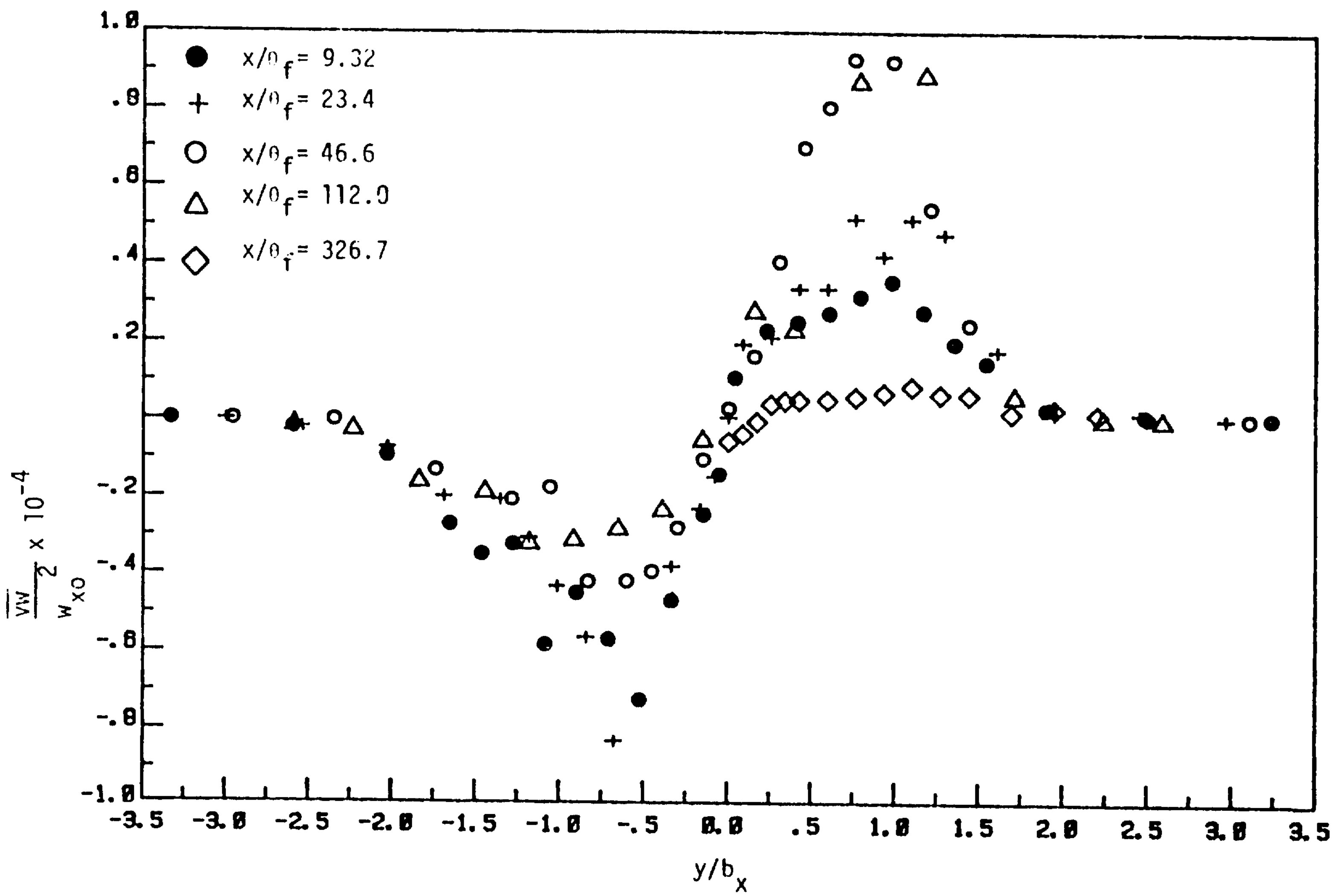

Figure 41. $\overline{vw}$ in self-preserving coordinates

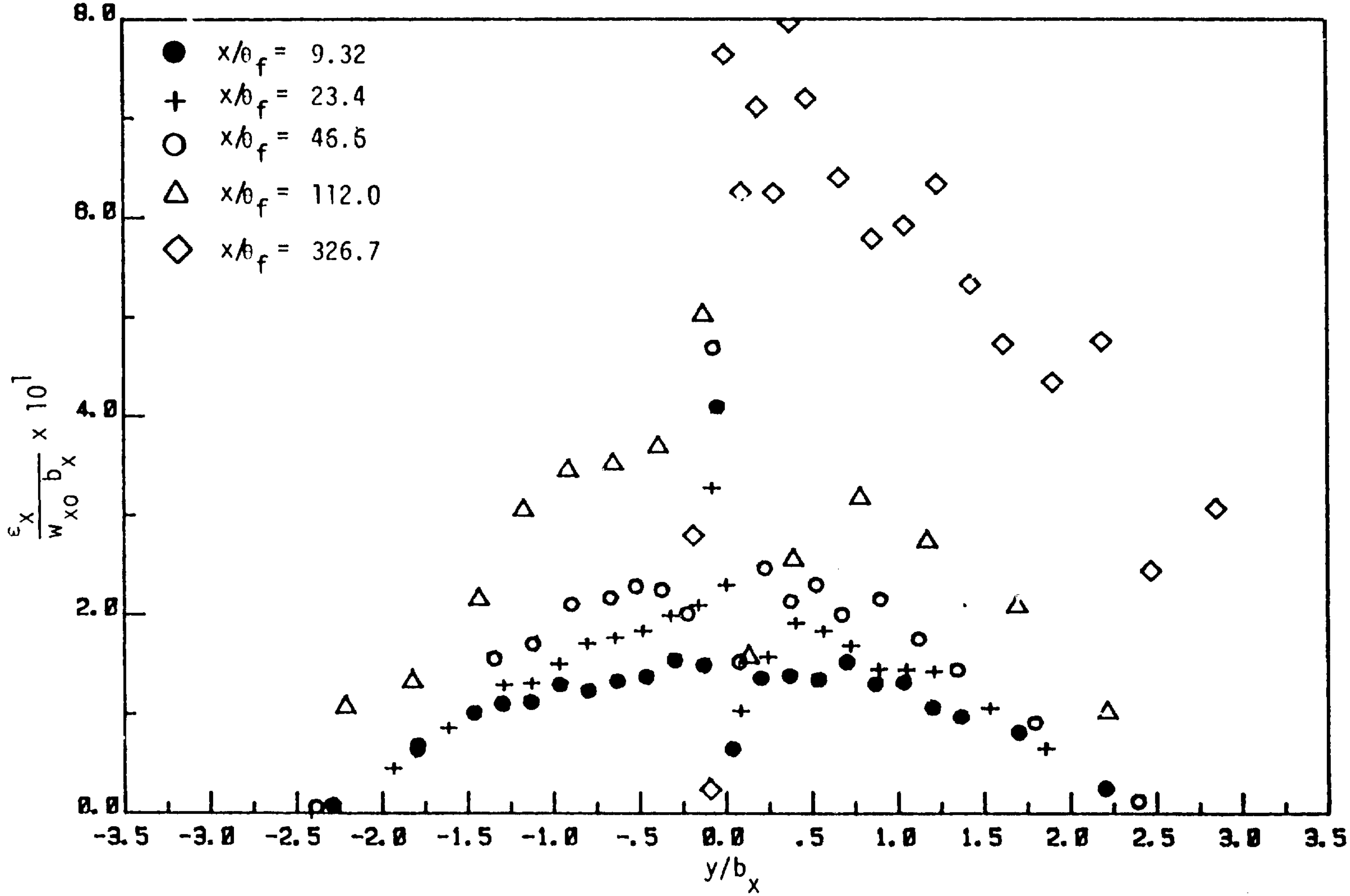

Figure 42. Eddy viscosity ε_x in self-preserving coordinates

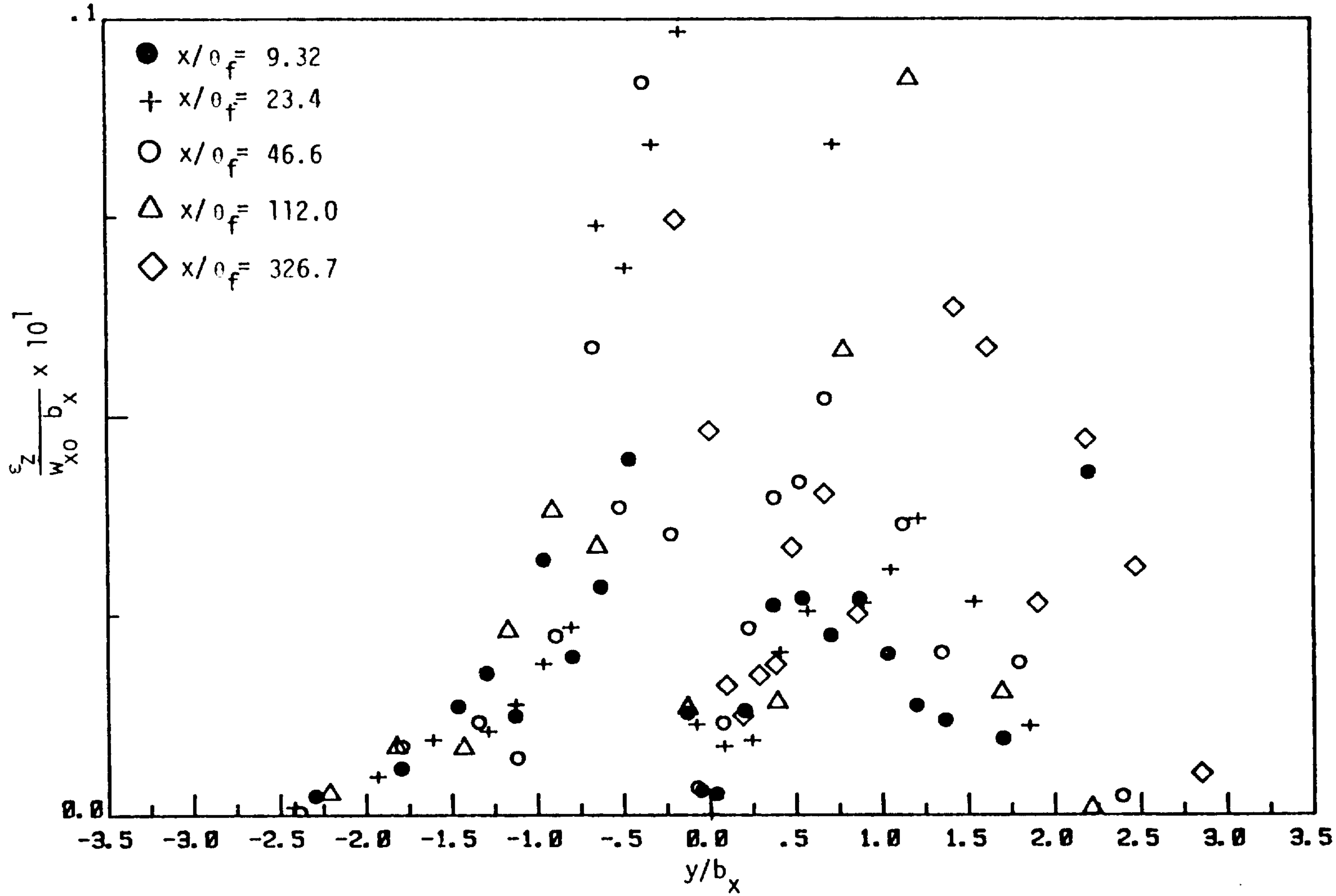

Figure 43. Eddy viscosity ε_z in self-preserving coordinates

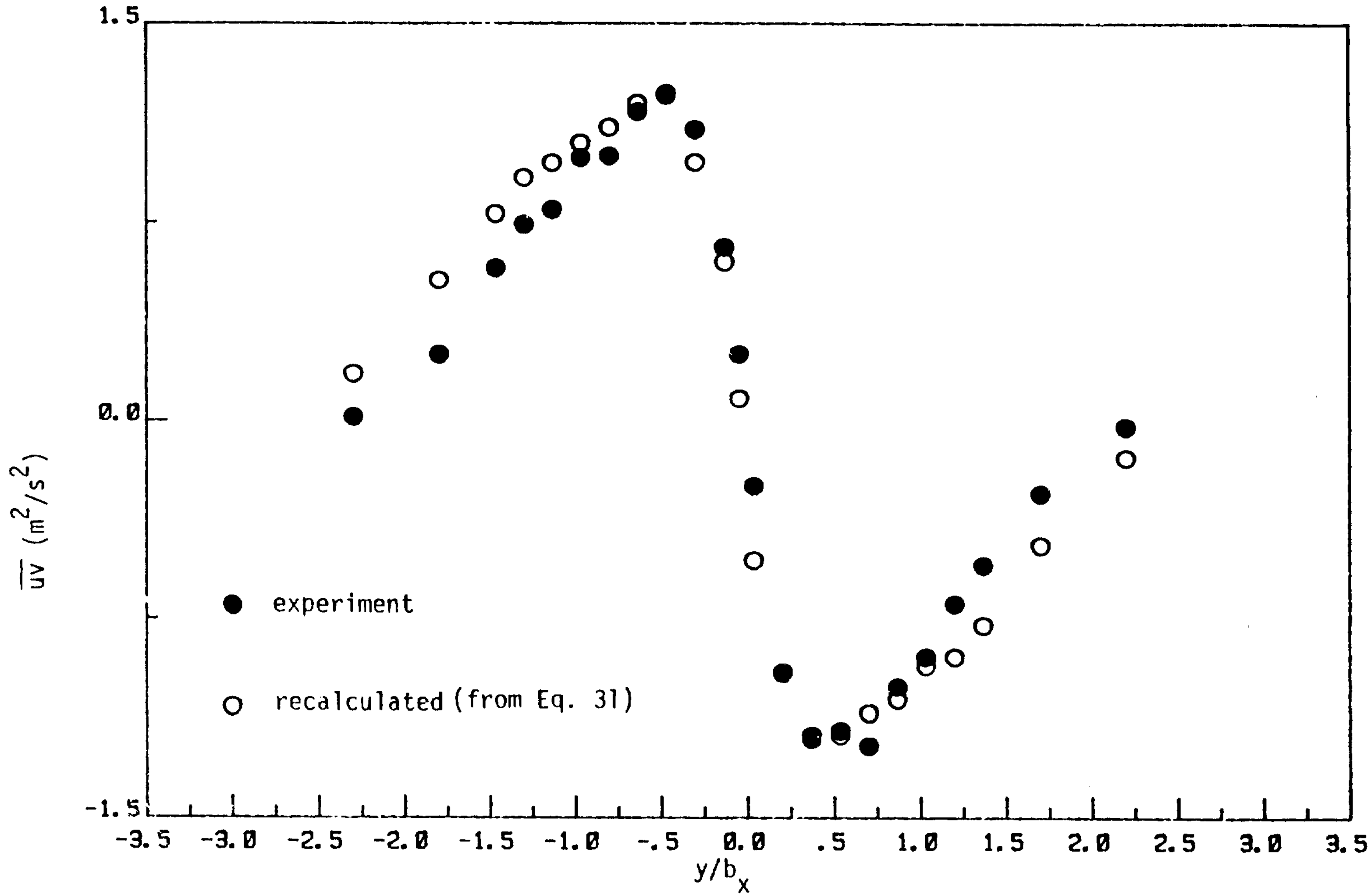

Figure 44. Recalculation of $\overline{uv}$ using ϵ_x compared to $\overline{uv}$ as determined experimentally: $x/L = .055^x$

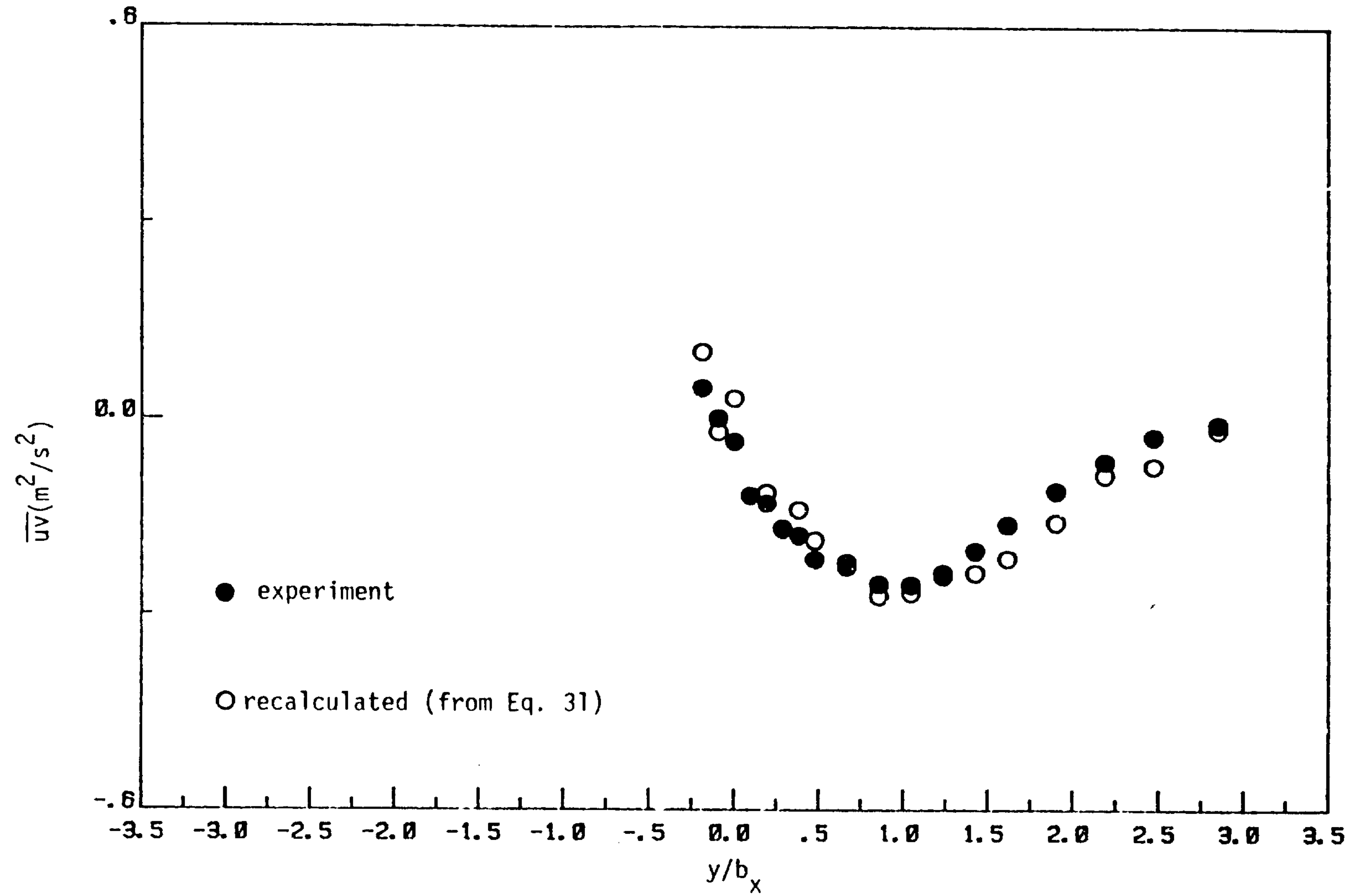

Figure 45. Recalculation of $\overline{uv}$ using ϵ_x compared to $\overline{uv}$ as determined experimentally: x/L = 1.928

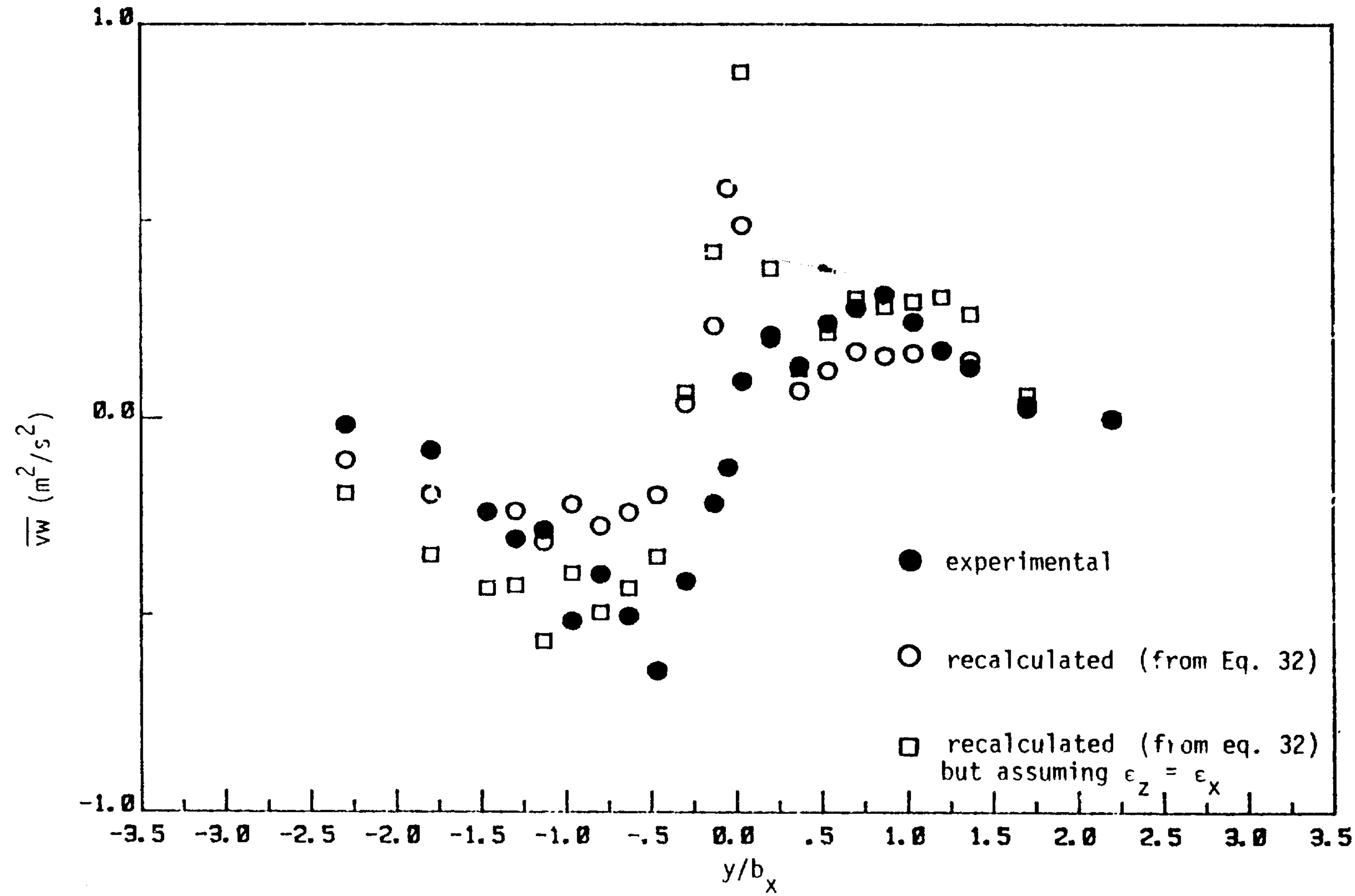

Figure 46. Recalculation of $\overline{vw}$ using ε_x and ε_z, compared to $\overline{vw}$ as determined experimentally: $x/L = 0.055$

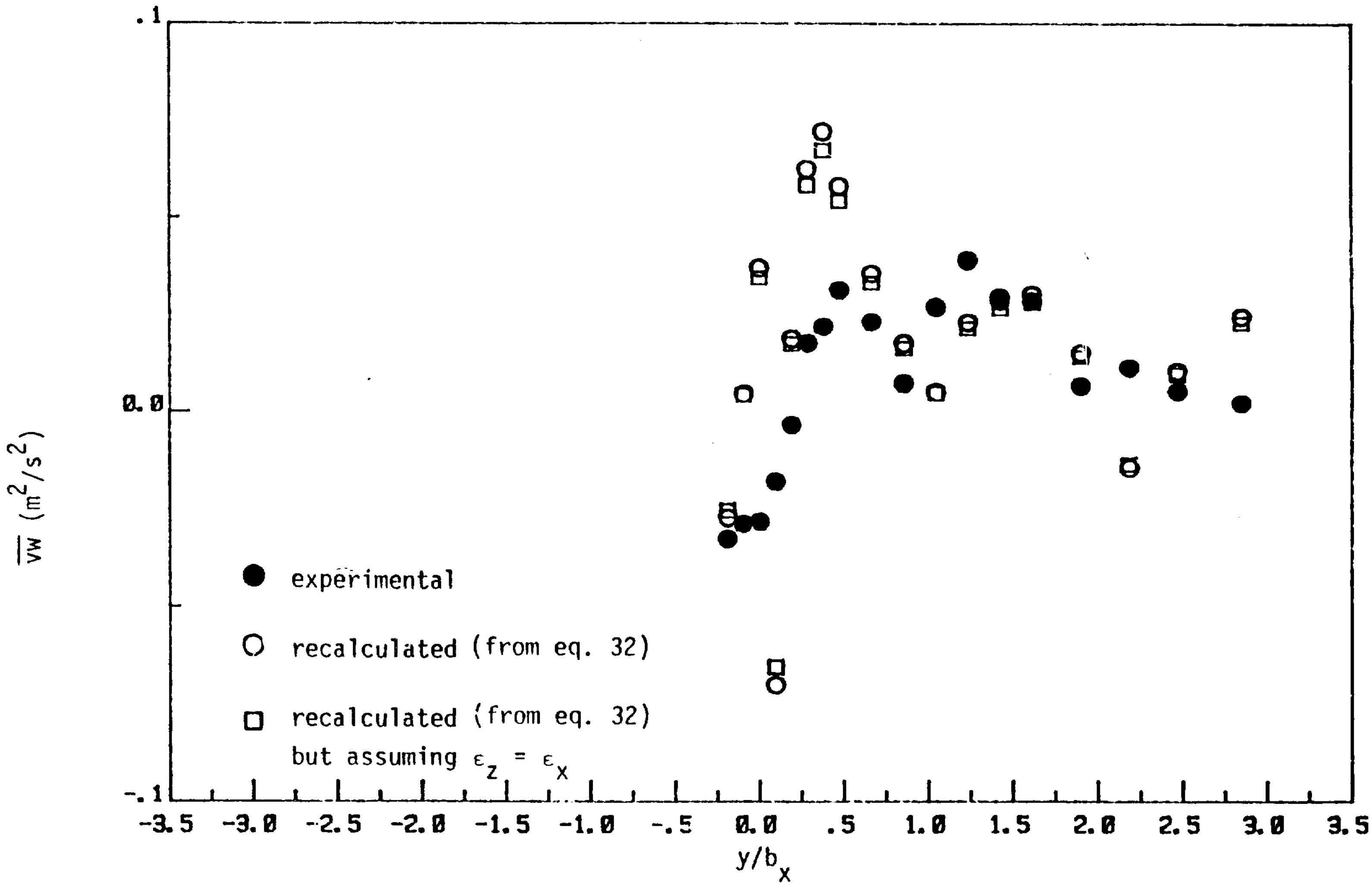

Figure 47. Recalculation of $\overline{vw}$ using ε_x and ε_z compared to $\overline{vw}$ as determined experimentally: x/L = 1.928

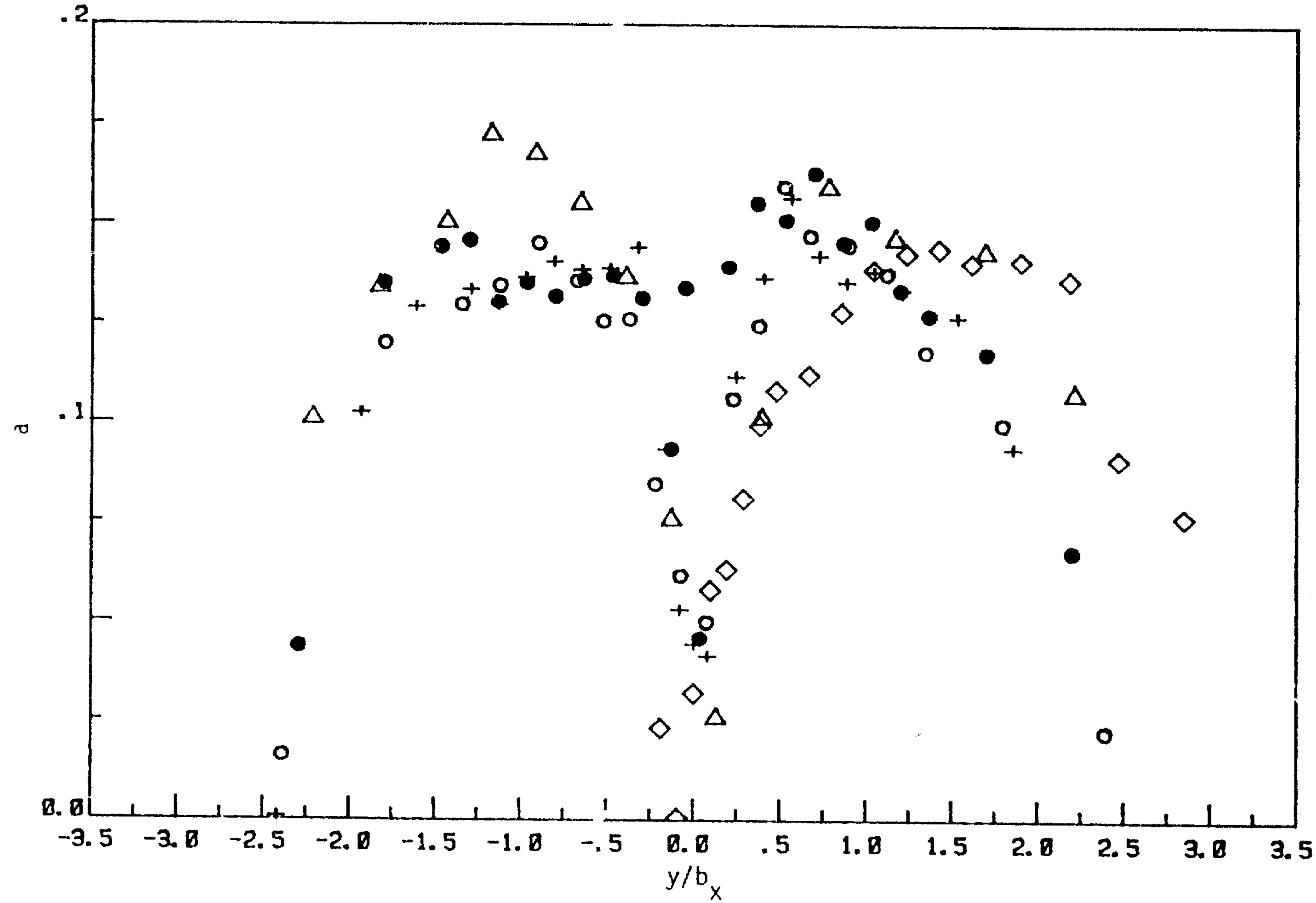

Figure 48. Structure parameter as calculated from eq. (34)
(symbols as in Figure 43)

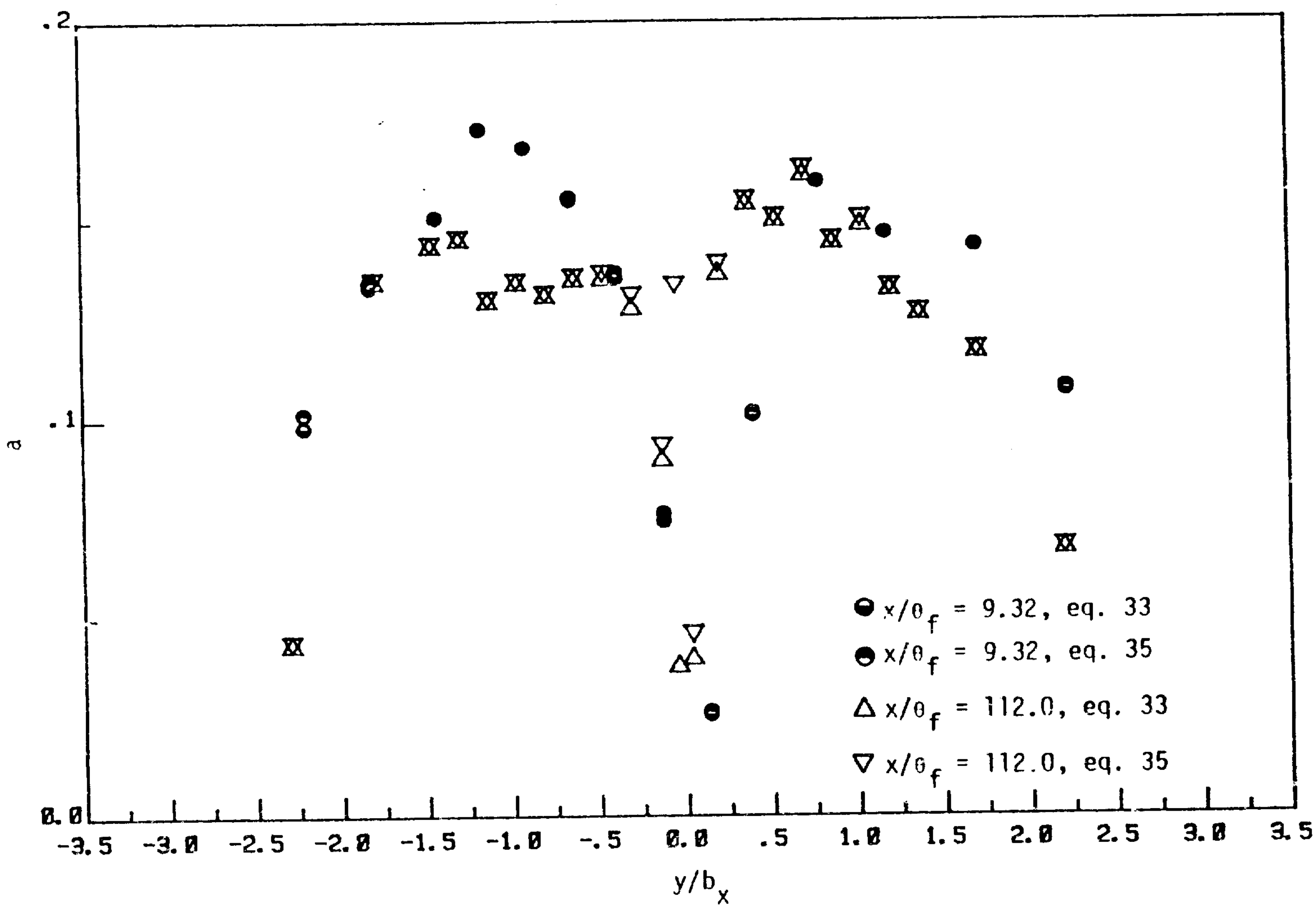

Figure 49. Comparison of structure parameter as calculated by from eq. 33 and eq. 35

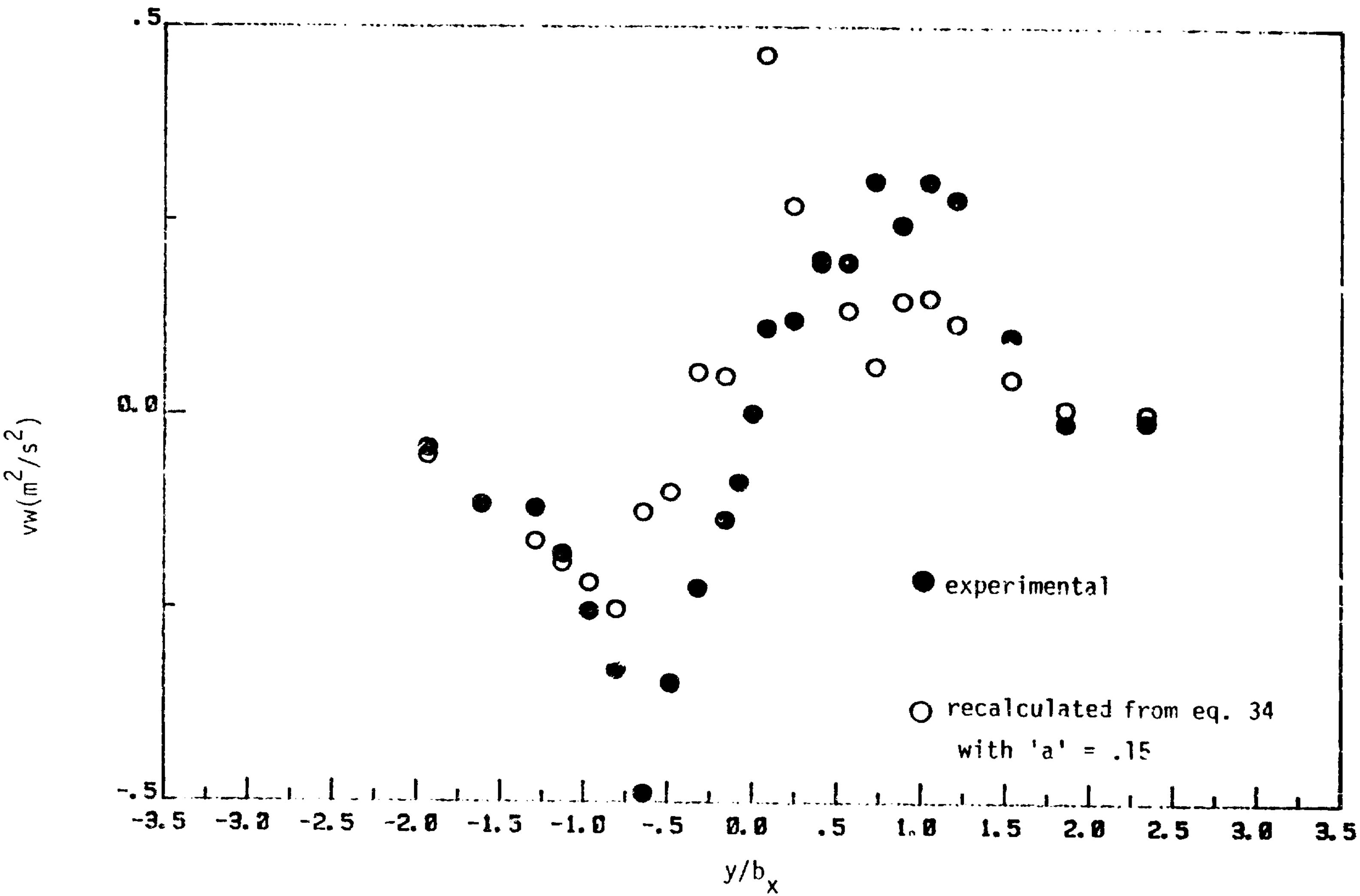

Figure 50. Recalculated value of $\overline{vw}$ with a = .15 compared to $\overline{vw}$ obtained experimentally at x/L = .138

APPENDIX

TABLES OF EXPERIMENTAL DATA

KEY TO SYMBOLS USED IN DATA TABLES

Beta	angle between mean flow vectors and the chordline
Gama	angle between mean flow vectors and the free streamline
Delta*sub x	δ_1 meters
Delta*sub z	δ_2 meters
Theta sub x	δ_{11} meters
Theta sub z	δ_{22} meters
Theta sub xz	δ_{12} meters
Theta sub zx	δ_{21} meters
Pstatic	static pressure in inches of alcohol
u/Uinf	local chordwise velocity/reference velocity
w/Uinf	local spanwise velocity/reference velocity
U bar 1	u/U_∞ from 3-D hot wire probe
V bar	normal velocity component/U_∞ from 3-D hot wire probe
W bar	W/U_∞ from 3-D hot wire probe
uu bar	$\sqrt{\overline{u^2}}/U_\infty \times 100$
vv bar	$\sqrt{\overline{v^2}}/U_\infty \times 100$
ww bar	$\sqrt{\overline{w^2}}/U_\infty \times 100$
uv bar	$\frac{\overline{uv}}{U_\infty^2} \times 10^4$
Y(mm)	distance from wake centerline or wall in millimeters
uw bar	$\frac{\overline{uw}}{U_\infty^2} \times 10^4$

vw bar	$\frac{\overline{vw}}{U_\infty^2} \times 10^4$
uuu bar	$\frac{\bar{u}^3}{U_\infty^3} \times 10^5$
vvv bar	$\frac{\bar{v}^3}{U_\infty^3} \times 10^5$
www bar	$\frac{\bar{w}^3}{U_\infty^3} \times 10^5$
uuv bar	$\frac{\overline{u^2 v}}{U_\infty^3} \times 10^5$
uuw bar	$\frac{\overline{u^2 w}}{U_\infty^3} \times 10^5$
vvu bar	$\frac{uv^2}{U_\infty^3} \times 10^5$
vvw bar	$\frac{\overline{v^2 w}}{U_\infty^3} \times 10^5$
wwu bar	$\frac{\overline{uw^2}}{U_\infty^3} \times 10^5$
wwv bar	$\frac{vw^2}{U_\infty^3} \times 10^5$
uvw bar	$\frac{\overline{uvw}}{U_\infty^3} \times 10^5$

Table A1

Symmetric Flat Plate Wake Data (x = 177.8) using IIHR probe

Y_{mm}	u/U_{inf}	uu_{bar}	vv_{bar}	ww_{bar}	uv_{bar}	vw_{bar}	uw_{bar}
9.62	.81	6.273	6.460	3.476	+10.879	-14.358	-7.370
5.81	.76	6.219	6.764	3.755	10.091	-13.694	-9.821
2.00	.72	5.381	6.709	.317	5.551	-6.361	-15.538
.73	.709	5.098	6.422	4.713	4.056	-1.497	-17.972
-.54	.710	4.933	6.009	5.075	-2.966	+4.693	-17.587
-1.30	.711	5.131	5.758	5.349	-4.775	6.742	-17.594
2.06	.714	5.292	5.645	5.613	-7.217	9.636	-17.105
2.32	.717	5.530	5.572	5.724	-12.607	10.014	-15.674
4.09	.729	5.799	5.084	5.873	-12.315	12.802	-14.390
5.36	.742	5.086	4.965	5.926	-15.098	14.263	-13.412
7.90	.769	6.409	4.931	5.829	-15.113	14.137	-11.317
12.98	.839	6.259	4.819	5.279	-13.286	12.468	-9.424
18.06	.882	5.397	4.504	4.570	-9.857	8.262	-6.942
23.84	.930	4.648	3.660	3.646	-6.184	5.515	-4.753
33.0	.982	2.199	2.063	1.837	-1.058	1.273	-2.113
48.24	1.00	.477	.792	.603	-.002	.099	-.339

TABLE A2

Airfoil Boundary Layer Data at x/L = -.220 (central plane)

```
RUN #       4
DATE OF RUN    1981

Urefernce (m/s)     =   21.84
X loca.=   -.220

Uinfinity (m/s)   =   23.19

Integral Parameters

Delta*sub x = .4776659E-02
Delta*sub z =.3158540E-01
Theta sub x = .3417375E-02

Theta sub z = .6247743E-03
Theta sub xz =  .2697690E-01
Theta sub zx =  .1681640E-03

Shape Factor H = 1.398

Boundary Layer Profile
```

Y mm.	u/Uinf	Gama	w/Uinf	Beta	Pstatic
.51	.454	3.37	.027	33.37	-.0016
.76	.500	4.18	.037	34.18	.0007
1.02	.522	4.57	.042	34.57	.0043
1.27	.535	4.51	.042	34.51	.0062
1.52	.550	4.43	.043	34.43	.0043
2.03	.574	4.47	.045	34.47	.0021
2.54	.596	4.35	.045	34.35	0.0000
3.05	.618	4.20	.045	34.20	-.0012
3.56	.639	4.10	.046	34.10	-.0099
4.83	.678	3.69	.044	33.69	-.0132
6.10	.716	3.26	.041	33.26	-.0252
7.37	.737	3.07	.039	33.07	-.0161
8.64	.762	2.68	.036	32.68	-.0206
9.91	.795	2.31	.032	32.31	-.0301
12.45	.842	1.77	.026	31.77	-.0294
14.99	.881	1.19	.018	31.19	-.0303
18.80	.942	.55	.009	30.55	-.0414
22.61	.984	.16	.003	30.16	-.0455
26.42	1.000	.05	.001	30.05	-.0429
30.23	1.000	0.00	0.000	30.00	-.0392

TABLE A3

Airfoil Boundary Layer Data at x/L = -.124 (central plane)

RUN # 1
DATE OF RUN 29881

Urefernce (m/s) = 21.[illegible]
X loca.= -.124

Uinfinity (m/s) = 22.61

Integral Parameters

Delta*sub x = .6346047E-02
Delta*sub z =.7913063E-01
Theta sub x = .4398430E-02

Theta sub z = .7212564E-03
Theta sub xz = .7305337E-01
Theta sub zx = .2687818E-03

Shape Factor H = 1.443

Boundary Layer Profile

Y mm.	u/Uinf	Gama	w/Uinf	Beta	Pstatic
.51	.416	4.80	.035	34.80	.0428
1.27	.480	6.09	.051	36.09	.0612
2.03	.526	6.27	.056	36.27	.0635
3.30	.576	5.87	.059	35.87	.0601
5.08	.630	5.20	.057	35.20	.0583
7.11	.678	4.36	.052	34.36	.0520
10.16	.742	3.27	.042	33.27	.0487
12.45	.798	2.44	.034	32.44	.0407
18.29	.887	1.20	.019	31.20	.0235
25.91	.977	.04	.001	30.04	.0173
33.53	.991	-.13	-.002	29.87	.0287
43.69	.997	-.28	-.005	29.72	.0214
58.93	.998	-.15	-.003	29.85	.0182
74.17	1.000	0.00	0.000	30.00	.0145

TABLE A4

Airfoil Boundary Layer Data at x/L = - .124 (-6" plane)

```
RUN #      2
DATE OF RUN  29881

Urefernce (m/s)      =   21.84
X loca.=    -.124

Uinfinity (m/s)   =   22.66

Integral Parameters

Delta*sub x = .5580028E-02
Delta*sub z =.4887007E-01
Theta sub x = .3946812E-02

Theta sub z = .9489292E-03
Theta sub xz =  .4355173E-01
Theta sub zx = .2616808E-03

Shape Factor H = 1.414

Boundary Layer Profile
```

Y mm.	u/Uinf	Gama	w/Uinf	Beta	Pstatic
.51	.435	4.35	.033	34.35	.0369
.76	.481	5.61	.047	35.61	.0425
1.27	.521	6.06	.055	36.06	.0459
1.78	.554	6.00	.058	36.00	.0465
2.54	.584	5.93	.061	35.93	.0434
3.30	.609	5.69	.061	35.69	.0412
4.57	.646	5.20	.059	35.20	.0377
5.84	.673	4.87	.057	34.87	.0365
8.38	.732	3.90	.050	33.90	.0355
11.18	.779	3.23	.044	33.23	.0294
13.46	.831	2.50	.036	32.50	.0236
18.54	.908	1.33	.021	31.33	.0177
23.62	.971	.43	.007	30.43	.0093
31.24	.998	.05	.001	30.06	-.0006
38.86	1.001	-.02	-.000	29.98	-.0002
46.48	1.000	0.00	0.000	30.00	-.0019

TABLE A5

Airfoil Boundary Layer Data at x/L = - .124 (+6" plane)

RUN # 3
DATE OF RUN 29881

Urefernce (m/s) = 21.84
X loca.= -.124

Uinfinity (m/s) = 22.65

Integral Parameters

Delta*sub x = .5613346E-02
Delta*sub z =.4455488E-01
Theta sub x = .3972160E-02

Theta sub z = .8642757E-03
Theta sub xz = .3918079E-01
Theta sub zx = .2392422E-03

Shape Factor H = 1.413

Boundary Layer Profile

Y mm.	u/Uinf	Gama	w/Uinf	Beta	Pstatic
.51	.418	5.36	.039	35.36	.1560
.76	.460	5.58	.045	35.58	.1640
1.02	.496	5.91	.051	35.91	.1640
1.27	.520	5.84	.053	35.84	.1000
1.78	.548	5.80	.056	35.80	.1620
2.29	.577	5.56	.056	35.56	.1560
3.05	.605	5.36	.057	35.36	.1540
4.32	.635	4.91	.055	34.91	.1520
5.59	.671	4.46	.052	34.46	.1450
6.86	.691	4.19	.051	34.18	.1560
8.13	.725	3.63	.046	33.63	.1450
10.67	.776	2.88	.039	32.88	.1380
13.21	.825	2.19	.032	32.19	.1280
15.75	.864	1.65	.025	31.65	.1260
19.56	.920	1.00	.016	31.00	.1200
23.37	.963	.49	.008	30.49	.1160
29.72	.997	.10	.002	30.10	.1110
36.07	1.001	.02	.000	30.01	.1130
42.42	1.000	-.03	-.011	29.97	.1070

TABLE A6

Airfoil Roundary Layer Data at x/L = - .014 (far side)

RUN # 5
DATE OF RUN 1981

Urefernce (m/s) = 21.84
X loca.= -.014

Uinfinity (m/s) = 22.23

Integral Parameters

Delta*sub x = .7026?38E-02
Delta*sub z =.5247342E-01
Theta sub x = .4873316E-02

Theta sub z = .1921229E-02
Theta sub xz = .4601236E-01
Theta sub zx = .5658745E-03

Shape Factor H = 1.442

Boundary Layer Profile

Y mm.	u/Uinf	Gama	w/Uinf	Beta	Pstatic
.51	.479	12.62	.107	42.62	.2285
.76	.489	12.53	.109	42.53	.2258
1.02	.495	12.55	.110	42.56	.2299
1.27	.507	12.23	.110	42.23	.2268
1.52	.517	12.01	.110	42.01	.2260
1.78	.523	11.93	.110	41.93	.2270
2.03	.534	11.44	.108	41.44	.2229
2.54	.551	10.82	.105	40.82	.2204
3.05	.560	10.72	.106	40.72	.2233
3.56	.573	10.33	.104	40.33	.2216
4.06	.584	10.03	.103	40.03	.2228
5.08	.607	9.46	.101	39.46	.2201
6.10	.637	8.55	.096	38.55	.2140
8.13	.678	7.36	.088	37.36	.2074
10.16	.702	6.72	.083	36.72	.2188
12.70	.762	5.26	.070	35.26	.1979
15.24	.811	4.17	.059	34.17	.1802
20.32	.885	2.60	.040	32.60	.1695
25.40	.948	1.43	.024	31.43	.1564
30.48	.978	.79	.013	30.79	.1527
35.56	.992	.47	.008	30.47	.1429
43.18	.999	.11	.002	30.11	.1214
50.80	1.000	0.00	0.000	30.00	.1216

TABLE A7

Airfoil Boundary Layer Data at x/L = - .014 (near side)

RUN # 6
DATE OF RUN 1981

Urefernce (m/s) = 21.84
X loca.= -.014

Uinfinity (m/s) = 22.07

Integral Parameters

Delta*sub x = .7871451E-02
Delta*sub z =.4484890E-01
Theta sub x = .5212710E-02

Theta sub z = .5540243E-02
Theta sub xz = .4255312E-01
Theta sub zx = .5575653E-02

Shape Factor H = 1.510

Boundary Layer Profile

Y mm.	u/Uinf	Gama	w/Uinf	Beta	Pstatic
.51	.452	12.23	.098	42.23	.2140
.76	.465	11.88	.098	41.88	.2121
1.02	.482	11.25	.096	41.25	.2080
1.27	.493	11.10	.097	41.10	.2051
1.78	.515	10.55	.096	40.55	.2012
2.29	.531	10.28	.096	40.28	.2025
2.79	.549	9.81	.095	39.81	.2007
3.30	.555	9.82	.096	39.82	.2057
4.32	.586	9.02	.093	39.02	.2021
5.33	.610	8.42	.090	38.42	.1988
6.35	.636	7.77	.087	37.77	.1931
8.38	.668	6.96	.082	36.96	.1952
10.41	.710	5.97	.074	35.97	.1951
12.95	.758	4.86	.064	34.86	.1832
15.49	.797	3.90	.054	33.90	.1800
20.57	.872	2.25	.034	32.25	.1649
25.65	.938	1.02	.017	31.03	.1475
30.73	.976	.41	.007	30.41	.1394
35.81	.989	.21	.004	30.21	.1322
43.43	.997	.07	.001	30.07	.1212
51.05	.999	.02	.000	30.02	.1022
58.67	1.000	0.00	0.000	30.00	.1065

TABLE A8

Airfoil Wake Data at x/L = .014 (central plane)

RUN # 7
DATE OF RUN 2981

Urefernce (m/s) = 21.84
X loca.= .140

Uinfinity (m/s) = 22.17

Integral Parameters

Delta*sub x = .1640730E-01
Delta*sub z =.1054121E+00
Theta sub x = .1085906E-01

Theta sub z = .4158555E-02
Theta sub xz = .9038031E-01
Theta sub zx = .1375550E-02

Shape Factor H = 1.51i

Wake Profile

Y mm.	u/Uinf	Gama	w/Uinf	Beta	Pstatic
46.74	1.002	01	.000	30.01	.1135
41.66	1.003	.11	.002	30.11	.1146
36.58	.996	.25	.004	30.25	.1295
31.50	.988	50	.009	30.50	.1293
26.42	.942	1.18	.019	31.18	.1444
23.88	.913	1.65	.026	31.65	.1558
21.34	.881	2.36	.036	32.36	.1653
18.80	.843	3.02	.044	33.02	.1720
16.26	.809	3.92	.055	33.92	.1739
13.72	.766	4.85	.065	34.85	.1837
11.18	.714	6.16	.077	36.16	.1953
9.65	.678	7.02	.084	37.03	.2032
8.13	.655	7.69	.088	37.69	.2035
6.60	.627	8.51	.094	38.51	.2019
5.08	.580	9.98	.102	39.97	.2172
4.32	.560	10.51	.104	40.51	.2170
3.56	.542	11.10	.106	41.10	.2180
2.79	.515	11.91	.109	41.91	.2186
2.29	.500	12.10	.107	42.10	.2192
1.78	.491	12.17	.106	42.17	.2141
1.27	.480	12.23	.104	42.23	.2088
.76	.453	13.21	.106	43.21	.2121
.25	.439	14.00	.109	44.00	.2152

TABLE A8 (Continued)

Wake Profile

Y mm.	u/Uinf	Gama	w/Uinf	Beta	Pstatic
-.25	.439	14.16	.111	44.16	.2154
-.76	.445	14.15	.112	44.15	.2140
-1.27	.465	13.34	.110	43.34	.2118
-1.78	.469	13.86	.116	43.86	.2221
-2.54	.499	12.82	.114	42.82	.2180
-3.30	.523	12.29	.114	42.29	.2200
-4.32	.554	11.29	.111	41.29	.2154
-5.33	.580	10.47	.107	40.47	.2157
-6.60	.604	9.69	.103	39.69	.2161
-7.87	.636	8.70	.097	38.70	.2046
-9.65	.669	7.87	.093	37.87	.2085
-11.43	.703	6.82	.084	36.82	.2071
-13.97	.747	5.76	.075	35.76	.2024
-17.78	.810	4.23	.060	34.23	.1964
-21.59	.869	2.91	.044	32.91	.1856
-26.67	.936	1.57	.026	31.57	.1673
-31.75	.976	.89	.015	30.89	.1545
-39.37	.991	.41	.007	30.41	.1408
-46.99	1.000	.12	.002	30.12	.1221
-54.61	1.000	0.00	0.000	30.00	.1205

TABLE A9

Airfoil Wake Data at x/L = .027 (central plane)

RUN # 8
DATE OF RUN 2981

Urefernce (m/s) = 21.84
X loca.= .027

Uinfinity (m/s) = 22.26

Integral Parameters

Delta*sub x = .1591637E-01
Delta*sub z =.1157773E+00
Theta sub x = .1095042E-01

Theta sub z = .3777430E-02
Theta sub xz = .1010357E+00
Theta sub zx = .1174841E-02

Shape Factor H = 1.453

Wake Profile

Y MM.	u/Uinf	Gama	w/Uinf	Beta	Pstatic
-54.86	1.001	.35	.006	30.35	.1121
-44.70	.993	.09	.001	30.08	.1317
-37.08	.987	.30	.005	30.30	.1453
-29.46	.969	.86	.015	30.86	.1500
-21.84	.879	2.48	.038	32.48	.1802
-16.76	.807	3.94	.056	33.94	.1871
-11.68	.722	5.93	.075	35.93	.1769
-9.14	.677	7.05	.084	37.05	.1980
-6.60	.631	8.27	.092	38.27	.1970
-5.08	.589	9.38	.097	39.38	.2045
-4.06	.558	10.76	.106	40.76	.2097
-3.05	.545	10.64	.102	40.64	.2047
-2.03	.522	10.71	.099	40.71	.2013
-1.02	.505	11.13	.099	41.13	.2009
0.00	.500	11.15	.099	41.15	.2012
1.02	.509	10.78	.097	40.78	.2002
2.03	.538	9.94	.094	39.94	.1912
3.05	.560	9.48	.093	39.48	.1947
4.32	.589	8.88	.092	38.88	.1927
5.59	.615	8.17	.088	38.17	.1931
7.37	.650	7.38	.084	37.38	.1918
9.91	.697	6.07	.074	36.07	.1893
12.45	.741	5.19	.067	35.19	.1871
14.99	.788	4.06	.056	34.06	.1771
20.07	.865	2.39	.036	32.39	.1585
25.15	.928	1.20	.019	31.20	.1491
32.77	.977	.43	.007	30.44	.1481
40.39	.992	.19	.003	30.19	.1304
48.01	.998	.07	.001	30.06	.1170
55.63	1.000	0.00	0.000	30.00	.1113

TABLE A10

Airfoil Wake Data at x/L = .027 (-6" plane)

RUN # 9
DATE OF RUN 3981

Urefernce (m/s) = 21.84
X loca.= .027

Uinfinity (m/s) = 21.94

Integral Parameters

Delta*sub x = .1524869E-01
Delta*sub z =.1011579E+00
Theta sub x = .1042631E-01

Theta sub z = .3805762E-02
Theta sub xz = .6703996E-01
Theta sub zx = .1130750E-02

Shape Factor H = 1.463

Wake Profile

Y mm.	u/Uinf	Gama	w/Uinf	Beta	Pstatic
51.82	1.003	.00	.000	30.00	.1243
44.20	.999	.14	.002	30.14	.1367
36.58	.998	.26	.005	[illegible].26	.1385
28.96	.977	.64	.011	[illegible]0.64	.1375
21.34	.876	2.27	.035	32.27	.1746
16.26	.806	3.70	.052	33.70	.1854
13.72	.758	4.69	.062	34.69	.1928
11.18	.717	5.58	.070	35.58	.1920
8.64	.673	6.57	.078	36.57	.1939
6.10	.618	7.84	.085	37.84	.1998
4.32	.579	8.63	.088	38.63	.2031
3.05	.552	8.98	.087	38.98	.2001
2.29	.539	9.50	.090	39.50	.2020
1.52	.526	9.88	.092	39.88	.2023
.76	.520	10.29	.094	40.29	.2029
0.00	.516	10.69	.097	40.69	.2057
-.76	.524	10.67	.099	40.67	.2045
-1.52	.529	10.86	.102	40.86	.2082
-2.29	.549	10.31	.100	40.31	.2052
-3.56	.563	10.19	.101	40.19	.2102
-5.33	.614	8.56	.092	38.56	.2014
-7.11	.642	7.85	.088	37.85	.2023
-9.65	.695	6.47	.079	36.47	.1969
-12.19	.738	5.43	.070	35.43	.1969
-17.27	.826	3.59	.052	33.59	.1860
-22.35	.903	2.23	.035	32.23	.1740
-29.97	.974	1.11	.019	31.11	.1630
-37.59	.997	.62	.011	30.62	.1470
-45.21	1.000	.54	.208	30.54	.1359

TABLE A11

Airfoil Wake Data at x/L = .027 (+6" plane)

RUN # 10
DATE OF RUN 3981

Urefernce (m/s) = 21.84
X loca.= .027

Uinfinity (m/s) = 22.15

Integral Parameters

Delta*sub x = .1577514E-01
Delta*sub z =.1282676E+00
Theta sub x = .1068428E-01

Theta sub z = .3449251E-02
Theta sub xz = .1135899E+00
Theta sub zx = .1097508E-02

Shape Factor H = 1.476

Wake Profile

Y mm.	u/Uinf	Gama	w/Uinf	Beta	Pstatic
60.96	1.010	-.18	-.003	29.82	.1106
53.34	1.008	-.11	-.002	29.89	.1207
45.72	1.006	-.03	-.000	29.97	.1295
38.10	1.000	.07	.001	30.07	.1421
30.48	.984	.36	.006	30.36	.1463
22.86	.907	1.39	.022	31.39	.1695
17.78	.826	2.58	.037	32.58	.1911
12.70	.743	4.14	.054	34.14	.2023
10.16	.702	5.07	.062	35.07	.2054
7.62	.651	6.08	.069	36.08	.2117
5.84	.610	7.12	.076	37.12	.2205
4.06	.569	8.01	.080	38.01	.2244
3.05	.543	8.61	.082	38.61	.2257
2.03	.527	9.11	.085	39.11	.2250
1.52	.520	9.29	.085	39.29	.2248
1.02	.513	9.74	.088	39.74	.2271
.51	.509	9.97	.089	39.97	.2287
0.00	.510	10.13	.091	40.13	.2275
-.76	.513	10.52	.095	40.52	.2348
-1.78	.523	18.61	.098	40.61	.2360
-3.05	.549	10.24	.099	40.24	.2361
-4.32	.574	9.72	.098	39.72	.2358
-6.10	.614	8.59	.093	38.59	.2302
-8.64	.658	7.29	.084	37.29	.2298
-12.45	.724	5.50	.070	35.50	.2266
-17.53	.809	3.59	.051	33.59	.2120
-22.61	.889	2.33	.036	32.33	.1975
-30.23	.961	.95	.016	30.95	.1866
-37.85	.991	.38	.007	30.38	.1654
-45.47	.995	.24	.004	30.24	.1519
-53.09	1.000	.05	.001	30.05	.1430
-60.71	1.000	0.00	0.000	30.00	.1369

TABLE A12

Airfoil Wake Data at x/L = .041 (central plane)

RUN # 11
DATE OF RUN 3981

Urefernce (m/s) = 21.84
X loca.= .041

Uinfinity (m/s) = 22.23

Integral Parameters

Delta*sub x = .1587362E-01
Delta*sub z =.1556493E+00
Theta sub x = .1118588E-01

Theta sub z = .4402381E-02
Theta sub xz = .1409030E+00
Theta sub zx = .1127246E-02

Shape Factor H = 1.419

Wake Profile

Y mm.	u/Uinf	Gama	w/Uinf	Beta	Pstatic
73.66	.999	-.01	-.000	29.99	.1135
63.50	.995	.46	.008	30.46	.1258
53.34	.994	.48	.008	30.48	.1289
43.18	.988	.64	.011	30.64	.1463
33.02	.982	.81	.014	30.81	.1483
22.86	.903	2.04	.032	32.04	.1658
15.24	.792	4.18	.058	34.18	.1883
7.62	.666	6.88	.080	36.88	.1940
5.08	.609	8.10	.087	38.10	.2011
3.05	.567	9.16	.091	39.16	.2054
1.52	.547	9.53	.092	39.53	.2017
.51	.538	9.81	.093	39.81	.2030
0.00	.532	10.15	.095	40.15	.2053
-.51	.538	9.88	.094	39.88	.2032
-1.02	.540	9.90	.094	39.90	.2035
-2.03	.552	9.56	.093	39.56	.2006
-3.56	.575	9.24	.094	39.24	.2050
-5.59	.614	8.37	.090	38.37	.2058
-8.13	.662	7.31	.085	37.31	.2067
-11.94	.732	5.70	.073	35.70	.2012
-15.75	.798	4.30	.060	34.30	.1936
-20.83	.875	2.83	.043	32.83	.1814
-27.18	.947	1.49	.025	31.49	.1676
-34.80	.976	.97	.017	30.97	.1640
-43.69	.991	.56	.010	30.56	.1401
-53.85	.994	.36	.006	30.36	.1308
-64.01	.997	.18	.003	30.18	.1199
-74.17	1.000	.00	.001	30.00	.1127

TABLE A13

Airfoil Wake Data at x/L = .055 (central plane)

RUN # 12
DATE OF RUN 3981

Urefernce (m/s) = 21.84
X loca.= .055

Uinfinity (m/s) = 22.14

Integral Parameters

Delta*sub x = .1459999E-01
Delta*sub z =.1879447E+00
Theta sub x = .1045328E-01

Theta sub z = .2475021E-02
Theta sub xz = .1742300E+00
Theta sub zx = .8853995E-03

Shape Factor H = 1.397

Wake Profile

Y mm.	u/Uinf	Gama	w/Uinf	Beta	Pstatic
-83.31	1.005	-.44	-.008	29.56	.0961
-73.15	1.002	-.38	-.007	29.62	.0961
-62.99	1.000	-.28	-.005	29.72	.1130
-52.83	.995	-.10	-.002	29.90	.1259
-42.67	.997	.00	.000	30.00	.1278
-33.78	.992	.21	.004	30.21	.1357
-26.16	.969	.70	.012	30.70	.1353
-19.81	.889	1.96	.030	31.96	.1658
-14.73	.819	3.26	.047	33.26	.1710
-10.92	.752	4.55	.060	34.55	.1818
-7.11	.696	5.65	.069	35.65	.1707
-4.57	.636	6.98	.078	36.98	.1869
-2.54	.602	7.69	.081	37.69	.1872
-1.02	.573	8.32	.084	38.32	.1909
0.00	.565	8.36	.083	38.36	.1897
.51	.569	8.23	.082	38.22	.1866
1.02	.575	8.01	.081	38.01	.1785
1.52	.569	8.21	.082	38.21	.1855
2.54	.575	8.14	.082	38.14	.1833
4.06	.587	7.83	.081	37.83	.1870
6.10	.627	6.88	.076	36.89	.1770
8.64	.672	5.93	.070	35.93	.1725
16.26	.798	3.31	.046	33.31	.1669
23.88	.910	1.40	.022	31.40	.1449
34.04	.978	.42	.007	30.42	.1514
44.20	.989	.19	.003	30.19	.1371
54.36	.993	.16	.003	30.16	.1291
64.52	.996	.17	.003	30.17	.1178
74.68	.997	.19	.003	30.19	.1126
56.90	1.000	-2.97	-1.147	27.03	.0993

TABLE A13 (Continued)

Turbulence Data

X/L Location = .055
Reference Velocity = 21.8 m/s

Wake Profile

Y mm.	Ubar	Vbar	Wbar	uubar	vvbar	wwbar
43.69	1.000	.000	.002	.558	.778	.890
33.53	.994	.001	.003	1.440	1.703	1.772
25.91	.952	-.000	.001	4.244	3.817	4.210
20.83	.895	-.002	.012	5.674	5.120	5.715
18.29	.859	-.002	.019	6.303	5.701	6.126
15.75	.825	.004	.026	6.788	6.052	6.570
13.21	.783	.006	.032	7.266	6.566	7.087
10.67	.740	.011	.038	7.724	6.940	7.211
8.13	.694	.015	.045	7.897	6.794	7.426
5.59	.644	.018	.046	7.723	6.993	7.435
3.05	.602	.023	.052	7.037	6.802	7.082
.51	.572	.033	.066	6.032	6.534	7.261
-.76	.570	.040	.081	6.036	6.564	7.588
-2.03	.579	.042	.086	6.616	6.709	7.952
-4.57	.613	.051	.092	7.876	6.894	8.355
-7.11	.662	.058	.085	8.313	7.037	8.485
-9.65	.711	.062	.077	8.089	6.848	8.242
-12.19	.755	.064	.063	7.538	6.677	7.601
-14.73	.798	.065	.057	7.335	6.555	7.592
-17.27	.837	.067	.043	6.801	6.006	6.772
-19.81	.876	.067	.034	6.087	5.709	6.063
-22.35	.909	.068	.024	5.335	5.190	5.314
-27.43	.962	.067	.007	3.637	3.728	3.361
-35.05	.992	.067	-.011	1.072	1.617	1.191
-45.21	.995	.068	-.015	.481	.817	.663

TABLE A13 (Continued)

Profile continued at X/L = .055

Y mm.	uvbar	uwbar	vwbar	uuubar	vvvbar	wwwbar
43.69	-.049	.027	.03	-.002	-.001	.001
33.53	-.547	.627	-.14	.630	.400	-.964
25.91	-5.893	2.112	.48	9.611	1.883	-4.075
20.83	-11.54	.705	2.67	10.649	1.743	-4.621
18.29	-14.57	1.907	3.59	11.487	5.278	-6.527
15.75	-18.7[illegible]	1.053	5.11	9.449	-.708	-5.240
13.21	-21.14	-.557	6.56	6.700	6.456	-6.142
10.67	-25.83	1.366	5.85	6.631	7.680	-2.970
8.13	-24.60	-3.301	5.04	-.253	8.800	-.094
5.59	-25.30	-2.125	2.79	-12.04	10.199	.203
3.05	-19.99	-6.099	4.23	-15.12	4.814	2.375
.51	-5.282	-6.074	1.96	-9.937	.018	-.447
-.76	5.226	-4.799	-2.67	-8.667	-5.607	-1.597
-2.03	13.694	-6.051	-4.59	-16.48	-3.931	-4.271
-4.57	23.008	-11.20	-8.72	-19.39	-9.639	-3.926
-7.11	25.856	-17.82	-13.48	-7.130	-5.490	1.066
-9.65	24.408	-13.18	-10.57	3.687	-4.966	2.195
-12.19	20.912	-10.44	-8.36	5.626	-7.206	-.188
-14.73	20.784	-15.07	-10.83	11.366	-10.72	3.759
-17.27	16.665	-9.671	-5.99	12.142	-5.797	2.727
-19.81	15.484	-8.233	-6.48	10.567	-5.905	8.045
-22.35	12.033	-6.786	-5.03	10.977	-4.757	6.772
-27.43	5.183	-3.994	-1.73	7.663	-4.198	5.875
-35.05	.226	-.327	-.38	.14[illegible]	-.415	.609
-45.21	-.021	-.043	-.04	-.001	-.002	.011

TABLE A13 (Continued)

Profile continued at X/L = .055

Y mm.	uuvbar	uuwbar	vvubar	vvwbar
43.69	-.001	.001	-.001	.004
33.53	-.188	.210	.460	.134
25.91	-3.774	.384	4.183	-.575
20.83	-4.480	.343	5.362	-1.671
18.29	-4.423	.089	6.221	-3.600
15.75	-4.651	-.488	5.771	-2.328
13.21	-4.200	-3.980	6.057	-2.786
10.67	-3.003	-2.856	3.313	-1.147
8.13	-.308	-1.178	.474	-2.308
5.59	2.917	.602	.411	-1.817
3.05	7.749	-.454	-5.626	.646
.51	3.282	1.600	-9.519	.829
-.76	-3.500	2.164	-10.83	2.869
-2.03	-8.349	3.249	-10.15	1.491
-4.57	-7.127	8.861	-4.662	.045
-7.11	-.462	4.791	.711	-4.309
-9.65	2.665	.542	2.788	-5.753
-12.19	3.265	-3.025	4.332	-5.778
-14.73	5.442	-2.940	5.843	-4.322
-17.27	4.715	-1.748	6.172	-3.445
-19.81	5.771	-1.614	6.650	-5.384
-22.35	6.059	-1.882	6.331	-4.016
-27.43	3.653	-1.522	4.503	-2.555
-35.05	.182	-.116	.159	-.180
-45.21	.002	-.000	-.002	-.001

TABLE A13 (Continued)

Profile continued at X/L = .055

Y mm.	wwubar	wwvbar	uvwbar
43.69	-.005	.002	-.008
33.53	.283	-.214	-.101
25.91	3.832	-1.834	2.551
20.83	3.540	-1.874	3.680
18.29	3.728	-.379	9.513
15.75	2.410	-1.286	7.529
13.21	2.438	.189	12.043
10.67	-.513	-1.607	7.365
8.13	-3.407	2.558	6.689
5.59	-3.774	1.391	4.080
3.05	-6.850	3.637	-1.596
.51	-6.891	1.370	-6.426
-.76	-6.671	-.676	-1.206
-2.03	-5.316	1.531	3.769
-4.57	-7.676	-2.180	14.242
-7.11	-1.750	2.923	.525
-9.65	-.173	2.772	-.869
-12.19	6.632	3.605	-9.651
-14.73	4.320	4.712	-7.104
-17.27	5.333	6.565	-5.291
-19.81	5.015	4.378	-8.378
-22.35	6.143	4.104	-8.294
-27.43	3.091	1.529	-1.898
-35.05	.143	.139	-.293
-45.21	-.001	.004	-.005

TABLE A14

Airfoil Wake Data at x/L = .138 (central plane)

RUN # 13
DATE OF RUN 8931

Urefernce (m/s) = 21.84
X loca.= .138

Uinfinity (m/s) = 22.10

Integral Parameters

Delta*sub x = .1171234E-01
Delta*sub z =.9371559E-01
Theta sub x = .8880582E-02

Theta sub z = .2588599E-02
Theta sub xz = .8256759E-01
Theta sub zx = .5643530E-03

Shape Factor H = 1.319

Wake Profile

Y mm.	u/Uinf	Gama	w/Uinf	Beta	Pstatic
48.26	.999	.53	.009	30.53	.1083
40.64	.997	.53	.009	30.53	.1101
33.02	.993	.60	.010	30.60	.1102
25.40	.952	1.17	.020	31.17	.1060
20.32	.896	1.82	.028	31.82	.1083
15.24	.829	2.86	.041	32.86	.1159
10.16	.756	3.91	.052	33.91	.1205
7.62	.716	4.46	.056	34.46	.1294
5.08	.685	4.98	.060	34.99	.1290
2.54	.666	5.18	.060	35.18	.1268
0.00	.660	5.20	.060	35.20	.1266
-2.54	.668	5.07	.059	35.07	.1273
-5.08	.691	4.71	.057	34.71	.1295
-7.62	.721	4.09	.052	34.09	.1279
-10.16	.763	3.61	.048	33.61	.1227
-15.24	.835	2.64	.039	32.64	.1213
-20.32	.905	1.62	.026	31.62	.1101
-25.40	.959	.85	.014	30.85	.1044
-33.02	.996	.06	.001	30.06	.0997
-40.64	1.000	0.00	0.000	30.00	.0990

TABLE A14 (Continued)

Turbulence Data

X/L Location = .138
Reference Velocity = 21.8 m/s

Wake Profile

Y mm.	Ubar	Vbar	Wbar	uubar	vvbar	wwbar
44.45	1.000	-.001	.001	.568	.772	.829
36.83	.997	-.003	.003	.970	1.227	1.340
29.21	.976	-.007	.003	2.938	2.937	3.186
24.13	.932	-.007	.006	4.383	4.357	4.868
19.05	.875	-.004	.015	6.142	5.577	6.109
16.51	.843	-.004	.020	6.668	5.919	6.576
13.97	.802	.002	.029	7.347	6.256	6.784
11.43	.768	.002	.030	7.510	6.466	6.886
8.89	.725	.005	.035	7.530	6.727	7.038
6.35	.695	.006	.039	7.210	6.454	6.703
3.81	.666	.012	.049	6.460	6.348	6.300
1.27	.648	.017	.055	5.804	6.238	6.219
0.00	.648	.022	.062	5.801	6.225	6.513
-1.27	.651	.021	.065	5.947	6.089	6.854
-2.54	.655	.024	.065	6.191	6.142	6.783
-5.08	.684	.030	.070	7.262	6.276	7.113
-7.62	.718	.031	.066	7.483	6.612	7.546
-10.16	.757	.035	.064	7.835	6.638	7.769
-12.70	.797	.037	.055	7.817	6.619	7.492
-15.24	.836	.038	.046	7.416	6.223	6.950
-17.78	.874	.040	.037	6.554	5.751	6.604
-20.32	.906	.040	.030	6.009	5.295	5.694
-25.40	.958	.037	.014	4.278	3.985	4.020
-30.48	.990	.035	-.001	2.306	2.614	2.210
-38.10	.999	.035	-.008	.728	1.119	.828
-45.72	1.000	.036	-.011	.521	.789	.700

TABLE A14 (Continued)

Profile continued at X/L = .138

Y mm.	uvbar	uwbar	vwbar	uuubar	vvvbar	wwwbar
44.45	-.006	.014	-.01	-.005	.009	.003
36.83	-.059	.155	-.16	.073	.373	-.070
29.21	-2.552	1.614	-.20	4.347	2.849	-2.461
24.13	-8.396	1.814	2.16	10.988	.823	-5.601
19.05	-14.13	-.226	5.90	12.998	3.305	-5.015
16.51	-16.91	.134	6.37	9.574	3.428	-5.948
13.97	-18.73	-2.641	5.20	12.278	5.502	-5.711
11.43	-20.66	-1.255	6.39	2.754	9.970	-.272
8.89	-23.61	-3.174	4.18	-5.766	8.583	-2.284
6.35	-18.79	-2.235	4.17	-11.04	1.992	.468
3.81	-13.27	-2.885	2.60	-14.57	2.154	2.532
1.27	-3.941	-3.369	2.39	-9.962	1.702	-.068
0.00	1.413	-3.024	.05	-8.554	-3.536	-.263
-1.27	6.307	-4.020	-1.86	-10.44	.508	-2.379
-2.54	10.508	-4.065	-2.88	-11.33	-1.125	-3.437
-5.08	20.346	-6.383	-4.75	-16.45	-3.784	-2.766
-7.62	21.694	-10.56	-7.36	-7.359	3.327	-2.435
-10.16	22.859	-13.51	-10.35	-2.119	-3.196	1.522
-12.70	22.570	-15.15	-7.01	10.174	-4.207	2.892
-15.24	19.343	-13.65	-5.38	15.361	-1.571	1.488
-17.78	15.484	-10.17	-3.81	12.004	-5.590	5.553
-20.32	12.865	-8.144	-2.57	13.738	-6.023	6.592
-25.40	6.482	-5.864	-2.47	9.877	-6.004	4.408
-30.48	1.741	-1.832	-.91	3.217	-1.538	2.130
-38.10	-.002	-.079	-.06	-.023	-.007	.104
-45.72	-.010	-.020	.02	-.001	-.002	.006

TABLE A14 (Continued)

Profile continued at X/L = .138

Y mm.	uuvbar	uuwbar	vvubar	vvwbar
44.45	-.001	.001	-.003	.003
36.83	-.068	.024	.056	.028
29.21	-1.735	.306	2.175	.095
24.13	-4.985	-.588	5.432	-1.816
19.05	-5.021	-2.110	7.200	-1.091
16.51	-3.191	-2.483	4.848	-1.570
13.97	-3.605	-2.623	4.730	-3.188
11.43	-.542	-1.952	2.488	-1.317
8.89	2.601	-1.023	-.253	1.436
6.35	6.625	-.707	-3.610	.453
3.81	7.794	.713	-6.815	1.028
1.27	3.210	1.364	-9.432	2.138
0.00	-1.102	1.284	-9.934	2.021
-1.27	-3.470	2.913	-8.629	.920
-2.54	-5.648	2.688	-8.714	1.400
-5.08	-7.232	5.439	-4.938	-1.293
-7.62	-3.552	3.602	-3.332	-1.153
-10.16	2.776	2.670	3.660	-3.459
-12.70	6.000	-1.368	5.990	-6.357
-15.24	8.467	-3.561	6.991	-6.042
-17.78	5.718	-1.549	6.281	-4.342
-20.32	6.543	-1.816	6.657	-4.105
-25.40	4.309	-2.791	5.008	-2.777
-30.48	.985	-.975	1.287	-.802
-38.10	.019	-.001	-.019	-.014
-45.72	.001	-.001	-.004	.002

TABLE A14 (Continued)

Profile continued at X/L = .138

Y mm.	wwubar	wwvbar	uvwbar
44.45	-.002	-.002	-.007
36.83	.093	-.176	-.115
29.21	2.186	-.807	-.302
24.13	4.013	-1.947	5.070
19.05	5.461	-1.316	8.473
16.51	2.466	-1.156	6.856
13.97	2.021	.301	6.356
11.43	.581	.188	8.123
8.89	-4.450	1.396	3.524
6.35	-4.411	2.869	4.682
3.81	-5.093	2.704	-.426
1.27	-5.440	.310	-3.292
0.00	-3.704	.243	.171
-1.27	-7.041	-3.591	6.080
-2.54	-4.778	-1.837	2.848
-5.08	-6.139	-2.059	6.899
-7.62	-4.458	-.590	6.842
-10.16	-1.203	1.012	-1.012
-12.70	3.147	4.042	-8.345
-15.24	4.169	3.455	-8.901
-17.78	5.546	4.172	-3.819
-20.32	7.090	2.998	-6.711
-25.40	4.589	2.750	-5.718
-30.48	1.397	.595	-1.432
-38.10	-.010	.026	-.032
-45.72	-.003	.001	-.005

TABLE A15

Airfoil Wake Data at x/L = .225 (central plane)

RUN # 19
DATE OF RUN 8981

Urefernce (m/s) = 21.84
X loca.= .275

Uinfinity (m/s) = 22.31

Integral Parameters

Delta*sub x = .1050085E-01
Delta*sub z =.8172131E-01
Theta sub x = .8346599E-02

Theta sub z = .2219180E-02
Theta sub xz = .7163467E-01
Theta sub zx = .4141984E-03

Shape Factor H = 1.258

Wake Profile

Y mm.	u/Uinf	Gama	w/Uinf	Beta	Pstatic
38.10	1.000	.67	.012	30.67	.0862
30.48	.987	.89	.015	30.89	.0847
22.86	.932	1.41	.023	31.41	.0849
15.24	.849	2.46	.036	32.46	.0947
10.16	.794	3.06	.042	33.06	.0954
6.35	.755	3.56	.047	33.56	.1012
3.81	.735	3.80	.049	33.79	.1040
2.54	.726	3.82	.049	33.82	.1037
1.27	.722	3.86	.049	33.86	.1047
0.00	.719	3.89	.049	33.89	.1057
-1.27	.719	3.88	.049	33.88	.1057
-2.54	.721	3.81	.048	33.81	.1056
-5.08	.734	3.60	.046	33.60	.1030
-7.62	.754	3.23	.043	33.23	.1005
-11.43	.790	2.78	.038	32.79	.1028
-16.51	.847	2.10	.031	32.10	.0973
-22.86	.920	1.19	.019	31.19	.0870
-30.48	.984	.36	.006	30.36	.0812
-39.37	1.000	0.00	0.000	30.00	.0797

TABLE A15 (Continued)

Turbulence Data

X/L Location = .275
Reference Velocity = 21.8 m/s

Wake Profile

Y mm.	Ubar	Vbar	Wbar	uubar	vvbar	wwbar
52.07	1.000	.004	.004	.495	.762	.811
41.91	1.000	-.000	.003	.775	1.034	1.026
31.75	.982	-.003	.002	2.896	2.686	3.028
24.13	.926	-.006	.007	5.409	4.618	5.183
20.32	.885	-.005	.017	6.251	5.321	5.815
16.51	.845	-.012	.015	6.761	6.103	6.270
12.70	.799	-.007	.022	6.743	6.069	6.257
10.16	.770	-.002	.027	6.602	6.002	5.997
7.62	.747	-.001	.032	5.938	5.905	5.828
5.08	.732	.001	.037	5.732	5.861	5.750
2.54	.719	.006	.041	5.243	5.515	5.614
0.00	.717	.009	.045	5.274	5.614	5.580
-2.54	.727	.013	.044	5.683	5.664	5.699
-5.08	.748	.014	.048	6.277	5.806	6.154
-7.62	.768	.019	.044	6.68[illegible]	5.826	6.497
-10.16	.795	.018	.043	7.10[illegible]	5.876	6.724
-13.97	.839	.017	.037	7.106	5.988	6.555
-17.78	.889	.020	.025	6.638	5.698	6.043
-21.59	.927	.017	.018	5.628	4.865	5.228
-29.21	.986	.016	.003	2.754	2.991	2.587
-39.37	.999	.015	-.006	.742	1.104	.828
-49.53	.998	.016	-.008	.479	.756	.756

TABLE A15 (Continued)

Profile continued at X/L = .275

Y mm.	uvbar	uwbar	vwbar	uuubar	vvvbar	wwwbar
52.07	.006	-.028	-.01	.000	-.001	.003
41.91	-.051	-.008	-.01	-.045	.021	-.060
31.75	-2.453	1.639	.19	4.557	1.699	-1.926
24.13	-9.112	1.762	1.95	13.305	2.161	-5.148
20.32	-13.87	-.933	4.34	13.430	2.918	-6.466
16.51	-17.63	-2.174	7.40	9.217	3.760	-5.441
12.70	-17.67	-2.639	7.45	-1.671	4.802	-2.570
10.16	-18.22	-2.728	6.44	-8.132	5.111	.811
7.62	-12.91	-3.501	5.60	-7.595	.298	1.789
5.08	-10.40	-3.807	3.25	-9.080	5.573	1.602
2.54	-4.087	-4.302	1.30	-6.399	3.501	1.296
0.00	2.821	-2.869	.22	-5.628	1.926	.072
-2.54	7.942	-3.368	-.84	-8.859	2.509	-1.808
-5.08	13.893	-5.263	-2.26	-10.26	4.494	-2.376
-7.62	15.022	-7.118	-3.17	-6.043	-.355	-3.026
-10.16	17.619	-8.591	-3.37	-.154	.883	-.353
-13.97	18.744	-10.22	-3.38	7.688	-6.160	3.368
-17.78	15.170	-7.134	-1.42	16.393	-4.547	6.841
-21.59	10.690	-7.571	-1.66	15.791	-4.276	5.619
-29.21	2.782	-2.022	-1.05	5.076	-3.106	3.512
-39.37	.040	-.049	.02	-.010	-.001	.150
-49.53	-.018	.010	.04	0.000	-.005	.000

TABLE A15 (Continued)

Profile continued at X/L = .275

Y mm.	uuvbar	uuwbar	vvubar	vvwbar
52.07	-.000	0.000	-.002	.004
41.91	-.009	-.002	-.013	-.005
31.75	-1.674	.415	2.249	-.318
24.13	-5.466	-.305	6.052	-1.843
20.32	-5.363	-1.169	6.557	-2.335
16.51	-4.243	-1.671	5.458	-1.317
12.70	2.163	-1.086	.918	-1.222
10.16	4.336	-.264	-2.432	-.210
7.62	5.680	-.056	-4.862	.119
5.08	4.192	1.309	-5.271	.748
2.54	2.281	1.249	-5.630	.998
0.00	-1.814	1.668	-5.349	.705
-2.54	-4.360	1.479	-6.622	.028
-5.08	-5.463	2.413	-4.165	-.657
-7.62	-2.350	4.173	-2.225	-1.487
-10.16	.077	1.773	.186	-1.496
-13.97	3.869	.871	4.052	-3.246
-17.78	6.736	-1.662	8.201	-4.458
-21.59	5.501	-2.744	5.813	-3.393
-29.21	2.270	-.958	2.214	-1.582
-39.37	.025	.002	.030	.006
-49.53	0.000	-.002	-.002	-.003

TABLE A15 (Continued)

Profile continued at X/L = .275

Y mm.	wwubar	wwvbar	uvwbar
52.07	-.004	.001	-.004
41.91	-.024	-.017	-.001
31.75	1.886	-.694	.737
24.13	5.259	-1.785	4.886
20.32	2.305	-.446	7.127
16.51	2.491	-.898	7.050
12.70	-1.851	1.469	4.444
10.16	-3.131	3.119	.700
7.62	-1.994	.391	-2.272
5.08	-3.984	1.529	-.429
2.54	-3.053	.405	-.095
0.00	-3.449	-.307	-.283
-2.54	-3.157	-1.114	-.638
-5.08	-3.346	-1.386	-.834
-7.62	-2.758	-.920	4.353
-10.16	-1.282	1.146	-1.531
-13.97	3.586	2.436	-3.597
-17.78	6.256	2.809	-1.561
-21.59	5.823	2.400	-3.919
-29.21	1.807	.686	-1.644
-39.37	.005	-.002	.012
-49.53	0.000	-.002	.004

TABLE A16

Airfoil Wake Data at x/L = .399 (central plane)

RUN # 14
DATE OF RUN 3981

Urefernce (m/s) = 21.84
X loca.. .399

Uinfinity (m/s) = 22.26

Integr. . Parameters

Delta*sub x = .9478079E-02
Delta*sub z = .1359371E+00
Theta sub x = .7767224E-02

Theta sub z = .1761364E-02
Theta sub xz = .1267331E+00
Theta sub zx = .2740450E-03

Shape Factor H = 1.220

Wake Profile

Y mm.	u/Uinf	Gama	w/Uinf	Beta	Pstatic
64.77	1.006	.25	.004	30.25	-.0736
54.61	1.005	.19	.003	30.19	-.0716
44.45	1.004	.14	.002	30.14	-.0748
34.29	.996	.33	.006	30.33	-.0801
24.13	.925	1.03	.017	31.03	-.0524
13.97	.835	2.07	.030	32.07	-.0212
6.35	.773	2.52	.034	32.52	-.0013
1.27	.760	2.59	.034	32.59	.0040
0 00	.759	2.56	.034	32.56	.0033
-1.27	.761	2.61	.035	32.61	.0047
-3.81	.771	2.47	.033	32.47	.0026
-6.35	.786	2.32	.032	32.32	-.0017
-11.43	.825	1.97	.028	31.97	-.0127
-16.51	.873	1.54	.023	31.54	-.0250
-24.13	.954	.74	.012	30.74	-.0660
-31.75	.985	.30	.005	30.30	-.0549
-41.91	.997	.08	.001	30.08	-.0618
-52.07	.998	.01	.000	30.01	-.0643
-62.23	1.000	0.00	0.000	30.00	-.0669

TABLE A17

Airfoil Wake Data at x/L = .661 (central plane)

RUN # 15
DATE OF RUN 3981

Urefernce (m/s) = 21.84
X loca.= .661

Uinfinity (m/s) = 22.31

Integral Parameters

Delta*sub x = .8875865E-02
Delta*sub z =.1211335E+00
Theta sub x = .7585780E-02

Theta sub z = .2496901E-02
Theta sub xz = .1125227E+00
Theta sub zx = .2651202E-03

Shape Factor H = 1.170

Wake Profile

Y mm.	u/Uinf	Gama	w/Uinf	Beta	Pstatic
62.23	1.008	.72	.013	30.72	-.0766
46.99	1.006	.70	.012	30.70	-.0757
31.75	.971	1.02	.017	31.02	-.0669
19.05	.888	1.81	.028	31.81	-.0387
11.43	.837	2.28	.033	32.29	-.0207
8.89	.826	2.37	.034	32.37	-.0161
7.62	.821	2.40	.034	32.40	-.0156
6.35	.816	2.42	.034	32.42	-.0170
5.08	.810	2.49	.035	32.49	-.0130
3.81	.807	2.42	.034	32.42	-.0123
2.54	.807	2.48	.035	32.48	-.0117
1.27	.806	2.49	.035	32.49	-.0092
0.00	.803	2.47	.035	32.47	-.0104
-1.27	.805	2.41	.034	32.41	-.0119
-3.05	.811	2.40	.034	32.40	-.0125
-4.83	.816	2.37	.034	32.37	-.0147
-7.37	.822	2.25	.032	32.25	-.0139
-9.91	.839	2.13	.031	32.13	-.0211
-13.72	.861	1.91	.029	31.91	-.0292
-18.00	.896	1.65	.026	31.65	-.0306
-25.15	.940	1.16	.019	31.16	-.0555
-32.77	.978	.74	.013	30.74	-.0592
-41.66	.984	.46	.008	30.46	-.0413
-51.82	1.000	.60	.234	30.60	-.0689

TABLE A17 (Continued)

Turbulence Data

X/L Location = .661
Reference Velocity = 21.8 m/s

Wake Profile

Y mm.	Ubar	Vbar	Wbar	uubar	vvbar	wwbar
53.34	1.000	.003	-.001	.712	.974	.795
43.18	.996	.001	.000	1.532	1.783	1.550
33.02	.965	-.000	.001	3.760	3.460	3.385
22.86	.903	-.001	.008	5.414	4.946	4.895
15.24	.847	-.001	.014	5.617	5.469	4.909
7.62	.804	.004	.026	5.046	5.204	4.656
2.54	.790	.007	.027	4.392	5.054	4.461
-2.54	.793	.008	.028	4.607	5.206	4.547
-7.62	.813	.011	.029	5.169	5.328	5.013
-12.70	.843	.015	.026	5.609	5.386	5.112
-17.78	.875	.015	.023	5.722	5.046	5.008
-22.86	.908	.014	.020	5.442	4.699	4.659
-27.94	.941	.013	.013	4.514	4.076	3.840
-35.56	.972	.009	.000	2.552	2.836	2.308
-43.18	.981	.008	-.003	1.137	1.683	1.203
-50.80	.982	.005	-.008	.749	1.049	.780

Profile continued at X/L = .661

Y mm.	uvbar	uwbar	vwbar	uuubar	vvvbar	wwwbar
53.34	-.002	.012	-.05	-.008	.011	-.070
43.18	-.847	.138	.01	.856	.277	-1.054
33.02	-5.382	1.373	.27	6.543	1.369	-4.095
22.86	-11.39	-.010	3.93	6.881	1.458	-6.974
15.24	-13.64	-.453	3.86	-.463	.810	-1.893
7.62	-7.482	-1.279	1.03	-4.980	1.646	-.007
2.54	-1.641	-1.578	1.25	-3.188	.803	.606
-2.54	5.110	-1.716	-.22	-2.761	.583	-1.288
-7.62	10.855	-2.805	-1.02	-4.115	-.215	-1.621
-12.70	13.426	-4.271	-1.23	-.419	-.097	1.957
-17.78	13.984	-4.990	-1.36	3.548	.334	2.347
-22.86	12.680	-5.607	-1.40	10.473	-3.069	4.595
-27.94	7.794	-4.646	-.81	10.951	-2.931	5.573
-35.56	2.648	-2.037	-.69	3.880	-1.895	3.100
-43.18	.546	-.240	-.10	.199	-.288	.836
-50.80	.150	-.028	-.05	.114	-.014	.204

TABLE A17 (Continued)

Profile continued at X/L = .661

Y mm.	uuvbar	uuwbar	vvubar	vvwbar
53.34	-.012	-.003	.010	-.013
43.18	-.586	-.003	.575	-.145
33.02	-2.751	.037	3.647	-.492
22.86	-2.923	-.686	4.345	-1.524
15.24	.355	-.518	.461	-.309
7.62	3.108	.114	-2.666	-.877
2.54	1.131	.341	-4.167	.228
-2.54	-2.075	.517	-4.330	-.954
-7.62	-2.915	.687	-2.521	-1.477
-12.70	-.536	.494	-.162	-2.081
-17.78	2.287	.152	2.786	-2.282
-22.86	4.882	-.928	4.124	-1.070
-27.94	4.636	-2.095	4.746	-1.639
-35.56	1.984	-1.011	2.293	-1.158
-43.18	.282	-.041	.397	-.161
-50.80	.153	-.016	.141	-.019

Profile continued at X/L = .661

Y mm.	wwubar	wwvbar	uvwbar
53.34	-.001	-.014	.025
43.18	.185	-.332	.315
33.02	2.586	1.343	.956
22.86	2.046	-1.253	5.694
15.24	-1.028	1.254	.878
7.62	-1.781	.725	.530
2.54	-1.591	.228	1.260
-2.54	-1.619	-.790	1.612
-7.62	-1.405	-.570	1.469
-12.70	-.945	-.047	-1.028
-17.78	1.696	1.469	-1.781
-22.86	3.982	3.350	-2.893
-27.94	3.675	2.300	-3.658
-35.56	1.247	.820	-1.938
-43.18	.126	.191	-.150
-50.80	.005	.002	-.046

TABLE A18

Airfoil Wake Data at x/L = .661 (+6" plane)

RUN # 16
DATE OF RUN 4981

Urefernce (m/s) = 21.84
X loca.= .661

Uinfinity (m/s) = 22.50

Integral Parameters

Delta*sub x = .8693721E-02
Delta*sub z =.9094906E-01
Theta sub x = .7425145E-02

Theta sub z = .2110851E-02
Theta sub xz = .8250125E-01
Theta sub zx = .2459053E-03

Shape Factor H = 1.171

Wake Profile

Y mm.	u/Uinf	Gama	w/Uinf	Beta	Pstatic
48.26	1.007	.86	.015	30.86	.0425
38.10	1.000	.92	.016	30.92	.0409
27.94	.959	1.25	.021	31.24	.0381
20.32	.915	1.52	.024	31.52	.0334
12.70	.861	1.96	.030	31.96	.0350
7.62	.833	2.07	.030	32.07	.0359
5.08	.818	2.26	.032	32.26	.0376
3.81	.812	2.27	.032	32.27	.0399
2.54	.807	2.31	.033	32.31	.0396
1.27	.800	2.36	.033	32.36	.0445
0.00	.796	2.37	.033	32.37	.0438
-1.27	.814	2.19	.031	32.19	.0184
-2.54	.810	2.30	.033	32.30	.0229
-4.57	.816	2.19	.031	32.19	.0140
-7.11	.822	2.22	.032	32.22	.0198
-9.65	.829	2.11	.030	32.11	.0176
-14.73	.854	1.86	.028	31.86	.0153
-21.08	.888	1.57	.024	31.56	.0192
-28.70	.941	.99	.016	30.99	.0122
-37.59	1.000	.44	.172	30.44	.0037

TABLE A19

Airfoil Wake Data at x/L = .661 (-6" plane)

RUN # 17
DATE OF RUN 4981

Urefernce (m/s) = 21.84
X loca.= .661

Uinfinity (m/s) = 23.04

Integral Parameters

Delta*sub x = .8813884E-02
Delta*sub z =.1470653E+00
Theta sub x = .7528187E-02

Theta sub z = .1666125E-02
Theta sub xz = .1384450E+00
Theta sub zx = .1935721E-03

Shape Factor H = 1.171

Wake Profile

Y mm.	u/Uinf	Gama	w/Uinf	Beta	Pstatic
87.63	1.003	.22	.004	30.22	.0299
74.93	1.006	.30	.005	30.30	.0284
64.77	1.002	.41	.007	30.41	.0337
54.61	1.001	.34	.006	30.34	.0334
44.45	.999	.32	.006	30.32	.0274
34.29	.977	.55	.009	30.55	.0232
24.13	.916	1.10	.018	31.10	.0242
16.51	.871	1.59	.024	31.59	.0196
11.43	.837	1.85	.027	31.85	.0266
8.89	.821	1.97	.028	31.97	.0321
7.62	.818	1.99	.029	31.99	.0303
6.35	.812	1.99	.028	31.99	.0306
5.08	.810	2.03	.029	32.03	.0289
3.81	.807	2.03	.029	32.03	.0309
2.54	.805	1.95	.027	31.95	.0284
1.27	.805	2.01	.028	32.01	.0311
0.00	.804	1.96	.028	31.96	.0328
-1.27	.806	1.86	.026	31.86	.0306
-3.81	.810	1.86	.026	31.86	.0328
-7.62	.827	1.60	.023	31.60	.0300
-11.43	.848	1.33	.020	31.33	.0277
-16.51	.886	1.01	.016	31.01	.0207
-22.86	.925	.58	.009	30.58	.0190
-30.48	.970	.14	.002	30.14	.0198
-39.37	.995	-.02	-.000	29.98	.0237
-49.53	1.000	0.00	0.000	30.00	.0219

TABLE A20

Airfoil Wake Data at x/L = .992 (central plane)

RUN # 21
DATE OF RUN 10981

Urefernce (m/s) = 21.84
X loca.= .992

Uinfinity (m/s) = 22.73

Integral Parameters

Delta*sub x = .8715063E-02
Delta*sub z =.1334729E+00
Theta sub x = .7656711E-02

Theta sub z = .1486612E-02
Theta sub xz = .1249248E+00
Theta sub zx = .1669065E-03

Shape Factor H = 1.138

Wake Profile

Y mm.	u/Uinf	Gama	w/Uinf	Beta	Pstatic
66.04	1.003	.47	.008	30.47	.0496
55.88	1.001	.43	.007	30.42	.0510
45.72	.995	.39	.007	30.39	.0478
35.56	.975	.65	.011	30.65	.0474
25.40	.928	1.01	.016	31.01	.0525
17.78	.887	1.37	.021	31.37	.0594
12.70	.865	1.57	.024	31.57	.0623
7.62	.850	1.69	.025	31.69	.0621
2.54	.837	1.69	.025	31.69	.0646
-2.54	.836	1.64	.024	31.64	.0630
-7.62	.846	1.51	.022	31.51	.0614
-12.70	.862	1.35	.020	31.35	.0595
-17.78	.883	1.04	.016	31.04	.0585
-22.86	.909	.74	.012	30.74	.0529
-27.94	.937	.44	.007	30.44	.0487
-35.56	.967	.05	.001	30.05	.0467
-43.18	.989	-.13	-.002	29.88	.0443
-50.80	.998	-.29	-.005	29.71	.0447
-58.42	1.000	-.43	-.172	29.57	.0467

TABLE A21

Airfoil Wake Data at x/L = 1.928 (central plane)

RUN # 18
DATE OF RUN 4981

Urefernce (m/s) = 21.84
X loca.= 1.928

Uinfinity (m/s) = 23.34

Integral Parameters

Delta*sub x = .3185820E-02
Delta*sub z =.1070817E+00
Theta sub x = .2963738E-02

Theta sub z = .3562933E-03
Theta sub xz = .1039173E+00
Theta sub zx = .2139227E-04

Shape Factor H = 1.075

Wake Profile

Y mm.	u/Uinf	Gama	w/Uinf	Beta	Pstatic
0.00	.899	.77	.012	30.77	.0116
3.81	.901	.51	.008	30.51	.0103
7.62	.907	.50	.008	30.50	.0084
12.70	.918	.47	.008	30.47	.0050
19.05	.930	.27	.004	30.27	.0001
26.67	.947	.55	.009	30.55	.0029
35.56	.968	.20	.003	30.19	-.0034
45.72	.981	.09	.002	30.09	.0039
57.15	.994	.13	.002	30.13	.0037
69.85	.999	.05	.001	30.05	.0035
83.82	1.001	.03	.001	30.03	.0041
99.06	1.000	.00	.001	30.00	.0072

TABLE A21 (Continued)

Turbulence Data

X/L Location = 1.928
Reference Velocity = 21.8 m/s

Half Wake Profile

Y mm.	Ubar	Vbar	Wbar	uubar	vvbar	wwbar
-6.35	.902	.004	.015	3.378	4.385	3.509
-5.08	.900	.003	.016	3.376	4.185	3.656
-2.54	.902	.005	.017	3.358	4.351	3.674
0.00	.900	.003	.014	3.439	4.245	3.637
2.54	.903	.004	.016	3.482	4.308	3.654
5.08	.904	.003	.016	3.454	4.293	3.726
7.62	.908	.004	.015	3.584	4.315	3.725
10.16	.911	.000	.014	3.650	4.127	3.841
12.70	.914	.002	.012	3.537	4.196	3.714
17.78	.923	.002	.011	3.669	3.973	3.710
22.86	.934	.001	.010	3.735	3.882	3.635
27.94	.946	.002	.010	3.504	3.730	3.593
33.02	.955	.002	.009	3.379	3.580	3.414
38.10	.965	.001	.008	3.129	3.257	3.086
43.18	.975	.001	.007	2.756	2.988	2.853
50.80	.987	-.000	.004	2.318	2.453	2.326
58.42	.992	.001	.006	1.766	1.967	1.909
66.04	.998	.002	.005	1.290	1.691	1.493
76.20	1.001	.001	.005	.883	1.162	1.044
86.36	1.000	-.000	-.000	.622	.930	.840

TABLE A21 (Continued)

Profile continued at X/L = 1.928

Y MM.	uvbar	uwbar	vwbar	uuubar	vvvbar	wwwbar
-6.35	.861	-.184	-.69	-.307	.906	-.389
-5.08	.961	-.979	-.70	-.331	.590	.159
-2.54	-.018	-.428	-.62	-.272	.271	-.345
0.00	-.782	-.257	-.60	-.217	.658	-.495
2.54	-2.540	.149	-.39	-.167	.175	-.065
5.08	-2.773	.312	-.08	.065	.849	-1.309
7.62	-3.602	.479	.37	.249	.212	-1.242
10.16	-3.806	.700	.46	.114	.967	-1.727
12.70	-4.577	.828	.66	.081	.771	-1.583
17.78	-4.812	1.428	.40	.669	.729	-1.746
22.86	-5.369	.967	.15	1.808	1.026	-2.480
27.94	-5.393	1.383	.56	2.084	1.374	-3.169
33.02	-5.111	1.249	.82	2.360	.682	-2.807
38.10	-4.289	1.004	.62	2.855	.421	-2.462
43.18	-3.451	.782	.60	1.969	.947	-2.459
50.80	-2.359	.781	.14	1.719	.687	-1.699
58.42	-1.412	.357	.24	.822	.256	-1.097
66.04	-.608	.157	.11	.309	.121	-.957
76.20	-.188	-.029	.04	.053	-.007	-.225
86.36	-.041	-.012	.03	-.003	.016	-.053

TABLE A21 (Continued)

Profile continued at X/L = 1.928

Y mm.	uuvbar	uuwbar	vvubar	vvwbar
-6.35	-.166	[illegible]	-1.831	-.402
-5.08	-.228	.004	-1.554	-.303
-2.54	.308	-.043	-1.494	-.401
0.00	.513	-.016	-1.632	-.151
2.54	.455	-.264	-1.694	-.210
5.08	.677	.135	-1.326	-.251
7.62	.492	-.550	-1.066	-.322
10.16	.326	-.307	-.584	.035
12.70	.383	-.005	-.404	-.077
17.78	.240	-.008	.038	-.038
22.86	-.335	-.063	.732	-.187
27.94	-.825	.222	1.265	-.458
33.02	-1.149	.169	1.508	-.535
38.10	-1.401	.056	1.461	-.408
43.18	-1.192	.286	1.301	-.428
50.80	-1.004	.152	1.149	-.085
58.42	-.577	.094	.657	-.189
66.04	-.217	.104	.172	-.180
76.20	-.088	.009	.068	-.026
86.36	-.012	.004	.005	.014

TABLE A21 (Continued)

Profile continued at X/L = 1.928

Y mm.	wwubar	wwvbar	uvwbar
-6.35	-.036	-.104	1.675
-5.08	.062	-.089	1.560
-2.54	-.228	.103	1.470
0.00	.061	.137	2.025
2.54	.147	.228	2.081
5.08	-.235	-.223	.959
7.62	.114	-.253	1.335
10.16	.135	.085	1.398
12.70	.295	.287	.948
17.78	.429	.054	.868
22.86	.660	-.511	.456
27.94	1.008	-.610	.244
33.02	.828	-.686	.718
38.10	1.020	-1.089	.765
43.18	.896	-.607	.711
50.80	.693	-.590	.253
58.42	.403	-.473	.060
66.04	.071	-.354	-.025
76.20	-.019	-.089	.017
86.36	-.002	-.015	.020